

# **A Fundamental study on the effects of cation substitution on the molecular chemistry and surface reactivity of sphalerite**

**By**

**Lebogang Babedi**

*Thesis submitted in fulfilment of the requirements for the degree  
of Master of Science (Geology)*



UNIVERSITEIT  
STELLENBOSCH  
UNIVERSITY

**Stellenbosch University**

Supervisor: Dr. B.P. von der Heyden

1918-2018

Co-supervisor: Dr. M. Tadie

Department of Earth Sciences

Faculty of Science

December 2018

## Abstract

Sphalerite exhibits multiple flotation responses because of its intricate mineral chemistry which arises from its ability to incorporate different metal impurities. Historical work has focussed largely on the influences of Fe impurities on the flotation behaviour of sphalerite. This has created a broad knowledge gap related to the influence of associated metal impurities (e.g. Cd, Co etc.) on the structure and surface chemistry and the consequent flotation response of sphalerite. The current study seeks to address the knowledge gap using sets of analytical techniques (XRD, Raman spectroscopy, UV-vis and zeta potential) to build a molecular-level link between the crystal structure distortions, surface characteristics, and electronic structure alteration. These properties are related to the ultimate flotation response of synthetic sphalerite doped with variable amounts (0-4 wt.%) of Cd, Co and Fe.

Sets of impurity (Cd, Co, Fe) bearing sphalerite samples were synthesised using a dry experimental method to ensure a controlled sphalerite composition when evaluating the influence of individual cation substitutions. The structural evaluations with XRD revealed that each metal impurity induced lattice distortion, as reflected by the varied unit cell constants with increasing impurity concentration. The magnitude of the lattice distortions can be correlated with impurity concentration and ionic size of each metal impurity. Raman spectroscopy showed that the different metal impurities induce new surface features in the form of an impurity mode, the position of which reflects the chemical nature of the metal impurity bond formed within sphalerite molecular cluster. The stronger bonds (Co and Fe) require higher vibrational energies thus occur at higher wavenumber (Fe  $300\text{ cm}^{-1}$ , Co  $303\text{ cm}^{-1}$ ) compared to the weaker bonds of Cd ( $295\text{ cm}^{-1}$ ). The intensity ratios between the Zn-S mode (TO) and the impurity mode can be correlated ( $r^2 = 0.9403$  Cd,  $r^2 = 0.7915$  Fe,  $r^2 = 0.961$  Co) as a function of increases in impurity concentration. My UV-Vis data indicates that the variations in the band gap of sphalerite changed as a function of cation substitution (Cd>Fe>Co), and these were found to correlate well ( $r^2 = 0.99$ ) with the measured position of the Raman impurity mode of the corresponding cation substituent.

The influence of each individual cation on the surface charge, Cu-activation and collector adsorption was assessed using electro-kinetic techniques (zeta potential), which provided valuable information on the surface reactivity of impurity bearing sphalerite. The study illustrates different electro kinetic characteristics of sphalerite depending on the nature of the substituting metal, which resulted in the formation of multiple surface products. The zeta potential responses varied between the different trace element substituted sphalerite reflecting differences in their nucleophilic and electrophilic properties. The results presented herein thus provide a systematic correlation between the structure and surface chemistry and illustrate how such changes manifest to the variation to the electronic structure and consequently the flotation response. This illustrates that maximum recovery of zinc can only be achieved through multidisciplinary study and fundamental understanding of the effects of cation substitution on mineral structure and surface chemistry, the latter necessarily affecting the flotation response.

## Opsomming

Sphalerite vertoon verskeie floteringsreaksies as gevolg van die ingewikkelde minerale chemie wat voortspruit uit die vermoë om verskillende metaal-onsuiwerhede in te neem, maar die groot interpretasies van sulke flotasiëgedrag word hoofsaaklik toegeskryf aan Fe-konsentrasie. Dit het 'n breë kennisgaping geskep oor die invloed van geassosieerde metaal onsuierhede (bv. Cd, Co, ens.) Op die struktuur en oppervlakkemie en die gevolglike flotasië-respons van sphaleriet. Die huidige studie poog om die kennisgaping aan te spreek deur gebruik te maak van stelsel analitiese tegnieke (XRD, Raman-spektroskopie, UV-vis en zeta-potensiaal om 'n molekulêre vlak te bou tussen die kristalstruktuurverdraaiings, oppervlakkenmerke, verandering van elektroniese struktuur en hul verhouding tot die flotasië reaksie van sintetiese sphalerite gedoteer met veranderlike hoeveelhede (0-4 gewig%) van Cd, Co en Fe.

Setse van onsuierheid (Cd, Co, Fe) dra sphaleriet monsters is gesintetiseer met behulp van 'n droë eksperimentele metode om 'n beheerde samestelling te help en die invloed van individuele kationvervanging te evalueer. Die strukturele evaluasies met XRD het aan die lig gebring dat elke metaal-onreinheid geïnduseerde roostervorming weerspieël word deur die gevarieerde eenheidselle konstantes met toenemende onreinheidskonsentrasie. Die grootte van die roostervorming kan korreleer word met onreinheidskonsentrasie en ioniese grootte van elke metaal-onreinheid. Raman-spektroskopie het getoon dat die verskillende metaal-onsuierhede nuwe oppervlakkenmerke in die vorm van 'n onreinheidsmodus veroorsaak, waarvan die posisie die chemiese aard van die metaal-onreinheidsbinding wat binne die sphaleriet molekulêre groep gevorm word, weerspieël. Die sterker bindings (Co en Fe) vereis hoër vibrasie-energieë, dus by hoër wawetal (Fe 300  $\text{cm}^{-1}$ , Co 303  $\text{cm}^{-1}$ ) in vergelyking met die swakker bindings van Cd (295  $\text{cm}^{-1}$ ). Die intensiteitsverhoudings tussen die Zn-S-modus (TO) kan gekorreleer word ( $r^2 = 0.9403$  Cd,  $r^2 = 0.7915$  Fe,  $r^2 = 0.961$  Co) met die toename in onreinheidskonsentrasie. Ons UV-Vis-data het aangedui dat die variasies in die bandgaping (Cd > Fe > Co) van sphaleriet verander as 'n funksie van kation-substitusie, en dit is gevind dat dit goed korrek is ( $r^2 = 0.99$ ) met die gemete posisie van die Raman-onreinheid modus van die ooreenstemmende katioensubstituent.

Die invloed van elke individuele katioon op die oppervlakkingslading, Cu-aktivering en kollektor-adsorpsie is beoordeel met behulp van elektrokinetiese tegnieke (zeta potensiaal), wat waardevolle inligting verskaf het oor die oppervlakreaktiwiteit van onreinheid wat sphaleriet bevat. Die studie illustreer verskillende elektrokinetiese eienskappe van sphaleriet, afhangende van die aard van die vervangende metaal, wat gelei het tot die vorming van verskeie oppervlakprodukte. Die zeta potensiele reaksies het gewissel tussen die verskillende spoorelement-gesubstitueerde sphaleriet wat verskil in hul nukleofiele en elektrofiliese eienskappe weerspieël. Die resultate wat hierin aangebied word, bied dus 'n sistematiese korrelasie tussen die struktuur en oppervlakkemie en illustreer hoe sulke veranderinge manifesteer in die variasie van die elektroniese struktuur en gevolglik die flotasierepons. Dit illustreer dat maksimum herwinning van sink dus slegs bereik kan word deur multidisiplinêre studie en fundamentele begrip van die effekte van katioonsubstitusie op minerale struktuur en oppervlakkemie, laasgenoemde wat noodwendig die drywingsreaksie beïnvloed.

## Declaration

In accordance with the Stellenbosch University regulation for a Master of Science degree, by making this submission the following declarations are made:

I hereby declare that the work presented in this thesis has not been used at any other institution for the award of any other academic qualification (degree or diploma) and that, the material contained in this thesis as my work with exception where reference is presented within the thesis.

I also declare that the work presented herein as my own contribution and any publication by Stellenbosch University will not be contravening third party copyrights. The thesis includes three conference papers (one as an appendix) submitted in both national and international peer reviewed conferences respectively. The writing up and compiling of the manuscripts was my sole responsibility as the main author working together with my supervisors Dr B.P. von der Heyden and Dr. M. Tadie. The inclusion of co-workers on the manuscript illustrate the collaborative nature of the work and acknowledges their contribution to the preparation of the manuscript.

Thesis chapter	Paper title	status	Candidate's contribution
Appendix 1	Impact of cation substitution (Cd, Co) on the geometallurgical response of sphalerite.	Accepted at International Mineral Processing Congress, 2018 (Russia)	Main author, responsible for data collection, interpretation and writing
Chapter 4	Mineral chemistry as a critical parameter in geometallurgical models: a case study using trace element-substituted sphalerite	Accepted at SAIMM 2018 Geometallurgy conference, Cape Town	Compilation of the data, interpretation and 65% writing of the final draft.
Chapter 5	Impacts of cation (Co, Cd, Fe) substitution on the geometallurgical response of sphalerite	Submitted to Minerals Engineering International, Process Mineralogy 2018 conference, Cape Town.	Main author, responsible for data collection, interpretation and writing

Signed:

Lebogang Babedi

Date: December 2018

Copyright © 2018  
Stellenbosch University  
All rights reserved

## Acknowledgments

Firstly, I would like to thank my mother and brother for being the best support structure since the start of this MSc. Special dedication to my mother for continuing to acknowledge and support my childhood dreams throughout my academic years. I am deeply grateful that you kept me at school throughout the years, your constant encouragement has been the catalyst for my academic progress even when we had nothing, your words made sure that giving up was not an option.

The research project was not going to be a reality if it was not for the financial support from both DST-NRF-CIMERA and Society of Economic Geology (SEG). I want to acknowledge and CIMERA for funding this project for the period of two years and SEG for providing additional funds to aid some shortfalls.

I would like to thank my supervisor, Dr Bjorn von der Heyden for the role he has played from the first email communication we had in late 2016 to the last days of writing this thesis. It was the first communication with you in 2016, which I still consider as a turning point in my life and which aligned me back to my lifelong dream of pursuing my studies until PhD. Over the period of two years, you have contributed immensely to my scientific growth with your continued encouragement, support and input. It is through you that I met Dr Margreth Tadie, my co-supervisor. Coming with a geological background and an interest in process mineralogy and geometallurgy, meeting Dr. Tadie has been a blessing. I am very grateful to her for introducing me to key fundamental aspects related to mineral processing. Working with both Dr. von der Heyden and Dr. Tadie has been a great experience and I hold both relationships very close to my heart.

I also want to acknowledge and give thanks to other individuals that played a key role in making the project a success, they are:

- Prof. Gary Stevens for allowing me to use his Experimental laboratory and teaching me key skills in experimental synthesis.
- Dr. Martina Frei for assisting with ordering the chemicals and equipment for the project.
- Dr. Pieter. H. Neethling for his contribution towards Raman and UV-vis spectroscopy analyses. Thank you for allowing me to use your Raman instrument and I greatly appreciate your efforts in setting up a new UV-vis which allowed me to analyse my samples.
- Dr. Remy Bruker at Ithemba labs for his assistance during the XRD analysis.
- The Central Analytical Facility staff in Stellenbosch, for their assistance with sample preparation, and SEM analysis.

Special thanks to everyone who I didn't mention above but who have been a part of this journey. Thanks to the entire Department of Earth Sciences staff and Economic geology study group (2017 and 2018).



## Table of Contents

<b>Abstract</b> .....	i
<b>Opsomming</b> .....	iii
<b>Declaration</b> .....	v
<b>Acknowledgments</b> .....	vi
<b>Abbreviations</b> .....	xiv
<b>Chapter one – Introduction and Thesis Overview</b> .....	1
Introduction .....	1
Key research questions.....	3
Thesis structure.....	4
References.....	6
<b>Chapter two – Relevant literature review</b> .....	8
Introduction .....	8
Massive sulphide deposits and mineralogy- The source of base metal minerals. ...	8
Chemistry and structure of sphalerite.....	9
Metallurgical treatment of sphalerite.....	14
Sphalerite flotation.....	15
Sphalerite activation.....	15
Sphalerite collector adsorption.....	18
The effect of transition-metal impurities on the metallurgical response of sphalerite .....	19
Reference.....	20
<b>Chapter three – Experimental sphalerite synthesis</b> .....	26
Evaluation of experimental methods used for sphalerite synthesis .....	26
Chemical Vapour Transport (CVT).....	27
Dry Experimental Synthesis .....	31

Co-precipitation .....	32
Hydrothermal Synthesis .....	34
Justification of the chosen experimental method .....	35
Experimental considerations and synthesis for sphalerite using dry method .....	37
Purity of the starting material .....	37
Stability of the reacting tubes .....	37
Phase stability of ZnS polymorphs .....	38
synthesis of sphalerite.....	39
References .....	42
<b>Chapter Four-</b> Structural, surface and electronic structure interrogations .....	45
<b>Chapter five</b> – Electro-kinetic studies .....	68
<b>Chapter Six</b> – Discussion .....	85
The impacts of the Cd on the structure, surface bonding, electronic structure and flotation response of sphalerite.....	87
Influence of Cd on the bulk structure and surface bonding of sphalerite.....	87
The relation of Cd induced surface bonding, electronic structure characteristics and the flotation (i.e. Cu-activation and collector adsorption) response of Cd-bearing sphalerite .....	91
The influence of Cd on Cu activation and the flotability of sphalerite .....	95
The influence of Cd on the electron transfer between collector and sphalerite surface .....	97
Impacts of Cd on the oxidation of xanthate to dixanthaogen.....	99
Major difference between the impacts of 3d (Fe and Co) and 4d (Cd) atoms on the bulk structure, surface bonding, electronic structure and flotation response. ....	100
The influence of both Co and Fe on Cu-activation and electron transfer between collector and sphalerite surface .....	103

The influence of metal impurities on the electrochemical oxidation of xanthate to dixanthogen .....	105
Overall inter-relation of the bulk structure, surface chemistry and electronic structure to the flotation response of sphalerite.....	105
Implications for sphalerite flotation and predictive capabilities during process design .....	108
<b>Chapter Seven – Conclusions and Recommendations .....</b>	<b>110</b>
References .....	115
<b>APPENDIX I .....</b>	<b>120</b>
Abstract.....	120
Key words: sphalerite, Surface chemistry, electro-chemistry, zeta potential, iso-electric point, flotation.Introduction .....	121
Methods .....	122
Synthesis of Impurity-doped Sphalerite.....	122
Chemical and Structural Characterizations .....	123
Zeta Potential Measurements .....	124
Results and Discussion.....	124
Chemical and Structural Characterization.....	125
Dopant Effects on the Reactivity of Un-activated Sphalerite .....	127
Implications to Sphalerite Flotation and Predictive Capabilities During Process Design.....	131
Conclusion .....	132
Acknowledgments .....	133
References .....	133
<b>APPENDIX II .....</b>	<b>136</b>
<b>APPENDIX III .....</b>	<b>137</b>
Impurity induced surface characteristics of sphalerite .....	137

Influence of impurities on the band structure of sphalerite .....	139
Influence of impurities on sphalerite flotation response as reflected by electro-kinetic measurements.....	140

## **Table of figures**

### **Chapter two**

<b>Figure 2.1:</b> Sphalerite crystal structure: small spheres represent Zn and the large S (Harmer et al., 2008). .....	10
<b>Figure 2.2:</b> Summary of the metal impurity contents obtained from different studies of sphalerite at varied ore deposits in the world. The full data set is shown in appendix II.....	11
<b>Figure 2.2:</b> schematic representation of copper activation mechanism of sphalerite in alkaline conditions (from Chandra and Gerson, 2009). .....	17

### **Chapter Three**

<b>Figure 3.1:</b> Schematic representation of a Chemical Vapor Transport crystal growth experiment under controlled temperature gradient (from Schmidt et al., 2013).....	29
<b>Figure 3.2:</b> Different designs of tubes employed in dry synthesis of sulphide minerals. A-E illustrate a simple sealed evacuated silica tube arrangement, F-G, a tube-in-tube arrangement, H, DTA (Differential Thermal Analysis) tube design and I-M, Collapsible tube arrangement (Kullerud, 1971).....	31
<b>Figure 3.3:</b> Flowchart for the preparation of Cu, Cd and Fe doped sphalerite by co-precipitation method (Chen et al., 2012).....	33
<b>Figure 3.1:</b> Phase Stability diagram of sphalerite-wurzite minerals as a function of temperature and Cd concentration.....	39
<b>Figure 3.5:</b> A graphical summary of a dry experimental synthesis of sphalerite used in this study. A detailed explanation of the method is presented below.....	40

### **Chapter Four**

**Figure 4.1a:** Shift in the  $2\theta$  diffraction peak position for the sphalerite 311 diffraction plane as a result of increasing concentrations of a Fe cation substituent. 1b. Linear correlation between the doped sphalerite unit cell constant and increasing concentrations of Fe cation substituent.....52

**Figure 4.2:** (a) Peak positions of the Raman shifts associated with a 0.71% Co-substituted synthetic sphalerite relative to the pure synthetic sphalerite Raman spectrum. (b). Variations in the peak height ratios of the impurity mode and the transverse optical (TO) mode as a function of dopant concentration in the Cd-, Co-, and Fe-doped synthetic sphalerites.....54

**Figure 4.3:** (a) Shifts in the UV-Vis reflection spectra of Co-doped synthetic sphalerites as a function of the dopant concentrations. (b). Shifts in the calculated size of the band gap for the Co-, Cd-, and Fe-doped synthetic sphalerites (using Equation [5]).....56

**Figure 4.4:** Diagrammatic overview of how cation substitution in the bulk mineral structure can manifest as modifications to the surface chemistry and thus flotation response of sphalerite. Techniques indicate a simplified work flow towards understanding the important interrelationships (XPS: X-ray photoelectron spectroscopy; XAFS: X-ray absorption fine structure).....59

**Figure 4.5:** Relationship between the band gap in substituted sphalerite and the strength of the bond between sulphur and the cation substituent as reflected in the wavenumber position of the impurity mode.....60

**Figure 4.6:** Distribution of Cd in sphalerite along strike in the lower orebody of the Swartberg deposit. This trace element data can be used to improve efficiencies when beneficiating Swartberg ore by modifying the flotation parameters (e.g. pH) according to the mineral chemistry of the two zones indicated.....62

## Chapter Five

**Figure 5.1a-b:** Correlation between the iso-electric point and the concentration of both iron and cadmium.....74

<b>Figure 5.2a-b:</b> Zeta potential distribution for Cu-activated impurity bearing sphalerite in alkaline media at pH 9. A represents Co-sphalerite, while B represents Fe-sphalerite.....	76
<b>Figure 5.3:</b> The variation on the onset pH of flotation with increasing iron concentration within an activated sphalerite conditioned in alkaline media.....	78
<b>Figure 5.4:</b> Correlation between the impurity concentration and the change in the critical pH point suitable for flotation in alkaline media.....	79
<b>Figure 5.5:</b> Zeta potential distribution for different impurity bearing synthetic sphalerite conditioned in an electrolyte solution containing $1 \times 10^{-4}$ M xanthate and $1 \times 10^{-4}$ M $\text{CuSO}_4$ in a 1:1 ratio. Figure 5a-b represents Fe- and Cd-bearing samples respectively.....	81
<b>Chapter Six</b>	
<b>Figure 6.2:</b> Evolution of the relative intensities (I/TO) of three sets of impurity bearing sphalerite samples as a function of the unit cell constant variations.....	90
<b>Figure 6.3:</b> Proposed band structure of pure sphalerite.....	92
<b>Figure 6.4:</b> Correlation between the strength of the bond as reflected by the impurity mode position with the variation of the individual band gap.....	94
<b>Figure 6.4:</b> Electron transfer process that occurs during the mineral surface interaction with collector and consequent oxidation (modified from Xu and Schoonen, 2000).....	98
<b>Figure 6.5:</b> Diagrammatic overview of how cation substitution in the bulk mineral structure can manifest as modifications to the surface chemistry and thus flotation response of sphalerite.....	108

## Tables

### Chapter Two

<b>Table 2.1:</b> ionic radius of common transition-metals found in tetrahedral coordination of sphalerite (Shannon, 1976).....	13
---	----

### Chapter Three

<b>Table 3.1:</b> Summary of the locations of the different analytical methods used for this study.....	26
---	----

<b>Table 3.2:</b> Summary of the CVT synthesis of sphalerite used in two studies.....	30
---	----

<b>Table 3.3:</b> A summarized comparison of the common experimental methods used for the synthesis of sphalerite.....	36
--	----

<b>Table 3.4:</b> Average Scanning Electron Microscopy (SEM) elemental spot analyses for the samples. All values reported in weight percentage and values in parentheses reflect the standard deviation.....	42
--	----

### Chapter Five

<b>Table 5.1:</b> Average Scanning Electron Microscopy (SEM) elemental spot analyses for the samples. All values reported in weight percentage and values in parentheses reflect the standard deviation.....	73
--	----

### Chapter Six

<b>Table 6.1:</b> Summary of the influence of metal impurities on the structure, surface bonding, electronic structure and flotation response of sphalerite.....	86
--	----

## Abbreviations

CVT – Chemical Vapour Transport

XRD – X-ray Diffraction

SEDEX – Sedimentary Exhalative Deposits

BHT – Broken Hill Type

VMS – Volcanic Massive Sulphide

ISP - Imperial Smelting Process

XPS - X-ray Photoelectron Spectroscopy

SIMS - Secondary ion mass spectrometry

IEP – Isoelectric Point



## Chapter one – Introduction and Thesis Overview

### Introduction

Zinc is an important metal used primarily in the alloying industry, particularly in the manufacture of brass. Although it can be won from non-sulphidic ores, its primary ore mineral is sphalerite (ZnS) which is commonly mined in association with zinc and copper minerals from a variety of base metal ore deposit types. The beneficiation of these complex ores relies heavily on the use of flotation technologies (e.g., Aghazadeh et al., 2015) which when optimised, enable exploitation of low-grade ores that would otherwise be uneconomical (Bicak and Ekmekci, 2012). Sphalerite exhibits a wide band gap resulting in different semi-conducting properties as compared to other sulphide minerals. This thus requires activation using copper sulphate or copper nitrate to improve the efficiency of collector adsorption reactions (Ejtemaei and Nguyen, 2017, Chandra and Gerson, 2009).

Several studies have illustrated that the incorporation of transition-metal impurities within the sphalerite lattice cause extensive changes to the crystal structure and consequently distort its electronic properties (Harmer et al., 2008, Chen et al., 2010, Cook et al., 2011). As a result, sphalerite tends to change its semi conducting properties due a wide deviation in the sphalerite stoichiometry (Chen et al., 2010). This results in severe challenges during sphalerite beneficiation, including variable Cu activation and collector adsorption responses due to the presence of transition-metal cation impurities (Chen et al., 2012). Improving metal recovery from sulphide ores with a great deal of cation substitution requires a high-level understanding of the physical and chemical characteristics of the impurity bearing sphalerite.

Several interpretations on sphalerite flotation response are largely attributed to Fe concentration with minimal available data-sets that expand to other associated metal impurities. It is postulated that the presence of other associated metal impurities even at minimal concentration, depending on their physico-chemical properties will affect the geometallurgical response of sphalerite. This is illustrated by contrasting flotation results at different iron concentrations reported by Nefedov et al., (1980), Popov and

Vucinic (1990), Boulton et al. (2005), Harmer et al. (2008), Chen et al. (2012) and thus indicating the importance of an expanded evaluation of the mineral chemistry impacts on flotation fundamentals. The key to a broader understanding of sphalerite flotation response is thus related to the impacts of other (Cd, Co, Mn etc.) associated metal impurities on the bulk structural, surface and electronic structure characteristics of sphalerite (Harmer et al., 2008). Establishing a thorough knowledge of the influence of the associated metal impurities is critical to the fundamental understanding of sphalerite behaviour in flotation systems characterised by interactions with reagents such as collectors and activators. Although mineral chemistry plays a critical role in the flotation of mineral constituents especially during the interaction with flotation collectors, it is not the sole factor that governs successful separation using flotation.

Kohad, (1998) suggested that a successful flotation operation requires a holistic knowledge and understanding of four critical components namely:

- Mineralogical characteristics (i.e. mineral association and liberation size)
- The chemistry of the reagents that are used to induce hydrophobicity
- Process design (i.e. cell design and the system controls)
- Operational parameters (e.g. pH, temperature, ionic strength etc).

The consideration of the above factors play a significant role in improving the efficiency of flotation of individual minerals species, however this study has taken a route that seeks to establish the importance of mineral chemistry on flotation of sphalerite. The interaction between the mineral surface and the flotation reagents (i.e. Cu activation and collectors) is highly dependent on the mineral chemistry thus making the assessment of the variation in the mineral chemistry a key part to fully understanding the fundamental controls for sphalerite flotation.

Critical to this study is the desire to establish a substantive correlation between the bulk structure, surface chemistry, electronic structure and the consequent surface reactivity of transition-metal impurity-bearing sphalerite. This is because several studies have focussed on understanding the Cu activation mechanism and collector adsorption during sphalerite floatation. However, minimal attention has been given to a systematic molecular-level experimental correlation of the crystal structure, surface properties and the electronic structure of sphalerite and how such correlations can

effectively assist the flotation recovery. The current study utilizes a series of impurity-bearing (Cd, Co and Fe) synthetic sphalerite samples to build up a thorough molecular-level understanding of the changes to structure, and how such variation can manifest to the surface and electronic characteristic. The alterations of the electronic structure would consequently relate to the flotation response. A series of impurity (Cd, Co, Fe) doped sphalerite samples are synthesized using the dry method to aid a detailed investigation of the impact of individual cation substitution. The samples ( $Zn_{1-x}M_x$ )S (where M represents the metals Cd, Co, Fe) are prepared from a stoichiometric mixture of high purity (>99.99%) elements, with the mass of the substituting metal ranging between 0-4 wt.%. By establishing a correlation, it is anticipated that the study will be enhancing the understanding and our predictive capabilities using routine techniques, we add meaningfully to the existing body of work geared towards increasing the efficiency of sphalerite ore beneficiation.

The approach used in this work is critical to relating complex mineral structures to processing performance. The multidisciplinary study will contribute to a comprehensive model that leads to an understanding of the flotation response of a substituted sphalerite. Cook et al., (2011) stated that a prerequisite to understanding the beneficiation of low-grade sulphide ores was a comprehensive mineralogical understanding. This includes an understanding on the distribution of transition-metal impurities within minerals and ores. It is anticipated that such an approach will give insights on the multiple flotation responses as seen in natural sphalerite containing some of the transition-metal impurities and provide an improved understanding of their influence on process design. This may contribute to a broader understanding of the geometallurgical complications associated with low-grade sulphide ores.

### **Key research questions**

This research aims to address the following key questions:

- 1) What are the common bulk structural distortions and surface characteristics associated with individual cationic substitution of Zn in lattice sites of sphalerite?

- 2) Can we relate such bulk structural distortions to the surface bonding characteristics of a Zn-S molecular cluster?
- 3) What are the influences of the metal impurities on the electronic structure of sphalerite?
- 4) How does the influence of cation substitution on the surface bonding environment be related to the changes to the electronic structure of sphalerite?
- 5) Do the different metal impurities give sphalerite different flotation response?
- 6) Can these molecular-level insights (1-4) positively impact predictive capabilities during the design of sphalerite beneficiation circuits?

My research hypothesis can thus be broadly stated as:

***“The application of a set of analytical techniques to build-up a thorough molecular-level insight of sphalerite mineral chemistry can be key to a substantive and predictable understanding of the fundamental flotation controls of sphalerite.”***

## **Thesis structure**

The thesis is made up of seven chapters of which two chapters are peer reviewed conference publications. It is anticipated that a third chapter (Chapter 6) will be summarized and formatted to meet the required standard of an international journal publication.

**Chapter two:** This chapter is an extended background and literature review of topics that are relevant to the current study. Specifically, the chapter introduces the concepts on sulphide deposits, the chemistry and structure of sphalerite, different metallurgical process routes for sulphide ores and flotation of sphalerite. The chapter also introduces reported processing challenges associated with sphalerite as function of transition-metal impurities.

**Chapter three:** This section presents an overview of both the experimental and analytical methods. The chapter provides a critical evaluation of four experimental

methods for synthesising trace-element doped sphalerite i.e., chemical vapour transport, dry synthesis, co-precipitation and the hydrothermal method (, Suchanek and Riman, 2006, Tesfaye and Taskinen, 2010, Gulshan and Okada, 2013). The chapter provides a detailed breakdown of the ultimate methodology used for sphalerite synthesis and documents all the subsequent analytical techniques. These include X-ray diffraction (XRD) for structural characterisation; Raman spectroscopy to establish the impacts of impurities on the surface bonding environment of sphalerite, UV-vis Diffuse reflectance spectroscopy to investigate the variation in the band gap of sphalerite as a function of cation substitution and finally zeta potential measurements to interrogate the surface reactivity of sphalerite.

**Chapter four:** The chapter present a conference paper that has been peer-reviewed and accepted for presentation at the South African Institute of Mining and Metallurgy (SAIMM) 2018 Geometallurgy conference, Cape Town. The paper presents a correlation concept that seeks to illustrate the role of molecular-level investigations as the missing link in geometallurgical frameworks. The approach used in this paper is one that build up on a linkage between the impurities (Cd, Co, Fe) induced structural distortions and relates them to the surface bonding environment. This also illustrate how such variation can relate to the change in the electronic properties, consequently the flotation response.

**Chapter five:** The chapter presents a conference paper that has been prepared and submitted to the Process Mineralogy 2018 conference, Cape Town (hosted by the Minerals Engineering International). The chapter provides experimental insights into the surface reactivity of sphalerite under flotation related conditions as a function of the incorporation of Cd-, Co- and Fe- impurities. The interpretations presented in the chapter are based on a thorough interrogation of the electro-kinetic results of sphalerite in the presence of  $\text{CuSO}_4$  and sodium isobutyl xanthate. Based on the electro-kinetic measurements presented in the chapter, the impacts of the three-common transition-metal impurities on the flotation response of sphalerite are established.

**Chapter six:** This chapter is an expansion of the two papers presented in chapter four and five. This section expands on the presentation of the two papers and will be summarized at a later stage for submission at an international journal publication. The

section establishes the key impacts of the three common metal impurities (Cd, Co, Fe) on the bulk structure and relates those structural distortions to the surface bonding environment features as observed in Raman spectroscopy. It is also shown in this section how the surface bonding can be related to the alteration in the electronic structure of sphalerite through correlating the variation of band gap to the nature of the metal impurity-sulphur bond. The chapter also illustrates how the surface charge of sphalerite is altered by the different impurities, while also such variations can manifest to the different response to the Cu-activation and collector adsorption. It also illustrates how the impurities alter the molecular-level character of sphalerite and how such changes will impact its interaction with xanthate. The last point conveyed in this section involves fitting the overall results on a broader scale and assess their implication to real world beneficiation of sphalerite and how to best predict the flotation response of sphalerite with the application of molecular-level investigations.

**Chapter seven:** The final chapter sums up the entire project by providing a summary of the key finding of the thesis. The chapter also provides possible interested future work that will benefit the continued exploitation of the low-grade sulphide ores.

## References

- Aghazadeh, S., Mousavinezhad, S.K., Gharabaghi, M., 2015. Chemical and colloidal aspects of collectorless flotation behavior of sulfide and non-sulfide minerals. [Advances in Colloid and Interface Science](#), Vol. 225, pp 203-217.
- Bicak, O., Ekmekci, Z. 2012. Prediction of flotation behavior of sulphide ores by oxidation index. *Mineral Engineering*, Vol. 36, pp 279-283.
- Boulton, A., Fornasiero, D., Ralston, J., 2005. Effect of iron content in sphalerite on flotation. *Minerals Engineering* 18, pp 1120–1122.
- Chandra, A.P., Gerson, A.R., 2009. A review of the fundamental studies of the copper activation mechanisms for selective flotation of the sulfide minerals, sphalerite and pyrite, *Advances in Colloid and Interface Science*, Vol.149, pp 97-110.

Chen, Y., Chen, J., Guo, J. 2010. A DFT study on the effect of lattice impurities on the electronic structures and floatability of sphalerite. *Mineral Engineering*, Vol. 23, pp 1120-1130.

Chen, Y., Chen, J., Lan, L., Yang, M., 2012. The influence of impurities on the flotation behaviours of synthetic ZnS. *Mineral Engineering*, Vol. 27-28, pp 65-71.

Ejtemaei, M., Nguyen, V.A., 2017. A comparative study of the attachment of air bubbles onto sphalerite and pyrite surfaces activated by copper sulphate. *Mineral Engineering*, Vol. 109, pp 14-20.

Harmer, S.L., Mierczynska-Vasilev, A., Beattie, D.A., Shapter, J.G., 2008. The effect of bulk iron concentration and heterogeneities on the copper activation of sphalerite. *Mineral Engineering*, Vol. 21, pp 1005-1012.

Nefedov, V.I., Salyn, Ya.V., Solozhenkin, P.M., Pulatov, G.Yu., 1980. X-ray photoelectron study of surface compounds formed during flotation of minerals. *Surface and Interface Analysis*, Vol 2, pp 170–172.

Popov, S.R., Vucinic, D.R., 1991. The ethylxanthate adsorption on copper –activated sphalerite under flotation-related conditions in alkaline media. *International Journal of Mineral Processing*, Vol. 30, pp 229-244.

## Chapter two – Relevant literature review

### Introduction

Sphalerite (ZnS) the main economic mineral of zinc metal exhibits multiple flotation responses during beneficiation (Chen et al., 2012). This chapter introduces different concepts that deal with the mineral chemistry (i.e. cation substitution) and flotation recovery of sphalerite. Firstly, this chapter introduces the different massive sulphide ores commonly exploited for their base metal resources (e.g. Zn, Pb, Cu) while also introducing the chemistry and structure of sphalerite. The chapter examines the mineral chemistry of sphalerite, with emphasis on the different cation substitutions that have been reported in literature. A background on the primary method of sphalerite beneficiation is covered in this chapter as a background to the relevant minerals processing technologies. A brief background to flotation, and how it can be optimised for successful recovery of sphalerite is discussed. This includes a brief background on the Cu activation and collector adsorption, the two critical fundamental controls for inducing a hydrophobic character in sphalerite thereby allowing it to float. The last part of this section includes several concepts reported that illustrated different flotation response of natural sphalerite and the associated challenges encountered during the beneficiation process.

### **Massive sulphide deposits and mineralogy- The source of base metal minerals.**

Massive sulphide deposits are the primary source of base metals across the world (Mclung, 2006). These polymetallic deposits can be classed according to their mode of occurrence and tectonic setting. The deposits are broadly classified as Sedimentary exhalative (SEDEX), Broken Hill-Type (BHT), and Volcanic Massive Sulphide (VMS). Sedimentary exhalative (SEDEX) and Broken Hill-type (BHT) deposits are the most important sedimentary hosted base metal deposits due to their superior metal quantities as compared to other deposits and are exploited for their lead and zinc metal



resources (McClung, 2006). The deposits are of economic interest because they represent a major source of both base and precious metals (copper, zinc, lead, silver and gold). The deposits are commonly characterized by coexisting base metals, suggesting co-crystallized assemblages at equilibrium with varied accumulations of primary sulphide minerals (pyrite and pyrrhotite) associated with economic minerals (sphalerite, galena, and chalcopyrite) (George et al., 2016). The deposits are also exploited for their silver, gold, tungsten resources when present at economically viable quantities (McClung, 2006).

The occurrence of SEDEX deposits has received extensive attention over the years with different authors proposing different genetic models to explain the way such deposits occur. Goodfellow et al., (2007) suggested SEDEX deposits are a result of the release of hydrothermal fluids on the seafloor. Conversely, McClung, 2006 and Leach et al., 2005 suggested that the deposits are a result of sub-seafloor replacements with no evidence of exhalative features. Typical examples of SEDEX deposits occur at cordillera, Canada and the Northern Australian Carpentarian Belt (Goodfellow, 2007)

Parr and Plimer, 1993 defined BHT deposits as stratiform base metal orebodies that occurred in close association with either pre-deposition or syn-deposition of sediments. According to McClung, 2006, BHT deposits can be distinguished from SEDEX and VMS through several attributes:

- They occur in Paleo-to-Mesoproterozoic intracontinental rift basins;
- A distinctive skarn resemblance assemblage of Fe-Si-Mn-Ca-rich;
- Hosted in a highly oxidized siliciclastic/calc-silicate/carbonate rocks;
- Base metal zonation (Cu→Zn/Pb→Pb/Zn, Ag→ Mn,Fe);
- Basement occurrence of volcanic rocks;

### **Crystal structure, chemistry and electronic structure of sphalerite**

Sphalerite is the cubic polymorph of the zinc blende (F4 (-3) m, Z=4) structural group and has a recorded unit cell constant of 5.406 Å (Harmer et al., 2008, Skinner, 1961). The mineral consists of a molecular cluster of both zinc and sulphur closely stacked together in a tetrahedral coordination, with the zinc atoms occupying the tetrahedral sites (figure 2.1) (Harmer et al., 2008, Chen et al., 2010). In nature, the chemistry of sphalerite varies due to its ability to incorporate different transition-metal impurities (e.g. Co, Fe, Ge, Mn, Cd, Cu, In etc.) which substitute for the Zn cation in lattices sites (Cook et al., 2009). Different trace element contents have been recorded within sphalerite, notably the iron content reaching up to 26 wt. % (Harmer et al., 2008, Cook et al., 2009). Sphalerite colour is dependent on the type of trace element incorporated into the structure, pure ZnS is clear while a Fe-bearing sphalerite is black (Harmer et al., 2008).

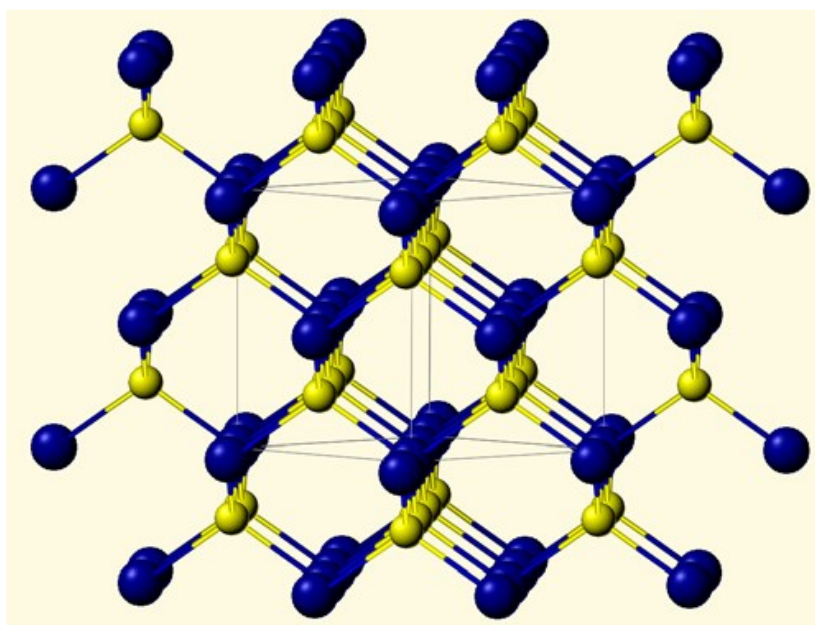


**Figure 2.5:** Sphalerite crystal structure: small spheres represent Zn and the large S (Harmer et al., 2008).

The major mineralogical characteristic of sphalerite is its ability to incorporate a broad range of transition-metal impurities (Co, Cd, Mn, Fe etc.) in varied concentrations (Ye et al., 1999; Gigowski et al., 1991). The occurrence of the impurities within sphalerite lattice is known to be in trace amounts, although in some rare cases up to 26 wt. % of Fe has been recorded (Harmer et al., 2008, Cook et al., 2009). According to Chen et al., (2012) the incorporation of these transition metal impurities relies on the temperature and chemistry of crystallization environment thus giving raise to the

different mineral chemistry and colour of sphalerite at different tectonic settings. Ye and Liu, (1999) Axelsson and Rodushkin, (2001), Cook et al. (2009) reported varied concentration of transition-metal impurities (Co, Cd, Ag, Ga, Bi, As, Cu, Fe, Mn, Mo, Ni, Tl, Pb, Sb, Se, Sn etc.) occurring within the lattice structure of sphalerite (Figure 2.2). The studies illustrated a large presence of trace elements at varying concentrations within sphalerite lattice structure while also confirming that some trace elements (e.g. Co, Cd, Mn) are present in solid solution.

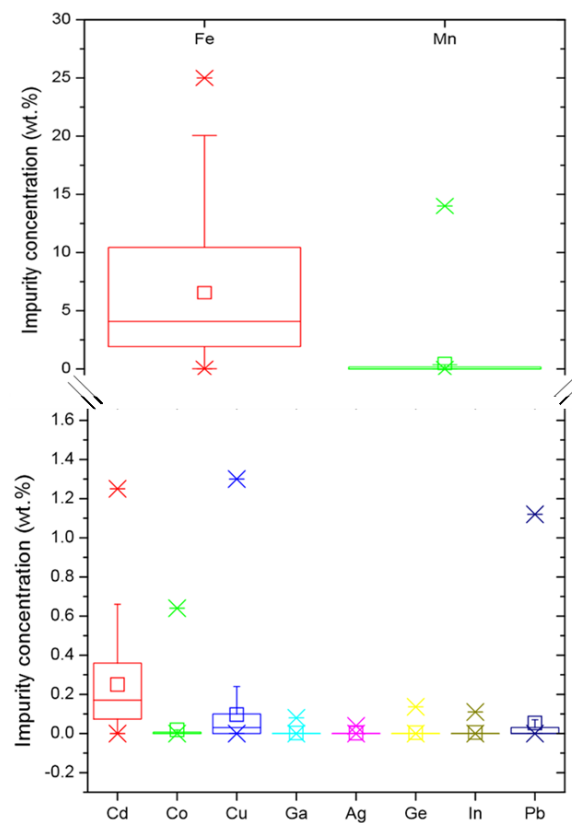


**Figure 2.2:** Summary of the metal impurity contents obtained from different studies of sphalerite at varied ore deposits in the world. The full data set is shown in appendix II.

The isoelectric cation substitution associated with sphalerite is greatly depended on the availability of major and minor trace elements with similar ionic size and charge as  $Zn^{2+}$  and its affinity for tetrahedral coordination (Cook et al., 2009). Several studies have illustrated the concentration of the transition-metal impurities (see Appendix III) within sphalerite at different ore bodies across the world. For example, Tong et al.

(2007) reported that sphalerite in Dachang, Guangxi, China was rich in iron content (up to 8-12 wt.%). Ye et al. (1999) found that the sphalerite in the Niujaotang deposits, Guizhou province, China incorporated high Cd impurities varying from 0.83% to 1.97%, in Long Lake, Canada, Beaudoin, 2000 reported that the sphalerite was enriched in Cu and Ag. McClung and Viljoen reported that the sphalerite was enriched with iron and manganese contents reaching up to 25 mol.% and 14 mol.% respectively at the Gamsberg orebody, Northern Cape Province, South Africa.

Studies of Lusk and Calder, (2004), Harmer et al., (2008), Cook et al., (2009), Chen et al., (2010), Osadchii and Gorbaty (2010), Wright and Gale, (2010) and Chen et al., (2012) interrogated presence of iron in lattice sites of sphalerite with major focus on understanding changes in surface chemistry of sphalerite because of iron presence. The work of Wright and Gate (2010) on the distribution of iron in sphalerite found that Fe is incorporated into sphalerite more easily when it is Zn deficient, i.e at high sulphur fugacity.

The work of McClung and Viljoen, (2011) and Schouwstra et al. (2010) interrogated the incorporation of manganese in simple cationic substitution ( $Zn^{2+} \rightarrow Mn^{2+}$ ) (Cook et al., 2009) within sphalerite at Gamsberg orebody, Northern Cape, South Africa. McClung and Viljoen, (2011) reported that the concentration of manganese at Gamsberg zinc ore reaches up to 14 mol %. Di Benedetto, (2005) states that the presence of Mn within the sphalerite structure at several ore bodies like the Gamsberg ore, South Africa and Santo Toribio, Peru is attributed to the presence of albanadite as the main source of the  $Mn^{2+}$ .

Cadmium like other associated transition-metal impurities occurs in trace amounts as reported by several studies (McClung and Viljoen, 2011, Buzatu et al., 2013). Chen et al., (2010) attributed the presence of Cd in the lattice of sphalerite to the broad range solid solution at high temperature and similar ionic size of  $Zn^{2+}$  and  $Cd^{2+}$ . The incorporation of Cd into the sphalerite mineral at Niujaotang deposits, Guizhou province, China was found to be between 0.383 wt.% and 1.97 wt.% (Ye and Liu, 1999). Karbish, (2007) reported a sphalerite from Abu Gurdi massive sulphides in South Eastern Desert, Egypt to have 7.25 wt.% Cd concentration. Cook et al., (2009) stated

that the concentration of cadmium in sphalerite ores could vary between 0.1-5 wt.% with possibilities of higher content more in some Mississippi Valley type deposits.

Cobalt ( $\text{Co}^{2+}$ ) exhibits an ionic radius closer to that of  $\text{Fe}^{2+}$  (see table 2.1) and it has been shown to substitute  $\text{Zn}^{2+}$  in sphalerite lattice sites depending on the crystallizing environment (McClung and Viljoen, 2011, George et al., 2016). The existence of a CoS-ZnS solid solution was interrogated by Becker and Luts, (1978) stating an intermediate composition of  $(\text{Zn},\text{Co})\text{S}$  with 40% CoS. McClung and Viljoen, (2011) reported a 0.64 mol.% of cobalt content at Gamsberg orebody, South Africa, while Cook et al., 2009 reported a 0.23 wt.% of cobalt in sphalerite at a skarn deposit in Paulus. The economic recovery of zinc from a substituted sphalerite through conventional flotation separation is negatively affected by the large presence of different trace elements in the processing stream.

**Table 2.2:** ionic radius of common transition-metals found in tetrahedral coordination of sphalerite (Shannon, 1976)

Metal Impurity	Ionic radius (pm)
Co	88.5
Fe	92.0
Cd	109.0
Zn	88.0

Sphalerite, cubic polymorph of the Zinc blend mineral group has received extensive research interest over the years due to its semi-conducting characteristics which include its diamagnetic character (Vaughan and Tossell, 1980). Pure sphalerite is known to exhibit a high resistivity which is as a function of a wide band gap exhibited (Vaughan and Tossell, 1980, Li et al., 2008). Over the years there has been several reported experimental and calculated band gap energies of a pure sphalerite, with a consensus amongst the several reports that a pure sphalerite has a wide band gap between 3.6 – 3.9 eV (Vaughan and Craig, 1978, Vaughan and Tossell, 1980, Lawniczak-Jablonska et al., 1999, Tsuji et al., 2005, Li et al., 2008). The incorporation of transition-metal impurities in sphalerite tetrahedral coordination induces a change in the conduction energies (Vaughan and Craig, 1978). Such variation results from the

transition of the nonbonding sulphur p electrons into the d orbitals of the metal impurity (Lawniczak-Jablonska et al., 1999). Tsuji et al. (2005) and Li et al. (2008) suggested that conduction band of sphalerite is made up of Zn 4s4p orbitals and the incorporation of the metal impurities such as Fe increases the valence band energies. Such variations led to sphalerite losing its diamagnetic character to paramagnetic and at elevated metal impurities such changes in the electronic structure leads to ferromagnetic coupling (Keys et al., 1968, Vaughan and Craig, 1978, Lawniczak-Jablonska et al., 1999).

### **Metallurgical treatment of sphalerite**

The treatment of low-grade complex sulphide ores for their zinc resources has been subject to intense research for several decades to understand the best possible method to aid maximum recovery of zinc. Abkhoshk et al., (2014) states that the treatment of zinc ores can be classified into two categories: Pyrometallurgical and physical separation (flotation) methods. Pyrometallurgical treatment of sulphide ores involves the recovery of target metal without the use of enriching chemical species at elevated temperature (Abkhoshk et al., 2014). The production of zinc metal through pyrometallurgical methods occurs at elevated temperatures greater than the 907°C boiling point of zinc to permit the recovery of the metal in liquid phase (Gordon et al., 2003, Abkhoshk et al., 2014). Gordon et al., (2003) stated that the four common pyrometallurgical techniques used in zinc production includes; imperial smelting process (ISP), horizontal retort, electric furnace, and vertical retort. However, pyrometallurgical methods are characterized by some common shortcomings; this includes the high costs due to the high consumption of energy and environmental hazards because of large emission of harmful gases (e.g. sulphur dioxide) (Harmer et al., 2007, Abkhoshk et al., 2014). It is due to the elevated running costs of pyrometallurgy that physical separation methods like flotation are regarded as the primary extraction methods for low-grade complex sulphide ores (Harmer et al., 2008). Flotation is regarded as the primary methods for the recovery of base metals from a low-grade sulphide ore using multiple chemicals and reagents (Abkhoshk et al., 2014).

In comparison to other extraction methods, flotation provides cheaper production costs, less environmental issues and allows direct recovery of metals in their purest form. Like any process, flotation separation presents its own challenges when dealing with low-grade sulphide deposits. The major challenge to flotation is its inability to successfully treat ores with intricate mineral chemistry and target minerals with close association with various minerals and gangue minerals with similar surface character (McClung and Viljoen, 2011). Flotation has acclaimed priority for processing of sulphide ores with varying proportion of mineral substitution due to its ability to treat variable minerals constituents contained in complex sulphide ores which were earlier considered to be uneconomical (Chandra and Gerson, 2009).

Flotation, a process that utilizes the surface properties of individual minerals to aid separation and recovery of metals of interest (Chandra and Gerson, 2009). The difference in the physio-chemical surface properties of different minerals permit the separation of the target metal (Cilek, 2009). The use of flotation in sulphide ore processing has become increasingly critical to global processing and recovery of base metal contents, dating back to the start of the 20th century (Chandra and Gerson, 2009). Bicak and Ekmekci, (2012) suggested that the chemical variation (i.e. mineralogical or elemental) associated with complex sulphide ores significantly affect the flotation performance. This is because the flotation response of complex sulphide ores is highly sensitive to the chemical and mineralogical phases involved, i.e. ores with a greater level of mineral variation or cation substitution are increasingly challenging to beneficiate (Bicak and Ekmekci, 2012). The increased transition-metal impurities content and mineral associates in processing stream are given greater precautions because of the negative implication which renders the concentrate uneconomical.

## **Sphalerite flotation**

### **Sphalerite activation**



The recovery of base metal sulphide minerals is typically achieved using flotation systems which are considered a key step towards achieving selective separation (Chandra and Gerson, 2009). In industrial processing plants, this involves initial depressing of sphalerite in both copper and lead circuits operated at mildly alkaline to neutral pH before the actual flotation recovery of sphalerite at alkaline pH 9 to allow separation with pyrite (Albrecht et al., 2016). The flotation system aims to achieve maximum recovery of target metals from weakly polar mineral species such as sphalerite (Chandra and Gerson, 2009). Such mineral species are characterized by mildly hydrophobic surfaces; thus, their flotation character is induced using organic chemical species called collectors (Chandra and Gerson, 2009).

Sphalerite is commonly known to react poorly with short-chained thiol collectors such as xanthate (Chandra and Gerson, 2009, Liu et al., 2014, Albrecht et al., 2016). This is because a non-activated sphalerite exhibits a wide band gap thus resulting in a poor electrochemical interaction between sphalerite surfaces and the collector due to the slow electron transfer (Ejtemaei and Nguyen, 2017). Several studies have suggested that this problem is best dealt with by using “activators” in the form of metal species abstracted from a nitrate or sulphate solution added to the processing stream prior to collector adsorption (Laskowski et al., 1997, Lascelles et al., 2001, Albrecht et al., 2016). Copper ions are commonly used activators during sphalerite flotation, however several studies have also illustrated the activating capabilities of other transition metals such as ferrous ions (Zhang et al., 1992), lead ions (Vucinic et al., 2006) and cadmium ions (Ralston and Healy, 1980).

The actual activation mechanism of sphalerite by Cu ions has been extensively interrogated over the last decade by different researchers (Lascelles et al., 2001, Chandra and Gerson, 2009, Albrecht et al., 2016). Lascelles et al. (2001) proposed that the activation of sphalerite in both acidic and alkaline pH is characterized by an initial uptake of Cu (II) resulting in the release of Zn (II) in a 1:1 ratio. In acidic medium, copper (II) ions ( $\text{Cu}^{2+}$ ) are the most stable species that are adsorbed to the mineral surface while at alkaline pH the surface is covered by copper hydroxide ( $\text{Cu}(\text{OH})_2$ ) (Chandra and Gerson, 2009). A reaction mechanism for the activation of sphalerite with Cu ions in acidic medium proposed by Gerson et al. (1999) can be represented by equation (1) while Popov and Vucinic, (1990), Lascelles et al., (2001) and Albrecht



et al., (2016) proposed equation (2) as a representation of the initial reaction in alkaline media.

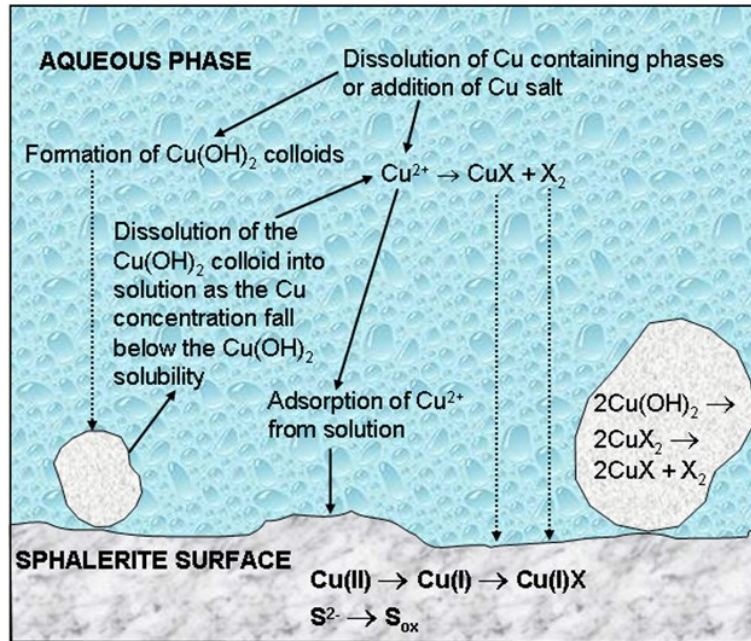
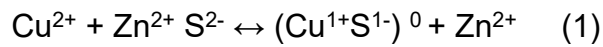
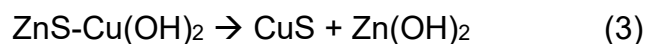


**Figure 2.3:** schematic representation of copper activation mechanism of sphalerite in alkaline conditions (from Chandra and Gerson, 2009).

Conventional flotation of sphalerite occurs at alkaline pH to aid the separation from associated metal sulphide minerals, predominately pyrite, thus the common activation mechanism in processing plants can be represented by equation 2. Prestige et al., (1997) and Gerson et al., (1999) used convention X-ray Photoelectron Spectroscopy (XPS) and Secondary ion mass spectrometry (SIMS) techniques respectively to study the surface species during sphalerite activation at pH 9, both confirming the formation of colloidal  $\text{Cu}(\text{OH})_2$  on the mineral surface (figure 2.3). The resultant zinc hydroxide formed from equation 2 undergoes dissolution which gives the mineral surface a different hydrophobic character. This can be represented by:



The resultant cupric sulphide (Cu(II)S) from equation 3 is subjected to redox disproportionation to form a more stable Cu (I) sulphide and elemental sulphur (equation 4) (Lascelles et al., 2001, Chandra and Gerson, 2009, Albrecht et al., 2016). The stable Cu (I) S will then react with the xanthate ions ( $X^-$ ) during the addition of collectors (equation 5) (Lascelles et al., 2001). Albrecht et al., (2016) stated that the electrostatics between the negatively charged sphalerite surface and the positively charged Cu ions is the fundamental control for the adsorption of Cu on mineral surface.

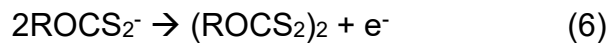


### **Sphalerite collector adsorption**

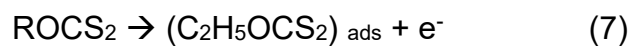
Mikhlin et al. (2016) stated that flotation recovery of sulphide minerals utilizes their surface characteristics to aid selective separation of the target mineral from the associated minerals due to the induced hydrophobic character by the adsorbed collectors such as thiols (xanthates) and dithiophosphates. The improved understanding of the flotation fundamentals in recent years has been attributed to the large research on Cu-activation and collector adsorption (Nedjar and Barkat, 2013). It is widely known that achieving maximum hydrophobicity/floatability of weakly polar sulphide minerals such as sphalerite requires adsorption of flotation collectors such as xanthates on the surface (Smit and Gnoinski, 2000). Flotation collectors used during the treatment of sulphide minerals are usually an organic species characterised by an ionic (i.e. hydrophilic) end and a non-ionic end (hydrophobic) (Smit and Gnoinski, 2000). The ionic end attaches on the mineral surfaces, while the non-ionic end creates hydrophobicity on the mineral surface.

Xanthate ions (O-alkyldithiocarbonate,  $\text{ROCS}_2^-$ ) collectors are frequently used in sphalerite flotation processes in use at different orebodies (Harmer et al., 2008, Wang et al., 2015, Smit and Gnoinski, 2000). This is because xanthate collectors induce the floatability of the target mineral by rendering the surface hydrophobic, thus facilitating the successful attachments of mineral particles on air bubbles during flotation (Wang et al., 2015). The semi-conducting properties of sphalerite reflect that the reaction

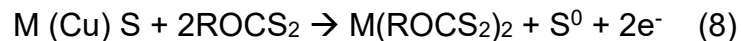
responsible to create a hydrophobic surface is electrochemical (Smit and Gnoinski, 2000). The reaction involves the oxidation of xanthate ions to form a more hydrophobic dixanthogen ion on the mineral surface (Smit and Gnoinski, 2000). According to Wood et al. (1990) hydrophobicity is conferred to a mineral surface in three steps. The first reaction involves the anodic oxidation to form dixanthogen ions represented by:



The second step involves distinguishing between dixanthogen ions produced from the anodic reaction and xanthate ions held electrostatically at lower potential.



The final step is the chemisorption of the oxidized xanthate ions on the metal sulphide:



The reason for Cu-activation is because the oxidation of xanthate to dixanthogen is more favourable on a copper like surface as compared to on an un-activated sphalerite surface (Chandra and Gerson, 2009).

### **The effect of transition-metal impurities on the metallurgical response of sphalerite**

It is well established that sphalerite exhibits multiple flotation responses attributed to the presence of multiple minor and trace transition-metal impurities within lattice structure. Several studies have illustrated multiple flotation responses of both natural and synthetic impurity bearing sphalerite samples, particularly the influence of iron concentration on the flotation response. Chen et al., 2012 stated that the collector adsorption and the consequent flotation response of sphalerite is highly dependent on the lattice defects induced by the transition-metal impurities. Popov and Vucinic, (1990), Harmer et al, (2008), Zhang et al., (1992), Boulton et al., (2005), Albretcht et al., (2016) studied the copper activation of impurity bearing sphalerite samples, with contrasting results reported. These studies postulated that heterogeneous mineral chemistry of sphalerite contribute significantly to the Cu activation and the consequent collector adsorption, thus resulting in the varied flotation responses.

The way sphalerite interacts with the flotation reagents (i.e. activators and collectors) is significantly influenced by its electronic properties (band gap, fermi level and ratio of free electron charge carrier concentration) and the consequent semi-conducting properties (Chen et al., 2010). Cook et al., (2011) and Chen et al., (2010) report that sphalerite's semi-conducting properties change from p-type to n-type due to the presence of transition-metal impurities (e.g. Fe, Co, Mn, In etc.) except for metals like Cd and Hg. Practically, depending on the chemical nature and concentration of the lattice impurities the extent of Cu-activated induced flotation of an impurity bearing sphalerite is lowered, thus resulting in lower flotation recovery (Boulton et al., 2005).

Boulton et al., (2005) studied the influence of iron concentration within the sphalerite lattice on the flotation response of the latter under alkaline pH (the operational pH for sphalerite flotation). The presence of iron within the sphalerite lattice negatively affect the flotation recovery due to the low Cu ion coverage on sphalerite surface, reducing the xanthate adsorption in the form of Cu (I) xanthate (Boulton et al., 2005). Similarly, Chen et al., (2012) reported the influence of Fe on the flotation response of synthetic sphalerite under flotation related conditions, reporting similar observations as stated for increasing iron concentration. Conversely, Harmer et al., (2008) and Nefedov et al., (1980) reported different flotation behaviour of sphalerite with increasing iron concentration, recording an increased copper activation with increased iron concentration. Harmer et al., (2008) attributed the increased Cu activation at high iron concentration to the number of cleavage steps and precipitates size. Gigowski et al., (1991) studied the effect of Fe-lattice ions on the flotation properties of sphalerite, stating that under flotation conditions sphalerite exhibits different behaviour because of iron concentration. Chen et al., 2012 illustrated the effect of both Cd and Cu ions on the flotation recovery of sphalerite. Compared to Fe-bearing sphalerite, both Cu and Cd improved the flotation recovery of sphalerite because of an improved xanthate adsorption aided by the two impurities.

## Reference

- Abkhoshk, E., Jorjani, E., Al-Harashsheh, M.S., Rashchi, F., Naazeri, M. 2014. Review of the hydrometallurgical processing of non-sulfide zinc ores. *Hydrometallurgy*, Vol. 149, pp 153-167.
- Albrecht, T.W.J., Addai-Mensah, J., Fornasiero, D., 2016. Critical copper concentration in sphalerite flotation: Effect of temperature and collector. *International Journal of Mineral Processing*, Vol. 146, pp 15-22.
- Axelsson, M.D., Rodushkin, I. 2001. Determination of major and trace elements in sphalerite using laser ablation double focusing sector field -ICP-MS. *Journal of Geochemical Exploration*, Vol. 72, pp 81-89.
- Beaudoin, G., 2000. Acicular sphalerite enriched in Ag, Sb and Cu embedded within colorbanded sphalerite from the Kokanee Range British Columbia, Canada. *Canadian Mineralogist*, Vol. 38, pp 1387–1389.
- Becker, W., Lutz, H., 1978. Phase studies in the systems CoS–MnS, CoS–ZnS, and CoS–CdS. *Material Research Bulletin*, Vol. 13, pp 907–911.
- Bicak, O., Ekmekci, Z. 2012. Prediction of flotation behavior of sulphide ores by oxidation index. *Mineral Engineering*, Vol. 38, pp 279-283.
- Boulton, A., Fornasiero, D., Ralston, J., 2005. Effect of iron content in sphalerite on flotation. *Minerals Engineering* 18, pp 1120–1122.
- Buzatu, A., Buzgar, N., Damian, G., Vasilache, V., and Apopei, A.I. (2013). The determination of the Fe content in natural sphalerites by means of Raman spectroscopy. *Vibrational Spectroscopy*, Vol. 68, pp 220-224.
- Chen, Y., Chen, J., Guo, J. 2010. A DFT study on the effect of lattice impurities on the electronic structures and floatability of sphalerite. *Mineral Engineering*, Vol. 23, pp 1120-1130.
- Cilek, E.C. 2009. The effect of hydrodynamic conditions on true flotation and entrainment in flotation of a complex sulphide ore. *International Journal of Mineral Processing*, Vol. 90, pp 35-44.

- Cook, N.J., Ciobanu, C.L., Pring, A., Skinner, W., Shimizu, M., Danyushevsky, L., Saini-Eidukat, B., Melcher, F. 2009. Trace and minor elements in sphalerite: A LA-ICPMS study. *Geochimica et Cosmochimica Acta*, Vol. 73, pp 4761-4791.
- Di Benedetto, R., Bernardini, G.P., Costagliola, P., Plant, D., Vaughan, D.J. 2005. Compositional zoning in sphalerite crystals. *American Mineralogist*. Vol. 90, pp 8-9.
- Harmer, S.L., Mierczynska-Vasilev, A., Beattie, D.A., Shapter, J.G., 2008. The effect of bulk iron concentration and heterogeneities on the copper activation of sphalerite. *Mineral Engineering*, Vol. 21, pp 1005-1012.
- George, L.L., Cook, N.J., Ciobanu, C.L. 2016. Partitioning of trace elements in co-crystallized sphalerite–galena– chalcopyrite hydrothermal ores. *Ore Geology Reviews*, Vol. 77, pp 97-116.
- Gerson, A.R., Lange, A.G., Prince, K.P., Smart, R.St.C. 1999. The mechanism of copper activation of sphalerite. *Applied Surface Science*, Vol. 137, pp 207-223.
- Gigowski, B., Vogg, A., Wierer, K., Dobias, B. 1991. Effect of Fe-lattice ions on adsorption, electrokinetic, calorimetric and flotation properties of sphalerite. *International Journal of Mineral Processing*, Vol. 33, pp 103-120.
- Goodfellow, W.D., Lydon, J.W. 2007. A synthesis of major deposit-types, district metallogeny, the evolution of geological provinces, and exploration methods: Geological Association of Canada, pp 163–184.
- Gordon, R.B., Graedel, T.E., Bertram, M., Fuse, K., Lifset, R., Rechberger, H., Spataro, S. 2003. The characterization of technological zinc cycles. *Resource Conservation Recycle*, Vol. 39, pp 107-135.
- Keys, J.D., Horwood, J.L., Bernsra, T.M., Cabrt, L.J., Henrus, D.C. 1968. Iron-iron interaction in iron-containing zinc sulphide. *Canadian Mineralogist*, Vol.9, pp 453-467.
- Kharbish, S. (2007). A Raman spectroscopic investigation of Fe-rich sphalerite: effect of Fe-substitution. *Physics and Chemistry of Minerals*, Vol. 34, pp 551–558.

Lawniczak-Jablonska, K., Kachniarz, J., Spolnik, Z.M. 1999. X-ray emission valence band spectra from  $Zn_{1-x}Fe_xS$  excited by electrons. *Journal of Alloys and Compounds*, Vol. 286, pp 71-75.

Li, Y., Lu, A., Wang, C., and Wu, X. 2008. Characterization of natural sphalerite as a novel visible light- driven photocatalyst. *Solar Energy Materials & Solar Cells*, Vol. 92, pp 953-959.

McClung, C.R., 2006. Basin Analysis of the Bushmanland Group, Namaqualand Metamorphic Complex of the Northern Cape Province, South Africa. Unpublished Doctoral Thesis, University of Johannesburg, pp 307.

McClung, C.R. and Viljoen, F., 2011. A detailed mineralogical assessment of sphalerites from the Gamsberg zinc deposit, South Africa: The manganese conundrum. *Minerals Engineering*, Vol.24, pp 930-938.

Mikhlin, Y., Karacharov, A., Tomashevich, Y., Shchukarev, A. 2016. Interaction of sphalerite with potassium n-butyl xanthate and copper sulfate solutions studied by XPS of frozen samples and zeta potential measurement. *Vacuum*, Vol. 125, pp 98-105.

Lascelles, D., Sui, C.C., Finch, J.A., Butler, I.S. 2001. Copper ion mobility in sphalerite activation. *Colloids and Surfaces*, Vol. 186, pp 163-172.

Laskowski, J.S., Liu, Q., Zhan, Y. 1997. Sphalerite activation: flotation and electrokinetic studies. *Minerals Engineering*, Vol. 10, pp 787-802.

Leach, D.L., Sangster, D.F., Kelly, K.D. 2005. Sediment-hosted lead-zinc deposit: A global perspective. *Economic Geology*, Vol.100, pp 307-324.

Lusk, J., Calder, B.O.E. 2004. The composition of sphalerite and associated sulfides in reactions of the Cu–Fe–Zn–S, Fe–Zn–S and Cu–Fe–S systems at 1 bar and temperatures between 250 and 535 °C. *Chemical Geology*, Vol. 203, pp 319-345.

Parr, J.M., Plimer, I.R. 1993. Models for Broken Hill-type lead-zinc-silver deposits. *Geological Association of Canada Special Paper*. Vol. 40, pp 253-288.

Prestige, C.A., Skinner, W.M., Ralston, J. and Smart, R.S.C. 1997. Copper (II) activation and cyanide deactivation of zinc sulphide under mildly alkaline conditions.



Applied Surface Science, Vol. 108, pp 333-344.

Ralston, J., Healy, T.W. 1980. Activation of zinc sulphide with  $\text{Cu}^{2+}$ ,  $\text{Cd}^{2+}$  and  $\text{Pb}^{2+}$ . Part III. International Journal Mineral Processing, Vol. 7, pp 279.

Schouwstra, R.P., de Vaux, D., Hey, P., Bramedeo, S. 2010. Understanding Gamsberg – A geometallurgical study of a large stratiform zinc deposit. Mineral Engineering, Vol. 23, pp 960-967.

Shannon, R. D. 1976. Revised effective ionic radii and systematic studies of interatomic distances in halides and chalcogenides. Acta Crystallography, Vol. 32, pp 751–767.

Skinner, B.J. 1961. Unit-cell edges of natural and synthetic sphalerites. American Mineralogist, Vol 46, pp 1399–1411.

Smit, J.T., Gnoinski, J., 2000. Electrochemistry: Contaminant Ions and Sulphide Mineral Interactions. Unpublished.

Tong, X., Song, S.X., He, J., Rao, F., Lopez-Valdivieso, A., 2007. Activation of high-iron

marmatite in froth flotation by ammoniacal copper(II) solution. Minerals Engineering, Vol. 20, pp 259–263.

Tsuji, I., Kato, H., Kudo, A. 2005. Visible-light-induced  $\text{H}_2$  evolution from an aqueous solution containing sulfide and sulfite over a  $\text{ZnS-CuInS}_2\text{-AgInS}_2$  solid solution Photocatalyst. Angewandte Chemie International, Edition. 44, pp 3565.

Vucinic, D.R., Lazic, P.M., Rosic, A.A. 2006. Ethyl xanthate adsorption and adsorption kinetics on lead-modified galena and sphalerite under flotation conditions. Colloids and Surfaces, Vol. 279, pp 96-104.

Vaughan, D.J., Craig, J.R. 1978. Mineral Chemistry of Metal Sulphides. Cambridge University Press



- Vaughan, D.J., Tossell J.A. 1980. The chemical bond and the properties of sulphide minerals: I. Zn, Fe and Cu in tetrahedral and triangular coordinations with sulfur. *Canadian Mineralogist*, Vol. 18, pp 157-163
- Wang, C., Wang, H., Fu, J., Liu, Y. 2015. Flotation separation of waste plastic for recycling-A review. *Waste Management*, Vol. 41, pp 28-38.
- Wright, K., Gale, J.D. 2010. A first principles study of the distribution of iron in sphalerite. *Geochimica et Cosmochimica Acta*. Vol. 74, pp 10-16.
- Woods, R., Young, C.A., Yoon, R.H. 1990. Ethyl xanthate chemisorption isotherms and Eh -pH diagrams for the copper/water/xanthate and chalcocite/water/xanthate systems. *International Journal of Mineral Processing*, Vol. 30, pp 17-33.
- Ye, L., Liu, T.G., 1999. Source sphalerite chemistry, niujiaotang cd-rich zinc deposit, guizhou, southwest China. *Chinese Journal of Geochemistry*, Vol. 18, pp 62–68.
- Zhang, Q., Rao, S.R., Finch, J.A. 1992. Flotation of sphalerite in the presence of iron ions. *Colloids and Surfaces*, Vol. 66, pp 81-89.

## Chapter three – Experimental sphalerite synthesis

The current chapter details the method used to aid the successful completion of the study. The large portion of the chapter provides a background on different experimental methods previously employed for sphalerite synthesis in the literature. This section also further provides comparative illustration of the major reasons why dry experimental technique was the preferred method of synthesis. A breakdown on key experimental considerations that permit a successful synthesis of sphalerite using dry synthesis are included, while the section is rounded off by providing a methodological procedure used for sphalerite synthesis followed in this study. The sets of analytical techniques applied throughout the study have been reported in both chapter 4 and 5. Table 3.1 provides details on where each of the different analytical methods used in this study are situated within the thesis.

**Table 3.1:** Summary of the locations of the different analytical methods used for this study.

Chapter	SEM	XRD	Raman	UV-vis	Zeta potential
Chapter 4	✓	✓	✓	✓	X
Chapter 5	✓	✓	X	X	✓

### Evaluation of experimental methods used for sphalerite synthesis

In recent years scientists have used synthetic minerals as a proxy to provide detailed interrogation on mineral systems (Skinner, 1961, Osadchii and Gorbaty, 2010 and Chen et al., 2012). One of the major advantages of employing synthetic material to any research scope is the ability to directly control the stoichiometric composition and size of the target synthetic mineral. This stands in contrast to natural sphalerite which has variable grain size, heterogeneous mineral chemistry, and is commonly associated with complex sulphide mineral parageneses. The use of such synthetic materials in geology and processing technologies has significantly contributed to the recent advancement in understanding a variety of minerals, largely through thermodynamic,

phase relations and solid solution studies. Kullerud, (1971) stated that the scientific advancement in natural material sciences research is attributed to the ability to experimentally produce synthetic materials that gives a good representation of the natural materials.

Experimental synthesis of sphalerite involves a carefully measured mass of the reacting material in an aqueous medium, except for dry recrystallization method, which involves synthesis of materials in the absence of an aqueous medium (Kullerud, 1971). The success of experimental synthesis is largely dependent on the purity of the starting material because the integrity of the final product is controlled by the purity and stoichiometric composition of the starting material (Kullerud, 1971, Kojima and Sugaki, 1984, Pring et al., 2008,). The success of experimental syntheses has paved a way for studies on complex sulphide minerals with a variety of substitution. Today, scientists can study and explain the effects of different cationic substitution on a wide range of sulphide minerals by using synthetic sulphide minerals. Experimental results obtained using synthetic minerals have been used to provide insights into the processing behaviours of natural sulphide minerals containing different proportions of trace elements (Skinner and Barton, 1960, Osadichii and Garborty, 2010, and Chen et al., 2012). For this study, four common experimental methods for the synthesis of sulphide minerals are compared to select the best method with reliable output. The methods evaluated in this critical comparison are; Chemical Vapor Transport, Dry Recrystallization Method, Co-Precipitation, and Hydrothermal Method.

### **Chemical Vapour Transport (CVT)**

This is an experimental technique widely used to promote chemical growth of high-quality single crystals in a gaseous media (Schmidt et al., 2013) depending on the crystalline nature of the reacting species and the presence of a transporting chemical species (Zavrazhnov et al., 2004). The CVT method utilizes high purity starting materials homogenized with a transporting chemical species (commonly bromine or chlorine) inside a sealed reacting tube which is kept at a temperature gradient (fig.3.1) (Chareev et al., 2017). Schmidt et al. (2013) stated that one characteristic feature of CVT is that the dissolution of a solid material in gaseous media is facilitated by a

transporting chemical species. In addition, Jiao et al., (2012) reports that the formation of the volatile reaction derivatives at different temperatures was dependent on the conversion of the non-volatile products permitted by the chemical vapour transport agent employed. Crystal growth using CVT thus relies on a successful selection of a vapour transport agent, however additional controlled parameters includes the temperature at the reaction zone and growth zone (Figure 3.1) and the molar ratios between the reacting species and the transport agent (Jiao et al., 2012).

The use of chemical vapour transport as a direct growth of pure metal sulphide crystals has been shown by several authors (Fiechter et al., 1986, Lepetit et al., 2003, Chareev et al., 2017). The use of this method has allowed direct synthesis of binary sulphide mineral crystals whose final composition can be controlled. The method was discussed thoroughly by Schmidt et al. (2013). Practically, the final composition of the mineral is controlled by the vapour pressure generated by the composition of the reactants, which in turn is a function of temperature (Zavrazhnov et al., 2004). Nitsche et al., 1966 proposed that the rate of chemical transport during crystal growth can be expressed mathematically as:

$$M = L dp (T', T'', dG, C_1) \quad [1]$$

Where both  $T'$  and  $T''$  represent two sites of different temperatures, one hot site and the other a cold site respectively. The difference in partial pressure at different temperatures  $T'$  and  $T''$  of the reaction is represented by  $dp$ , while the transporting agent concentration is denoted by  $C_1$ . The conductance of the overall system is represented by  $L$ , which depend on the geometry of the reacting tubes and the overall reaction involved in the vapour transport.  $dG$  represents the change in the Gibb's free energy during the reaction. Nitsche et al., (1967) proposed that crystal growth using chemical vapour transport can follow in three possible mechanism. First possible mechanism is the one where the transport mechanism is permitted by the low pressure and small diameter of the reacting tube, secondly, the reaction occurring at elevated pressure and bigger tubes depending on the thermal gradient. The final mechanism that can be used involves the formation of reaction products from equal amounts of the reacting species and the transporting agent. This depends on an equal distribution of the vapour phase to avoid the creation of a pressure gradient within the reaction tubes.

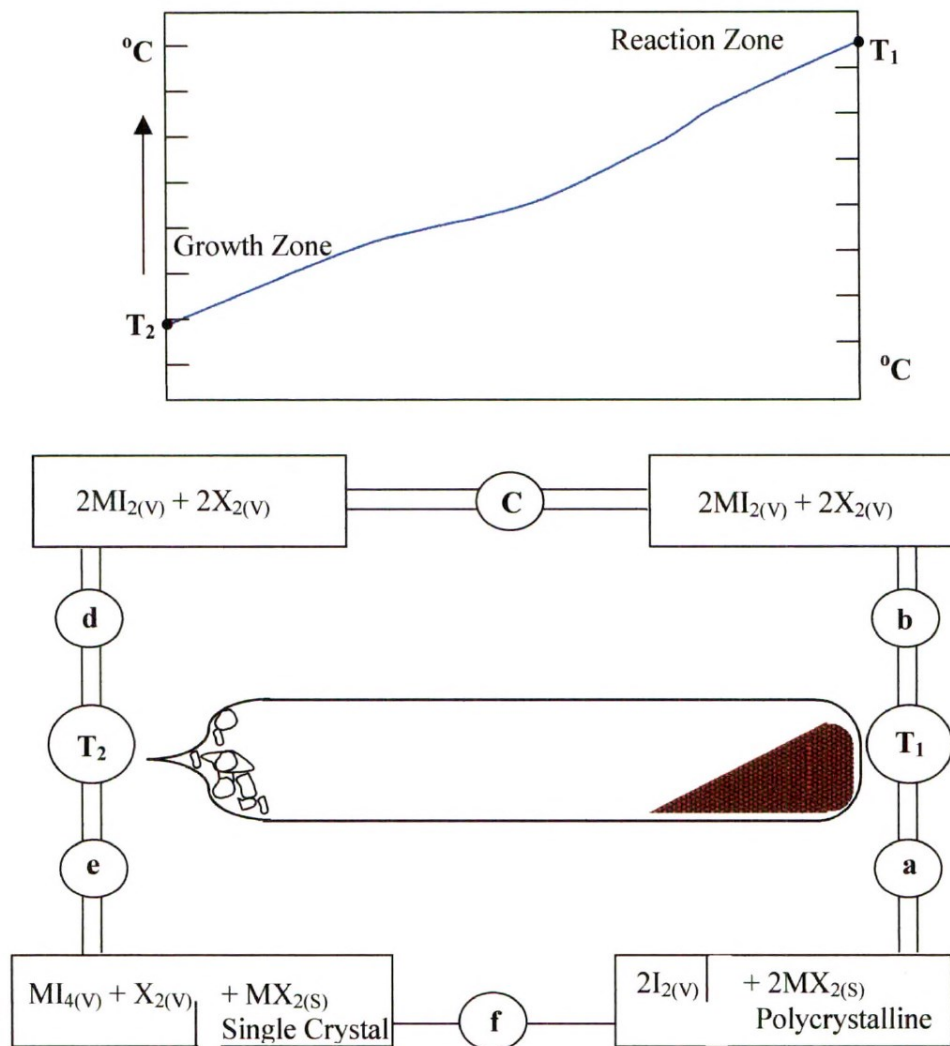


**Figure 3.1:** Schematic representation of a Chemical Vapor Transport crystal growth experiment under controlled temperature gradient (from Schmidt et al., 2013).

Nitche et al., (1967) suggested that a successful crystal growth using chemical vapour transport method is permitted by careful consideration of different fundamental controls such as:

1. A controlled rate of transport to ensure that the rate of crystal growth is always higher than the rate of transport.
2. Constant evaluation of the internal temperature to avoid the possible polymorphism during crystal growth.
3. A bigger size of the reacting tubes to regulate the possibility of crystal intergrowth.

4. A uniform distribution of the temperature across the reacting tubes to counter the possible re-evaporation of pre-existing crystals.
5. The formation of large crystals is regulated by employing a larger reacting tube whereby the main driver of large crystal growth is transporter convection.
6. The regulation of the temperature variation in both the growth chamber and reacting chambers in instances where the gas flow is the main control.

In recent times, different studies have shown varied experimental setups that allows the chemical vapour transport growth of binary sulphide crystals within a regulated temperature gradient environment, typically a dual zone horizontal furnace (Schmidt et al., 2013). The orientation of the furnace makes it possible to have two sets of points with varying temperatures (temperature gradient  $>700^{\circ}\text{C}$ ) across the length of the reacting tube. During CVT, the reaction is usually carried out using quartz or pyrex tubes which are characterized by a high melting point (approx.  $1500^{\circ}\text{C}$ ).

The growth of large crystals through CVT can be achieved using different sets of reacting tubes, however it is common to use reaction tubes with internal diameter of around 22 mm and 250 mm long to aid the synthesis of larger crystals (Schmidt et al., 2013). The tubes are sealed at one end prior to introducing the reacting species and sealed at the other end after a thorough evacuation. Both Lepetit et al., (2003) and Chareev et al., (2017) used chemical vapour transport method to synthesis high quality Fe-bearing sphalerite samples. The summary of the experimental setup used by both studies is presented in table 3.2.

**Table 3.2:** *Summary of the CVT synthesis of sphalerite used in two studies.*

Authors	Length of tube (mm)	Diameter (mm)	Crystallite size (mm)	Temp gradient	Transporting agent
Lepetit et al., (2003)	150	5	Not given	720 – 800 $^{\circ}\text{C}$	-
Chareev et al., (2017)	100	8	1–2	780 – 850 $^{\circ}\text{C}$	NH <sub>4</sub> Cl

## Dry Experimental Synthesis

The Dry method is a time dependent experimental method for synthesizing high purity homogeneous material under strict and controlled internal (reacting phases) and external (i.e. annealing temperature) conditions (Firdu and Taskinen, 2010). This method produces synthetic final products from the reaction of solid starting material without any catalyst or an aqueous media. This involves measured stoichiometric mass of the starting materials which are reacted within sealed quartz tubes at elevated temperature. The method usually employs high temperature resistant silica or pyrex tubes sealed to avoid contamination of the reacting phases. The method has been universally adopted by several scientists based on the consistency and compositional control achieved with this method (Firdu and Taskinen, 2010).

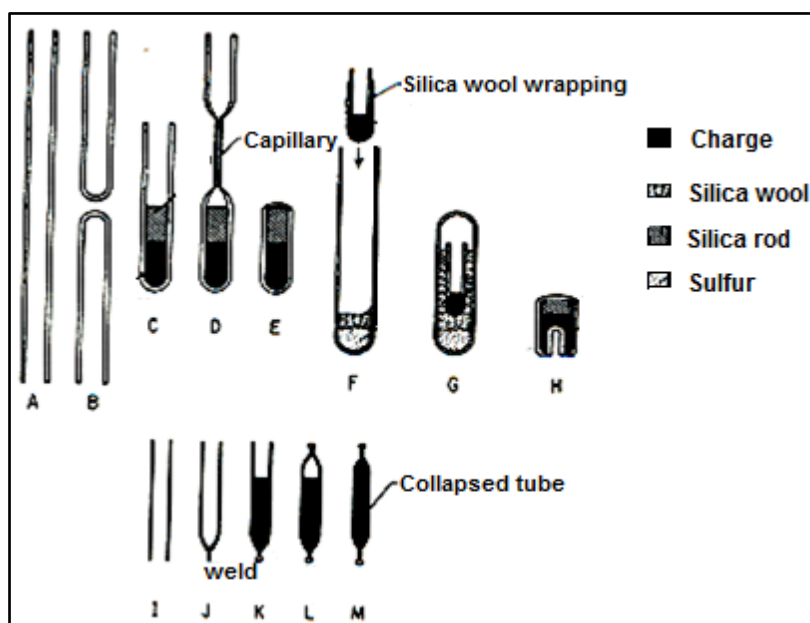


**Figure 3.2:** Different designs of tubes employed in dry synthesis of sulphide minerals. A-E illustrate a simple sealed evacuated silica tube arrangement, F-G, a tube-in-tube arrangement, H, DTA (Differential Thermal Analysis) tube design and I-M, Collapsible tube arrangement (Kullerud, 1971).

Experimental synthesis of common sulphide minerals usually takes place in a furnace under elevated temperature ( $>500^{\circ}\text{C}$ ) conditions depending on the mineral of interests (Kellerud, 1971). The high temperature reaction environment requires that the reacting phases be contained in a tube/capsule which does not devitrify nor react with sulphur at elevated temperatures (Firdu and Taskinen, 2010). For this reason, majority of recorded sulphide synthesis studies make use of reaction tubes with different experimental designs. Figure 3.2 shows different tubing designs employed for sulphide synthesis, selection of tubes of interest depend on the nature of the experiment, the quantity of the product required and the reacting phases.

In figure 3.2, experimental designs A-E are used for synthesis of mineral phases in a simple evacuated and sealed silica tube to avoid contamination of the reaction, F-G represent a tubing design whereby the tube arrangement is used for compositional determination and cation to ratios, H represent a setting for differential thermal analysis on sulphide type materials while I-M tubing illustrate a tubing design used for experiments on sulphide phases in the absence of vapour.

For synthesis of sulphide phases stable at elevated temperatures ( $>700^{\circ}\text{C}$ ), the reaction tube properties should be critically considered (e.g., some tubes become unstable due to their diameter). According to Kullerud, (1971) the wall thickness and inside diameter of the tube must be considered when selecting the tubes to use. For example, at elevated temperatures up to  $1000^{\circ}\text{C}$  a tube with an inside diameter of 3-7 mm and wall thickness of 0.5-2 mm can survive the vapour pressure created by the reacting sulphur compared to a tube with an outside diameter of 0.3 mm and wall thickness of 0.01 mm which can only be applicable to reactions that are limited to low temperature.

### **Co-precipitation**

The co-precipitation method for sulphide mineral synthesis is a simple, quick method to produce powdered materials from dissolved salt precursors (i.e. chlorite, nitrate or oxychloride) (Gulshan and Okada, 2013). The production of sphalerite is achieved through a reaction of zinc salts and  $\text{H}_2\text{S}$  or  $\text{Na}_2\text{S}$  (source of  $\text{S}^{2-}$ ) in an aqueous media



under controlled experimental conditions (fig.3.3) (Vacassy et al., 1998, Chen et al., 2012).

The experimental success of a given synthesis under the co-precipitation method is dependent on temperature, concentration of the anion source and pH parameters (Vacassy et al., 1998). The method is considered energy efficient because it occurs at low temperature reaction environment in contrast to other high temperature methods of synthesis. According to Gulshan and Okada, (2013) one of the major setbacks of the co-precipitation method involves its inability to control the morphology and size of the precipitated material. Consequently, the chemical and physical properties of the synthesized materials are poorly established due to poorly constrained mineral size, morphology and shape (Vacassy et al., 1998).

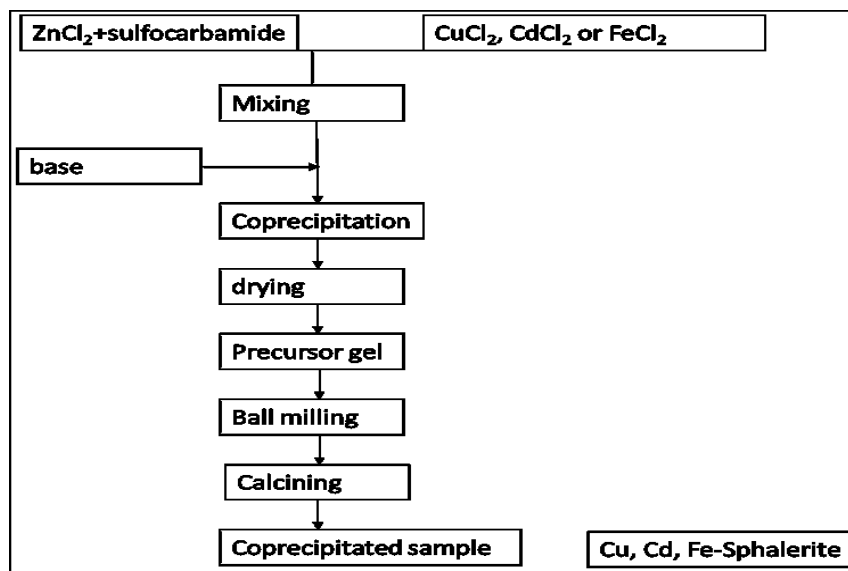


**Figure 3.3:** Flowchart for the preparation of Cu, Cd and Fe doped sphalerite by co-precipitation method (Chen et al., 2012).

Several of studies (notably Chen et al., 2012; Bredol and Merikhi, 1998; and Vacassacy et al., (1998)) have illustrated the application of co-precipitation to sulphide mineral synthesis. According to Bredol and Merikhi (1998) the co-precipitation of ZnS powders is a three-step process that involves the precipitation of ZnS in aqueous solution after the homogenization of the precursor salts and the precipitating anions. In their study Bredo and Merikhi, (1998) was able to successfully co-precipitate both CuS and ZnS.

Under controlled synthesis it is expected that CuS will be precipitated first due to its lower solubility allowing the ZnS to be precipitated last.

Figure 3.3 illustrates a flowsheet for the co-precipitation of doped synthetic sphalerite. Salt precursors were used as the source of zinc, while sulfocarbamide was the source for sulphur ions. In contrast to Chen et al., (2012), Bredol and Merikhi, (1998) used thioacetamide as the source of sulphur anions because the decomposition of thioacetamide to H<sub>2</sub>S can be controlled and monitored by pH and temperature (i.e. high temperatures and low pH promote the formation of H<sub>2</sub>S).

The most critical step in sphalerite synthesis through co-precipitation is calcination of the obtained material. The ZnS mineral occurs in different structures, prior to calcination, the obtained precipitate exhibits a hexagonal (wurtzite) structure, thus to convert it into sphalerite, the homogenous sample must be extensively calcined at a temperature below 1000°C (Vacassy et al., 1998).

### **Hydrothermal Synthesis**

The hydrothermal synthesis method was established as an experimental method to simulate and provide understanding of natural hydrothermal ore forming processes (Suchanek and Riman, 2006). Over the years different authors have proposed different explanation of hydrothermal method. As one of the earliest studies on hydrothermal synthesis, Morey and Niggli, (1913) explained hydrothermal methods as a technique of synthesis that utilizes water as a growth medium within reacting temperature higher than the critical temperature of water of 370°C. Byrappa, (2001) defined the hydrothermal method as a chemical reaction within an aqueous medium at temperatures higher than room temperature and at > 1 atm pressure within a closed reaction tube. Suchanek and Riman, (2006) stated that the method involves a single or multiple phased reaction in an aqueous media at varying temperature ( $T > 25^{\circ}\text{C}$ ) and pressure ( $P > 100\text{KPa}$ ) to crystallize solid synthetic materials. The hydrothermal reaction of sphalerite crystals usually a mixture of zinc acetate and thio-urea as source of both zinc and sulphur in an aqueous solution at temperature around 160°C for a day (Ibupoto et al., 2013).

In the 20<sup>th</sup> century, the hydrothermal procedure was the principal method for the synthesis of solid materials largely because of its desirable conditions of synthesis below 350°C (Suchanek and Riman, 2006). In contrast to other methods, hydrothermal procedure exhibits a wide variety of advantages that include the ability to continuously produce materials without stopping the process and its low energy usage (Suchanek and Riman, 2006).

### **Justification of the chosen experimental method**

The synthesis of solid material can be achieved using several experimental methods depending on the requirements of the final product (i.e. quality or morphology). The selection of the experimental method used for this study involved a careful comparison between the above-mentioned experimental methods. A dry experimental method was chosen to carry out the synthesis of impurity bearing sphalerite samples for this study, amongst several reasons behind the selection was that several studies have illustrated stoichiometric control of the final product (Skinner, 1961, Barton and Toulmin, 1966, Shoji and Sugaki, 1984, Daskalakis and Helz, 1993, Osadchii and Gorbaty, 2010).

The selection of dry method was dictated by careful consideration of key fundamental aspects governing experimental synthesis, this include experimental set up, duration of synthesis, level of complexity, nature and quantity of the final product. Practically, the preparation of sphalerite using dry method is a straight forward procedure, which require minimal specialized equipment. Key to the success of dry synthesis is the availability of a standard furnace (1000°C) and the reacting tubes with adequate internal diameter to withstand the vapour pressure at high temperature. The setup for both Hydrothermal and Coprecipitation requires a complete overhaul of the experimental laboratory, which will be both time consuming and logistically inefficient. Several studies have illustrated that the use of a standard furnace will not be enough for the chemical vapour transport method, which requires a strong temperature gradient (Zavrazhnov et al., 2004, Schmidt et al., 2013, Chareev et al., 2017). The formation of the final products is independent on any catalyst or any additional

component to aid the chemical reaction between sulphur and the metal species. A comparative summary of the four experimental methods is presented in table 3.3 based on their suitability to produce synthetic sphalerite samples.

**Table 3.3:** A summarized comparison of the common experimental methods used for the synthesis of sphalerite.

Method	Possible impurities	Advantages	Disadvantages
Chemical Vapour Transport	<ul style="list-style-type: none"> <li>Minimal contamination from the transport agent.</li> </ul>	<ul style="list-style-type: none"> <li>Unlimited sample quantity</li> <li>Grows large crystal</li> </ul>	<ul style="list-style-type: none"> <li>Challenging stoichiometric balance</li> <li>Time consuming. Require a specialized furnace to regulate the temperature gradient</li> <li>Costly transporting agents</li> </ul>
Dry synthesis	<ul style="list-style-type: none"> <li>No chance of impurities due to the use of high purity starting material.</li> </ul>	<ul style="list-style-type: none"> <li>Easy control of the stoichiometry</li> <li>No need to use additional chemical species to aid the reaction.</li> <li>Uses conventional furnace.</li> <li>Allow morphological control</li> </ul>	<ul style="list-style-type: none"> <li>Occurs in a closed system, progress of the reaction cannot be monitored.</li> <li>Takes longer to grow solid crystals.</li> </ul>
Co-precipitation	<ul style="list-style-type: none"> <li>Possible contamination from the s</li> </ul>	<ul style="list-style-type: none"> <li>Low temperature synthesis</li> <li>Quick to produce target mineral.</li> <li>Easy to regulate external contamination</li> </ul>	<ul style="list-style-type: none"> <li>Recrystallization of the material during calcination.</li> <li>Difficult to control the morphology</li> <li>Limited sample quantity.</li> </ul>
Hydrothermal	<ul style="list-style-type: none"> <li>Low chances of contamination from starting materials and reaction tubes.</li> </ul>	<ul style="list-style-type: none"> <li>Low temperature of synthesis</li> <li>Well controlled particle morphology</li> </ul>	<ul style="list-style-type: none"> <li>Agglomeration of the final product.</li> <li>Costly due to additional precursor and aqueous solvents.</li> </ul>

		<ul style="list-style-type: none"> <li>• Purity of the final product better than of the starting material.</li> </ul>	
--	--	---	--

## Experimental considerations and synthesis for sphalerite using dry method

The success of the dry experimental synthesis is aided by careful consideration of two factors i.e. external and internal factors. The external factors such as the presence of oxygen and contamination of the reacting species play a critical role in the success and integrity of the final products. The internal factors include the nature of the starting materials used for the synthesis, a careful consideration for such is important to make sure the integrity of the final product is maintained. The experimental design typically includes measures that should account for the integrity of the final products, these include the type of apparatus used, working environment, experimental conditions, nature of the starting material, and duration of the synthesis reaction.

### Purity of the starting material

Initially, like any experimental synthesis, the integrity of the final products is largely dependent on the nature and quality of the starting material. For this study high purity (>99.99%) starting materials were used to allow the reaction to proceed only between the required species with no foreign species thus increasing the chances of forming the desired material. The size of the material also plays a crucial part to the success of the reaction. The reaction between sulphur and metals is relatively quick, thus for complete reaction it is imperative that the smallest materials be used as this allows complete reactions between the reacting components. The study used relatively small size powdered material (<150  $\mu\text{m}$ ) hence it was possible to obtain complete reaction in the duration set for synthesis.

### Stability of the reacting tubes

Dry synthesis of metal sulphide typically occurs at high temperature conditions and thus makes it important to consider the nature of the reacting tubes and their stability

at high temperature ( $>600^{\circ}\text{C}$ ). Both silica and pyrex tubes are the commonly used reacting tubes largely because both exhibit high melting point (approx.  $1500^{\circ}\text{C}$ ). The high melting point of pyrex tubes used in this study eliminates the possibility of the material-tube interactions thus allowing the reaction to proceed without any materials from the tubes incorporated into the overall reaction. At  $850^{\circ}\text{C}$ , sulphur creates a high vapour pressure, which results to the breaking of the tubes during high temperature synthesis. To counter the high vapour pressure during the synthesis of metal sulphide, the reaction is kept at relatively lower temperature ( $<400^{\circ}\text{C}$ ) for several hours to allow sulphur to react fully with the metals. The vapour pressure is also controlled by correct selection of tube with the right internal diameter to be able to withstand the vapour pressure at high temperature without being destroyed. Depending on the amount of sulphur contained in the starting material, tubes with bigger internal diameter are suitable to withstand the vapour pressure, hence for this study tubes with 12 mm internal diameter were used.

### **Phase stability of ZnS polymorphs**

It is well known that sphalerite is a low temperature cubic polymorph of zinc blend, which can exist as wurtzite at high temperature (Tiwary et al., 2011). Skinner, (1961) and Tiwary et al., (2011) state that sphalerite is stable at low temperature and the phase transformation of pure sphalerite to wurtzite phase occurs at  $1020^{\circ}\text{C}$ . The study requires that the final product be a cubic impurity bearing sphalerite phase. Several studies have illustrated that the incorporation of oxygen and different metal impurities at varied concentrations lowers the onset of the sphalerite-wurtzite transformation (Skinner, 1961, Zhang et al., 1988)).

A prior knowledge of the onset of sphalerite-wurtzite transformation is thus crucial to establishing the composition and the temperature of synthesis to avoid the formation of wurtzite. The dependence of the sphalerite-wurtzite inversion temperature on the impurity concentration is illustrated in figure 3.4 (Zhang et al., 1988). It is shown that the increase in Cd concentration in sphalerite affects the onset of the inversion temperature. The temperature of synthesis of this study was set at  $900^{\circ}\text{C}$  to allow complete reaction and while eliminating any chance of forming wurtzite. Skinner and

Barton, (1960) reported on the substitution of sulphur by oxygen leading to the formation of ZnO instead of ZnS. To eliminate any chances of incorporating oxygen into the system, the material mixture of the starting is transferred to a reaction tube sealed at one end and connected to a suction pump for evacuation and flushing with argon gas several times before sealing. All the measures taken enabled successful synthesis of the sphalerite samples with known chemistry.

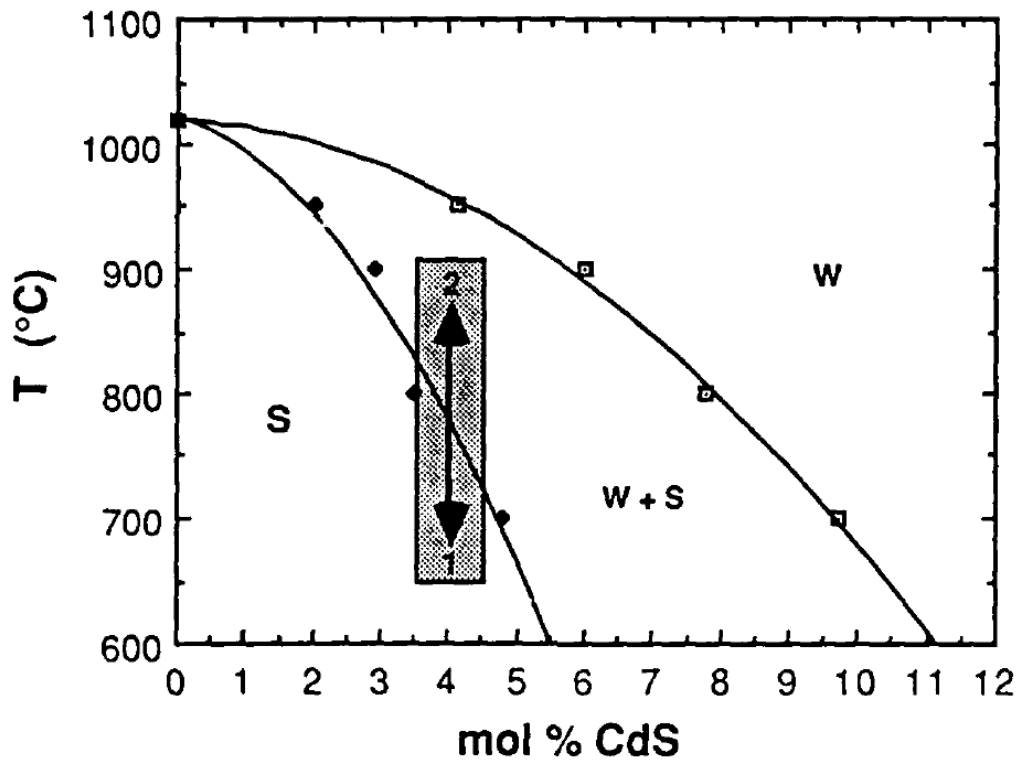


**Figure 3.6:** Phase Stability diagram of sphalerite-wurzite minerals as a function of temperature and Cd concentration (Zhang et al., 1988).

### Synthesis of sphalerite.

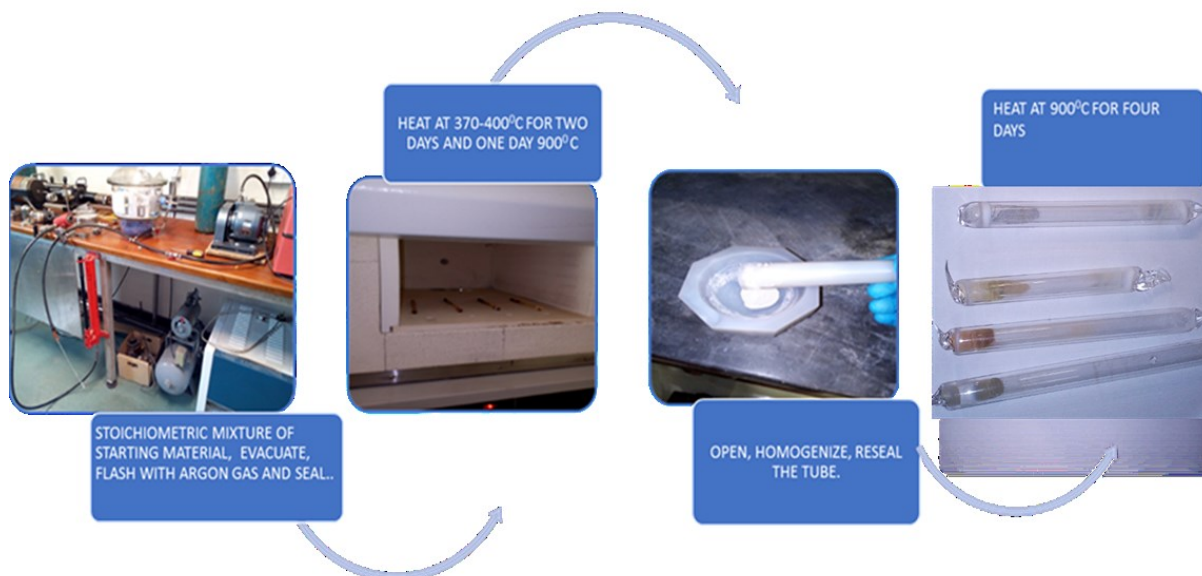


**Figure 3.5:** A graphical summary of a dry experimental synthesis of sphalerite used in this study. A detailed explanation of the method is presented below.

Numerous studies (Skinner, 1961, Kullerud, 1971, Kojima and Sugaki, 1984, Daskalakis and Helz, 1993, Pring et al., 2008, Osadchii and Gorbaty, 2010) have illustrated successfully the use of the dry experimental technique to produce different sphalerite samples. Kullerud, (1971), outlines the background of the method, with emphasis on key fundamental controls to achieving successful mineral synthesis. The current study uses dry synthesis technique (Figure 3.5) to synthesise sets of mixed crystal systems ( $M_xZ_{1-x}S$ , where M represent the metal impurities Cd, Co and Fe). The method provides a controlled stoichiometric composition of the final product, thus permitting synthesis of mixed crystal sulphide mineral (impurity bearing sphalerite).

The synthesis of pure and impurity (Cd, Co and Fe)-bearing sphalerite samples was carried out using high purity elements purchased from Sigma Aldrich as starting material. The synthesis used high purity zinc powder (<150 $\mu$ m, >99.995% trace metal basis), sulphur (trace metal grade >99.99%), iron powder (<150 $\mu$ m, >99.99% trace metal basis), cobalt powder (<150 $\mu$ m, >99.99% trace metal basis), and cadmium powder (<150 $\mu$ m, >99.99% trace metal basis). Additional material and equipment required includes Acetone (lab grade), mortar and pestle, desiccator, acetylene and



oxygen gas cylinder, oxyacetylene torch, argon gas cylinder, standard furnace (max temp 1200°C) and pyrex tube with an internal diameter of 12mm. It is critical that all the chemical species be stored in a desiccator, flushed with argon gas prior to closing to ensure that no oxidation of the chemical and their quality is retained throughout the duration of the experiments.

For this study, 1g each of pure and impurity-bearing sphalerite samples were synthesised by firstly, weighing stoichiometric masses of the Zn, S and metal impurity M (where the mass of M ranging between 0-4 wt. % for both Fe and Cd and 0 – 0.71 wt.% for Co) in a mortar and pestle under acetone. The mixture was ground and homogenized without oxidizing the reacting species and allowed to dry inside a fume cupboard for 30 minutes. The dried and homogenized mixture was transferred into a pyrex tube which was sealed (using oxyacetylene torch) at one end. The safety procedure on the operation of oxyacetylene torch can be found in Appendix II. The pyrex tube was evacuated using a suction pump and flushed with argon gas for several minutes to eliminate excess oxygen within the tube thus resulting in minimal chances of forming ZnO instead of ZnS. The flushing and suction processes were repeated until the material was settled and compact at the bottom of the pyrex tube without any visible gas spaces. The tube was sealed without switching off the suction pump or disconnecting the tube, this allowed for easy sealing of the tube and prevention of oxygen from entering the system.

The sealed tubes were carefully placed inside a pre-heated (100°C) furnace, and due to the volatile nature of sulphur at temperature, the furnace is pre-heated at lower temperature and gradually increased over a period of 2 hours. The temperature of synthesis for sphalerite as illustrated by several studies is between 800-900°C. However, a rapid increase of the temperature to 900°C creates high vapour pressure because of sulphur, thus resulting to the tubes bursting. To counter such challenge, the tubes were heated at 400°C for two days and at 900°C for one day to allow reaction of the phases without bursting the tubes at high temperature. To ensure a complete homogeneous reaction of the reacting species, the tubes were taken out and the mixture re-homogenised under acetone. The tubes are heated at 400°C for 5 hours and then heated for 4 days at 900°C to allow the complete reaction and formation of sphalerite. After a total of seven days of synthesis, the furnace is switched off to cool

off for several hours before removing the tubes. The chemical composition of each sample was confirmed through elemental spot (10 spots per sample) analysis using Scanning Electron Microscope (SEM)-Energy Dispersive Spectroscopy (EDS). The composition of each sample are summarized in table 3.4, where the presented values represent the averages of the 10 spots and the consequent standard deviation presented within the parentheses.

**Table 3.4:** Average Scanning Electron Microscopy (SEM) elemental spot analyses for the samples. All values reported in weight percentage and values in parentheses reflect the standard deviation.

Sample	Zn (wt. %)	S (wt. %)	Co (wt. %)	Cd (wt. %)	Fe (wt. %)
ZnS	66.93 ( $\pm 0.42$ )	33.07 ( $\pm 0.42$ )	-	-	-
(Co <sub>0.6</sub> ,Zn <sub>99.4</sub> )S	68.11 ( $\pm 1.70$ )	31.52 ( $\pm 1.68$ )	0.36 ( $\pm 0.05$ )	-	-
(Co <sub>0.9</sub> ,Zn <sub>99.1</sub> )S	66.47 ( $\pm 1.32$ )	32.95 ( $\pm 1.37$ )	0.56 ( $\pm 0.06$ )	-	-
(Co <sub>1.1</sub> ,Zn <sub>98.9</sub> )S	68.08 ( $\pm 1$ )	31.2 ( $\pm 0.98$ )	0.71 ( $\pm 0.05$ )	-	-
(Cd <sub>0.9</sub> ,Zn <sub>99.1</sub> )S	65.66 ( $\pm 1.49$ )	33.2 ( $\pm 1.61$ )	-	1.02 ( $\pm 0.28$ )	-
(Cd <sub>1.8</sub> ,Zn <sub>98.2</sub> )S	65.54 ( $\pm 0.26$ )	32.45 ( $\pm 0.32$ )	-	2.01 ( $\pm 0.08$ )	-
(Cd <sub>3.3</sub> ,Zn <sub>96.7</sub> )S	62.89 ( $\pm 0.32$ )	33.42 ( $\pm 0.56$ )	-	3.68 ( $\pm 0.1$ )	-
(Fe <sub>0.9</sub> ,Zn <sub>99.1</sub> )S	65.93 ( $\pm 1.2$ )	33.29 ( $\pm 0.2$ )	-	-	0.77 ( $\pm 0.35$ )
(Fe <sub>1.8</sub> ,Zn <sub>98.2</sub> )S	64.74 ( $\pm 0.72$ )	33.20 ( $\pm 0.06$ )	-	-	2.07 ( $\pm 0.83$ )
(Fe <sub>3.3</sub> ,Zn <sub>96.7</sub> )S	63.77 ( $\pm 0.49$ )	32.82 ( $\pm 0.1$ )	-	-	3.41 ( $\pm 0.67$ )

## References

Bredol, M., Merikhi, J. 1998. ZnS precipitation: morphology control. Journal of Material Science, Vol. 33, pp 471-476.

Byrappa, K., Yoshimura, M. 2001. Handbook of Hydrothermal Technology, A Technology for Crystal Growth and Material Processing, Noyes, New Jersey.

Chareev, D.A., Osadchii, V.O., Shiryayev, A.A., Nekrasov, A.N., Koshelev, A.V., Osadchii, E.G. 2017. Single-crystal Fe-bearing sphalerite: synthesis, lattice parameter, thermal expansion coefficient and microhardness. Physical Chemistry Minerals, Vol. 44, pp 287-296.

- Chen, Y., Chen, J., Lan, L., Yang, M. 2012. The influence of impurities on the flotation behaviours of synthetic ZnS. *Mineral Engineering*, Vol. 27-28, pp 65-71.
- Daskalakis, K.D., Helz, D.R. 1993. The solubility of sphalerite (ZnS) in sulfidic solutions at 25°C and 1 atm pressure. *Geochimica et Cosmochimica Acta*, Vol. 57, pp 4923-4931.
- Fiechter, S., Mai, J., Ennaoui, A., Szacki, W. 1986. Chemical vapour transport of pyrite (FeS<sub>2</sub>) with halogen (Cl, Br, I). *Journal of Crystal Growth*, Vol. 78, pp. 438-444.
- Firdu, F.T., Taskinen, P. 2010. Densities of Molten and Solid Alloys of (Fe, Cu, Ni, Co) - S at Elevated Temperatures - Literature Review and Analysis. Aalto University Publications in Materials Science and Engineering, ISBN 978-952-60-3272-6.
- Gulshan, F., Okada, K. 2013. Preparation of Alumina-Iron Oxide Compounds by Coprecipitation Method and Its Characterization. *American Journal of Materials Science and Engineering*, Vol. 1, pp 6-11.
- Ibutopo, H.Z., Khun, K., Liu, X., Willander, M. 2013. Hydrothermal synthesis of nanoclusters of ZnS comprised on nanowires. *Nanomaterials*, Vol.5, pp 364-371.
- Jiao, W.H., Jiang, S., Feng, C.M., Xu, Z.A., Cao, G.H., Xu, M., Feng, D.L., Yamada, A., Matsubayashi, K., Uwatoko, Y. 2012. Growth and characterization of Bi<sub>2</sub>Se<sub>3</sub> crystals by chemical vapor transport. *American Institute of Physics*, Vol. 2, 022148.
- Kojima, S., Sugaki, A. 1984. Phase relations in the central portion of the Cu-Fe-Zn-S system between 800 and 500°C. *Mineralogical Journal*, Vol. 12, pp 15-28.
- Kullerud, G. 1971. Experimental Techniques in Dry Sulfide Research. In , Ulmer, G. C., Ed., *Research Techniques for High Pressure and High Temperature*. Springer-Verlag, pp. 288 – 315.
- Morey, G. W., Niggli, P. 1913. The Hydrothermal Formation of Silicates, A Review, *Journal of American Chemistry Society*, Vol. 35, pp 1086-1130.
- Nitsche, R., Sargent, D.F., Wild, P. 1967. Crystal growth of quaternary 1<sub>2</sub>246<sub>4</sub> chalcogenides by iodine vapour transport, *Journal of Crystal Growth*, Vol. 1, pp 52-53.

- Osadchii, E.G., Gorbaty, Y.E. 2010. Raman spectra and unit cell parameters of sphalerite solid solutions ( $\text{Fe}_x\text{Zn}_{1-x}\text{S}$ ). *Geochimica et Cosmochimica Acta*, Vol. 74, pp 568-573.
- Pring, A., Terantino, S.C., Tenailleau, C., Etschmann, B., Carpenter, M.A., Zhang, M., Liu, Y., Withers, R.L. 2008. The crystal chemistry of Fe-bearing sphalerites: An infrared spectroscopic study. *American Mineralogist*, Vol 93, pp 591-597.
- Schmidt, P., Binnewies, M., Glaum, R., Schmidt, M.P. 2013. Chemical Vapor Transport Reactions—Methods, Materials, Modeling. *Advanced Topics on Crystal Growth*, Vol. 132, pp. 227-306.
- Skinner, B.J., Barton Jr, P.B. 1960. The substitution of oxygen for sulfur in wurtzite and sphalerite. *American Mineralogist*, Vol 45, pp 612-625.
- Skinner, B.J. 1961. Unit-cell edges of natural and synthetic sphalerites. *American Mineralogist*, Vol 46, pp 1399–1411.
- Suchanek, L.W., Riman, E.R. 2006. Hydrothermal Synthesis of Advanced Ceramic Powders. *Advances in Science and Technology*, Vol. 45, pp. 184-193.
- Tiwary, C.S., Srivastava, C., Kumbhakar, P. 2011. Onset of sphalerite to wurtzite transformation in ZnS nanoparticles. *Journal of applied physics*, Vol. 110, 034908.
- Vacassy, R., Scholz, S.M., Dutta, J., Plummer, C.J.G., Houriet, R., Hofmann, H. 1998. Synthesis of Controlled Spherical Zinc Sulfide Particles by Precipitation from Homogeneous Solutions. *Journal of American Ceramic Society*, Vol. 81, pp 2699-2705.

## **Chapter Four- Structural, surface and electronic structure interrogations**

### **Mineral chemistry as a critical parameter in geometallurgical models: a case study using trace element-substituted sphalerite**

*A presentation of a prepared conference paper*

The conference manuscript has been prepared and accepted (after a thorough review process) for presentation at the SAIMM 2018 Geometallurgy conference held in Cape Town between 7 and 8 August 2018. The manuscript was prepared between myself and Dr. B.P. von der Heyden. Dr. M. Tadie and Dr. P.H. Neethling contributed in an editorial capacity towards the final version of the manuscript.

The key concept underpinning the paper was to illustrate the importance of substantive molecular-level interrogation as a key missing parameter in geometallurgical frameworks and approaches. We emphasised the importance and inter-relationships between the bulk structure, surface characteristics and electronic structure in trace-element substituted sphalerite. The paper illustrates the correlation between the bulk structural distortions to the surface characteristics, and how those changes can manifest as the electronic structure variations arising from cation substitution (e.g., Cd, Co and Fe substituents).

The acquisition of experimental data, and 65% of the writing was performed by myself, while in his capacity as the second author, Dr. von der Heyden contributed towards finalizing the manuscript and the addition of a case study to augment our experimental results. Both Raman spectroscopy and diffuse UV-vis reflectance measurements were performed under the guidance of Dr. P.H. Neethling, hence he is acknowledged for his contribution to the manuscript. Dr. M. Tadie in her capacity as second supervisor assisted during the zetasizer measurements and was also involved in the review of the final draft and provided insightful points that assisted in improving the standard of the paper. I also acknowledge the reviewers for their useful comments and suggestions that helped to improve the paper.

### **Mineral chemistry as a critical parameter in geometallurgical models: a case study using trace element-substituted**

# sphalerite

**L. Babedi<sup>1</sup>, B.P. von der Heyden<sup>1\*</sup>, P.H. Neethling<sup>2</sup>, and M. Tadie<sup>3</sup>**

1 Department of Earth Sciences, Stellenbosch University, South Africa

2 Department of Physics, Stellenbosch University, South Africa

3 Department of Process Engineering, Stellenbosch University, South Africa

Global zinc supply is dependent on the mining and efficient beneficiation of the sulphide mineral sphalerite (ZnS). The sphalerite crystal structure commonly incorporates a range of substituting metal ions (*e.g.*, Fe, Mn, Co, Cd) that can substantially modify the structure and surface chemistry. The links between trace element concentration and type, sphalerite structure, surface chemistry, and flotation response have not yet been fully determined. Here we apply a range of analytical techniques (X-ray diffraction (XRD), Raman spectroscopy, and UV-Vis spectroscopy) to better quantify these links, such that mineral chemistry and surface chemistry parameters can be incorporated into geometallurgical models. It is anticipated that these results can be used towards optimizing mine design and operations, specifically through improving beneficiation efficiencies. The potential mine-scale application of the approach is highlighted using mineral chemistry data from the Swartberg base metal sulphide deposit in South Africa. It is hoped that this approach, particularly once applied to other sulphide ore minerals and their substituent ions, will ultimately lead to the development of more robust and transferrable geometallurgical models that will improve the yields and efficiencies of the 'mine of the future'.

## INTRODUCTION

Comprehensive mineralogical characterization is the first step towards developing robust geometallurgical models that can be used to optimize mining and beneficiation of an ore deposit. Importantly, these models are built on discrete geometallurgical units (*e.g.*, Lotter *et al.*, 2003; Fragomeni *et al.*, 2005), which are defined using mineralogical

parameters such as metal grade, mineral abundance, mineral texture, and liberation size. Less frequently, these models can incorporate details of the mineral chemistry, *e.g.*, from QEMSCAN (Gottlieb *et al.*, 2000) and, even less frequently, mineral surface chemistry. Because flotation technology is commonly used in beneficiating sulphide minerals (*e.g.*, Aghazadeh, Mousavinezhad, and Gharabaghi, 2015), understanding the links between mineral chemistry, surface chemistry, and flotation response is increasingly important for developing robust geometallurgical models for complex (low-grade) sulphide ores (*e.g.*, Bradshaw, 2014).

In this contribution, we focus on the effects of trace element substitutions in sphalerite on downstream processing of zinc ores. Current geometallurgical models for sphalerite ores largely apply one of two approaches; utilizing either quantitative/qualitative mineralogical characterization, or empirical metallurgical test work results. These approaches typically acknowledge the importance of understanding the effects of liberation size and variability in the mineral associations (*e.g.*, Lund, Lamberg, and Lindberg, 2013). However, barring a few studies (*e.g.*, Schouwstra *et al.*, 2010), only limited attention has been paid to the geometallurgical implications arising from variability in sphalerite mineral chemistry. Our study seeks to address this knowledge gap using synthetic sphalerite doped with known concentrations of the deleterious elements Cd, Co, and Fe, all of which can substitute into the lattice structure of natural sphalerite. These elements are also important in that their presence results in elevated smelter costs, a decreased product quality, and increased environmental disposal costs (*e.g.*, Lane *et al.*, 2016).

We foresee that the improved understanding derived from our study will enable better definition of geometallurgical units, *i.e.*, those that incorporate mineral chemistry as an important input parameter having fundamental control on mineral behaviour. Furthermore, our results provide important insights into the potential applicability of existing analytical techniques towards parameterizing mineral chemistry information for incorporating into future geometallurgical models. Understanding the links between trace metal substitution and flotation response will enable optimization of the beneficiation design, and opens avenues for selective beneficiation as a means to

decrease deleterious element concentrations in the product stream, thereby reducing smelter costs and improving environmental management planning.

## METHODOLOGY

This experimental work focused on characterizing the bulk and surface properties of synthetic sphalerite, as a controlled analogue for trace-element-substituted natural sphalerite.

### Sphalerite Synthesis and Characterization

Sphalerite was synthesised following the established dry synthesis protocol (e.g., Kullerud, 1953; Pring *et al.*, 2008) using high-purity chemical reagents from Sigma-Aldrich. Synthetic sphalerite was produced by mixing stoichiometric masses of zinc powder (<150 µm, trace metal basis 99.995% purity), sulphur (trace metal basis >99.99% purity), and a trace metal dopant phase (iron powder, trace metal basis >99.99% purity; cobalt powder, <150 µm, trace metal basis >99.99% purity; or cadmium powder, <150 µm, trace metal basis >99.99% purity). Stoichiometric mixtures (dopant concentrations ranging between zero and 4 wt.%) were finely ground and homogenized under acetone (to prevent oxidation) using a mortar and pestle. The homogeneous mixture was added to a 12 mm diameter Pyrex tube, which was then flushed with argon gas and evacuated to ensure that no extraneous oxygen entered into the chemical system. Sealed tubes were heated in a muffle furnace at 380–400°C for two days and at 900°C for one day to ensure controlled reaction of the elemental constituents. To ensure complete chemical homogeneity, the reacted sample was reground under acetone, sealed in a new Pyrex tube, and further reacted at 400°C for one day, and then at 900°C for four days.

The chemical and textural homogeneity of the synthetic sphalerite were confirmed using a reflected light microscope (Nikon Eclipse E200), and a Zeiss® EVO MA 15 scanning electron microscope (SEM) equipped with a wavelength dispersive spectroscopy (WDS) sensor (Central Analytical Facility, Stellenbosch University). Data



was collected in both backscatter mode and using WDS elemental mapping, and operating conditions were set at an accelerating voltage of 20 kV and a current of between –19 nA and –21 nA. The X-ray diffraction and Raman spectroscopy results further confirmed the purity and mineralogy of the synthetic minerals.

### **X-ray Diffraction (XRD) Analysis**

X-ray powder diffraction (XRD) data was collected using a Bruker D8 powder diffractometer at iThemba laboratories, Cape Town, South Africa. Synthetic sphalerite crystals were ground to a top size of 50  $\mu\text{m}$  and evaluated for mineral composition and possible spectrum shifts using a  $2\theta$  data collection step size of 0.0340. The diffractometer utilized Cu  $K\alpha$  radiation and was operated at an accelerating voltage of <40 kV and current of 25 mA. Data reduction and phase identification were performed using PANalytical X'pert HighScore Plus software.

### **Raman Spectroscopic Analysis**

Raman spectroscopy was conducted at room temperature using a MicroHR Horiba Jobin Yvon Raman spectrometer equipped with two-dimensional Synapse ICCD detector (Department of Physics, Stellenbosch University). The Raman spectra resulted from irradiating sphalerite powder samples using a frequency-doubled Nd:YAG laser (wavelength: 532 nm). Spectra were collected over the region 200–400  $\text{cm}^{-1}$  with a spectral accuracy of better than 1  $\text{cm}^{-1}$  and an exposure time of 1 second. Collected spectra were processed using PeakFit v. 4.12, and SYSTAT software, by truncating and correcting for background signal drift using a Gaussian fit.

### **Ultraviolet-Visible (UV-Vis) Spectroscopic Analysis**

The UV-vis diffuse reflectance spectra (DRS) measurements (200–500 nm) were collected using a Thorlabs spectrometer (CC5200/M) with 2 nm resolution at Stellenbosch University (Department of Physics) utilizing a deuterium lamp as source of light. A small portion of sample was ground and homogenized using a mortar and pestle and a small aliquot transferred onto a silver mirror, which was used as the blank stage. The acquisition time for the spectra was 500 milliseconds for samples with better absorption signals, and 1 second for samples with poor absorption signals.

## Zeta Potential Measurements

The zeta potential distribution measurements were collected using a Malvern Zetasizer Nano ZS instrument (University of Cape Town, South Africa). The stock solutions for zeta potential measurements were prepared from analytical grade reagents. Freshly prepared 0.001 M KNO<sub>3</sub> was used as the background electrolyte, with the pH regulated with 0.01 M HCl and 0.01 M NaOH stock solutions. Each sample was ground under acetone using a mortar and pestle to ensure a nominal top size of <50 μm. After sample drying, a small sub-sample (0.01 g) was transferred into a 15 ml test tube containing 10 ml of 0.001 M KNO<sub>3</sub>. This mixture was shaken vigorously and allowed to condition for 10 minutes, then a 2 ml aliquot was transferred into an electrophoretic cell. For activation and collector adsorption,  $1 \times 10^{-4}$  M of both CuSO<sub>4</sub> and sodium isobutylxanthate in solution was made up by adding separately 10 μL of each 0.1 M stock solution (CuSO<sub>4</sub> and sodium isobutylxanthate) to the 10 ml electrolyte solution with the sample and allowed to condition for 10 minutes. For these experiments, the pH was slightly alkaline (pH ± 9) and the temperature was controlled at 25°C for Cu activation and collector adsorption, while unactivated samples were analyzed in both acidic and alkaline media.

## RESULTS

The synthetic sphalerite showed a high degree of chemical and textural purity. Chemical SEM mapping, in backscatter mode as well as with the WDS sensor revealed that the crystals were chemically homogeneous, with an average crystallite size between 10 and 18 μm. Mineralogical purity was further confirmed by the XRD results, which showed only the characteristic 2θ diffraction peaks for sphalerite (*i.e.*, no wüstite peaks, which would indicate significant oxygen in the reaction system; and no FeS (*e.g.*, pyrrhotite), CdS, or CoS diffraction peaks, which would have indicated that the dopants formed discrete phases instead of substituting into the sphalerite mineral structure).

## X-ray Diffraction (XRD) Results

The incorporation of trace amounts of the transition metal dopants into the sphalerite crystal structure results in subtle shifts in the  $2\theta$  peak positions in the XRD spectra (Figure 4.1a). The prominent diffraction peaks occurring in sphalerite are positioned at  $28.5^\circ$ ,  $47.5^\circ$ , and  $56.4^\circ$  and are attributed to the 111, 220, and 311 planes respectively. Using these three prominent planes, as well as the 200, 222, and 400 planes, we were able to evaluate the shifts in the unit cell parameter (Figure 4.1b). These dopant-induced changes to the unit cell parameter reflect the strains and the geometric distortions occurring in the local (molecular-level) structure of the bonding environment (*i.e.*, the unit cell).

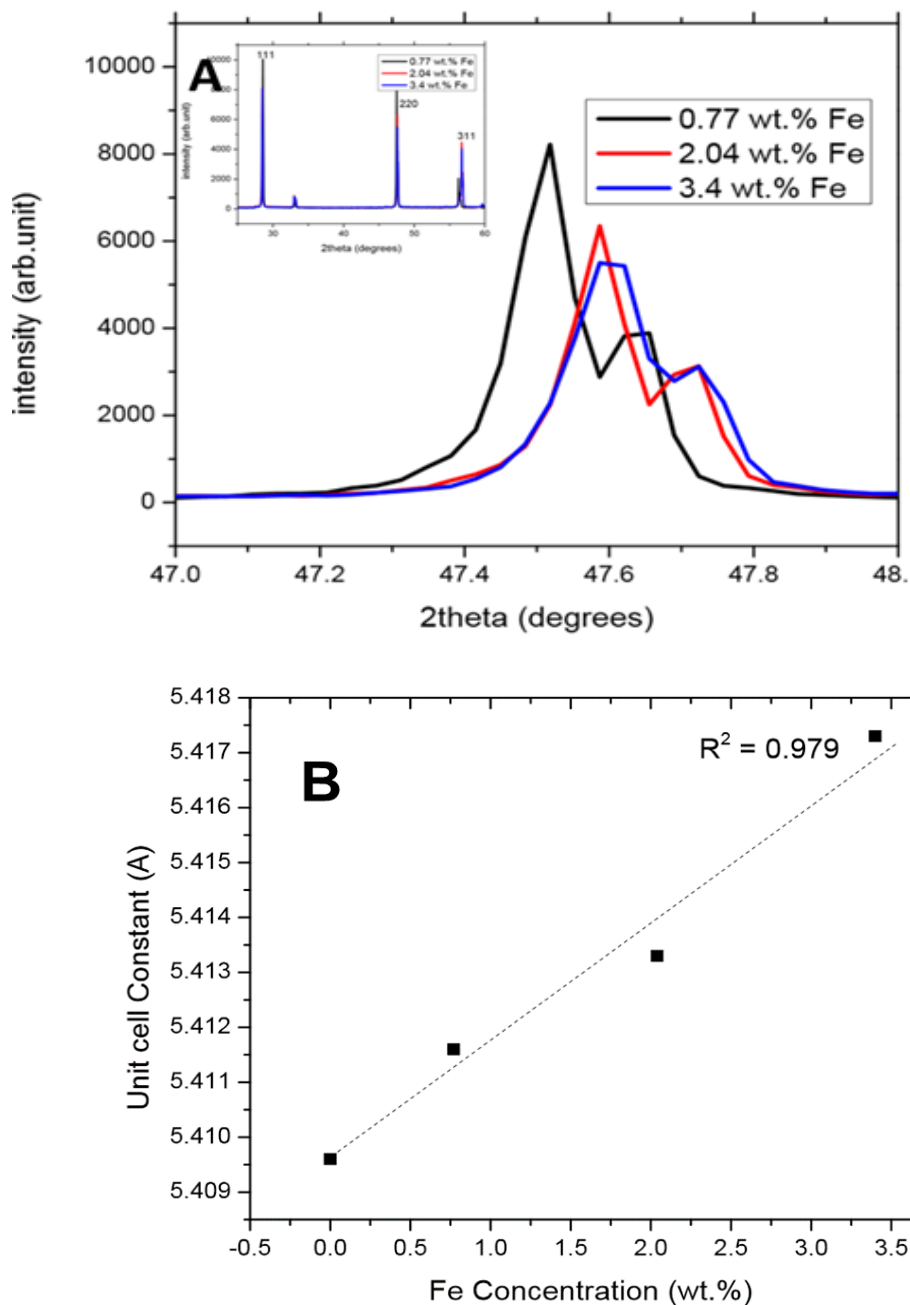


**Figure 4.1a.** Shift in the  $2\theta$  diffraction peak position for the sphalerite 311 diffraction plane as a result of increasing concentrations of a Fe cation substituent. 1b. Linear correlation between the doped sphalerite unit cell constant and increasing concentrations of Fe cation substituent.

For the Fe-doped sphalerite mineral structure, the unit cell parameter (calculated according to Equation [1]) varies linearly between 5.410 and 5.417 as the concentration of the Fe substituent increases from 0 to 3.40 wt.% ( $r^2 = 0.98$ ; Figure 4.1b). Similarly, the variation in the unit cell parameter in the Co-doped sphalerite mineral system ranges between 5.410 and 5.412 for Co concentrations between 0–0.71 wt.% ( $r^2 = 0.74$ ). For Cd concentrations ranging between 0–3.7 wt.%, the unit cell parameter showed a strong positive correlation ( $r^2 = 0.96$ ) and ranged between 5.410 and 5.424. The results from the Cd-substituted sphalerite are in good agreement with previous data reported by Skinner (1961).

$$\frac{1}{D^2} = \frac{h^2+k^2+i^2}{a^2} \quad [1]$$

### Raman Spectroscopy Results

Raman spectra reflect the scattering interactions between monochromatic light and the molecular vibrations or crystal phonons present in a mineral structure (Neuvill, de Ligny, and Henderson, 2014). Specifically, the cubic sphalerite mineral structure lacks a center of inversion and is characterized by two dominant first-order modes *viz.* the transverse optical mode (TO) and the longitudinal optical mode (LO). The TO mode reflects atomic vibrations that are perpendicular to the incident light and occurs at approximately  $350 \text{ cm}^{-1}$ ; whereas the LO mode occurs at  $272 \text{ cm}^{-1}$  and arises from vibrations that are parallel to the incident light (Hope, Woods, and Munce, 2000; Karbish, 2007; Krauzman, 1968; Oschadii and Gorbaty, 2010). The Raman spectra of our synthetic sphalerite minerals are more surface-sensitive and are dominated by these two first-order modes, as well as an impurity mode ( $295\text{--}305 \text{ cm}^{-1}$ ) that arises when trace amounts of cation substituents are incorporated in the sphalerite mineral structure (Figure 4.2a).

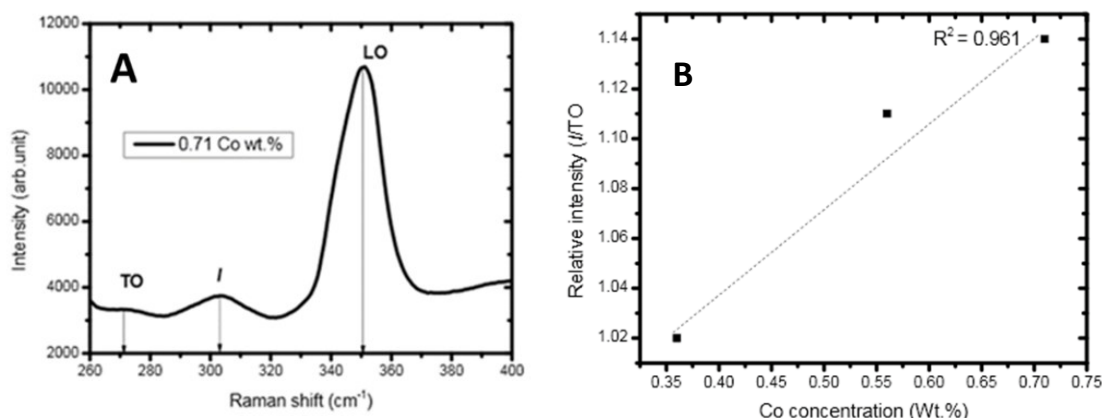


**Figure 4.2.** (a) Peak positions of the Raman shifts associated with a 0.71% Co-substituted synthetic sphalerite relative to the pure synthetic sphalerite Raman spectrum. (b). Variations in the peak height ratios of the impurity mode and the transverse optical (TO) mode as a function of dopant concentration in the Co-doped synthetic sphalerites.

The peak position of the impurity mode differs according to the identity of the cation substituent in the sphalerite structure. For Cd substitution, the impurity mode occurs at 295.6 cm<sup>-1</sup>; for Fe substitution it occurs at 300.0 cm<sup>-1</sup>; and for Co substitution the peak is centered on 303.5 cm<sup>-1</sup>. Importantly, the position of the impurity mode Raman shift shows a strong positive linear correlation ( $r^2 = 0.96$ ) with the electronegativity of the divalent cation substituent; and a strong negative linear correlation ( $r^2 = 0.95$ ) with the atomic radii of the divalent cation substituents (assuming tetrahedral coordination). Substitution of Cd and Fe further results in shifts to the peak position of the LO and TO without a clear correlation with increasing concentration. This is interpreted to reflect substituent-induced changes to the bonding environment in the Zn-S bonds, resulting in shorter, stronger bonds with increased levels of substitution (e.g., Buzatu *et al.*, 2013). This was not observed in the Co-substituted sphalerites, perhaps because of the low levels of the substitution (0–0.71 wt.%).

Figure 4.2b illustrates the strong linear relationships ( $r^2$  values between 0.79 and 0.96) between the dopant concentration and the ratio of the peak intensities of the impurity mode and the transverse optical mode. For all three substituting systems, the peak

height ratio increases as the dopant concentration increases. The dopant concentration is related to this peak height ratio by the formulae:

$$[\text{Cd}] = (\text{IM}_{\text{Cd}}/\text{TO} - 0.0.7963) / 0.082 \quad [2]$$

$$[\text{Co}] = (\text{IM}_{\text{Co}}/\text{TO} - 0.9006) / 0.3486 \quad [3]$$

$$[\text{Fe}] = (\text{IM}_{\text{Fe}}/\text{TO} - 1.032) / 0.0489 \quad [4]$$

The ratio between the peak height of the impurity mode and the peak height of the longitudinal optical mode (LO) does not show any similar distinctive trends.

### Ultraviolet-visible (UV-Vis) Spectroscopy Results

To complement the bulk mineral structure measurements (XRD) and the surface structural measurements collected from the Raman spectra, we applied UV-Vis spectroscopy to interrogate the changes that cation substituents induced in the molecular-level electronic structure of the synthetic sphalerites. Our UV-Vis measurements probed the energy range between 200 nm (mid-UV) through to 500 nm (visible light), and the absorption measurements primarily reflect d-d electronic transitions occurring between the various orbital subsets in the valence band of the synthetic sphalerites (Rossman, 2014; Li *et al.*, 2008). The minimum wavelength at which absorption occurs was used to qualitatively infer the size of the band gap existing between the valence band and the conduction band (*i.e.*, the densities of states are assumed for a direct band gap occurring in an ideal crystal). Equation [5] relates the wavelength of energy absorption ( $\lambda_{\text{red}}$ ) to the size of the band gap ( $E_g$ ) using Planck's constant ( $h$ ) and the speed of light ( $c$ ):

$$E_g = hc/\lambda_{\text{red}} \quad [5]$$

Figure 4.3a indicates the shifts that occur when cobalt substitutes into the synthetic sphalerite structure. As Co concentration increases, the UV-vis reflection spectra shift towards higher wavenumbers (Figure 3a), translating to a decrease in the inferred size of the band gap (Figure 4.3b) to energy differences as small as 3.0 eV at Co

concentrations between 0.56 and 0.71 wt. %. Cation substitution with Cd and Fe similarly results in decreases in the sizes of the band gap to 3.4 eV (Cd concentration 3.68 wt.%) and 3.35 eV (Fe concentration 3.40 wt.%). However, the UV-vis reflection data from the Fe-doped sphalerite system showed poor reflection and were thus more difficult to conclusively evaluate. Li *et al.*, 2008 reported the band gap of a Fe-bearing natural sphalerite to be 2.9 eV, thus illustrating the influence of the impurities on the band gap.

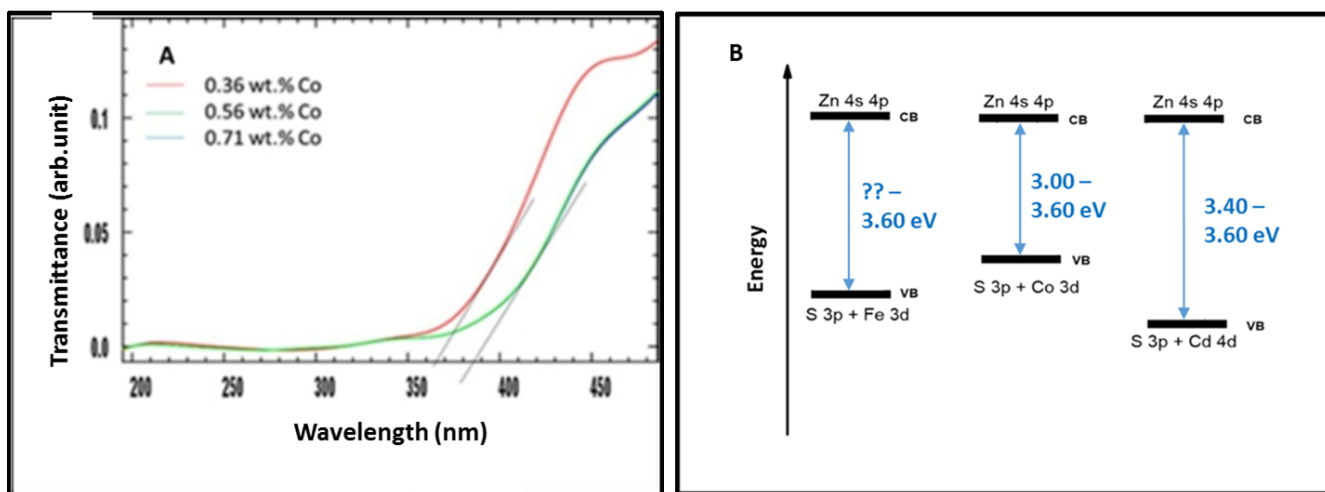


**Figure 4.3.** (a) Shifts in the UV-Vis reflection spectra of Co-doped synthetic sphalerites as a function of the dopant concentrations. (b). Shifts in the calculated size of the band gap for the Co-, Cd-, and Fe-doped synthetic sphalerites (using Equation [5]).

### Zeta Potential Results

Zeta potential measurements were conducted on substituted sphalerites to assess the variation in surface charge under both alkaline and acidic pH conditions, and to investigate the sphalerite responses to Cu activation and collector adsorption at alkaline pH. Unactivated synthetic sphalerites exhibit variable surface charges (reflected in their respective zeta potential distributions) as a function of the chemical nature of the transition metal impurity present in the mineral structure. The negative zeta potential distributions for Cd- and Fe-substituted sphalerites shift towards more alkaline pH values relative to pure sphalerite, whereas the incorporation of Co lowers



the zeta potential towards a more neutral pH. Similarly, the trace element substituents result in shifts in the isoelectric point (iep) towards higher pH values, with the largest shift observed in the Co-substituted sphalerites, where the iep shifts to pH 6 at 0.36 wt.% Co.

Zeta potential measurements recorded for Cu-activated sphalerite in an alkaline pH (*i.e.*, relevant to typical flotation circuits) reveal that the decrease in the negative zeta potential distributions can be correlated to increasing concentrations of both Cd and Fe. Furthermore, the presence of the different impurities has a profound influence on the onset pH related to flotation processing. Pure un-substituted sphalerite exhibits an onset pH of 9.13, which is higher than the onset pH recorded for both the Fe- and the Cd-bearing samples. The levels of Cd and Fe substitution both correlate positively with the recorded onset pH. For example, the onset pH for the Cd-bearing samples shifts from pH 8.6 for 1.02 wt.% Cd to pH 8.99 for 3.68 wt.% Cd samples. Similarly, the onset pH in the Fe-substituted sphalerites shifts from pH 8.7 for 0.77 wt.% Fe, to pH 8.8 for 3.4 wt.% Fe. Conversely, Co-bearing sphalerite shows a negative relationship between the onset pH and Co concentration, *i.e.* increased Co contents from 0.36 wt.% to 0.71 wt.% decrease the onset pH from 9.4 to pH 8.8. Based on the aforementioned results, understanding the mineral chemistry will enable careful adjustment to the operational pH during flotation, thus potentially optimizing flotation design during large-scale processing. Improving metal recovery from impurity-bearing sphalerite requires a high-level understanding of the chemical nature of the substituting metal ions as this also has a bearing on the hydrophobic species forming on the mineral surface during collector adsorption.

## DISCUSSION

Sphalerite beneficiation, and indeed the beneficiation of most sulphide minerals, is strongly reliant on the effectiveness and efficiencies of flotation technologies (Harmer *et al.*, 2008, Chandra and Gerson,

2009). Flotation response, in turn, is strongly dependent on the surface chemistry and, importantly, on the electronic interactions taking place at the interface between the surface and the aqueous medium (Chen, Chen, and Guo, 2010). Here we explore the effects that trace metal incorporation into the bulk sphalerite mineral structure have on the resultant surface chemistry and electronic structure. We further discuss the implications that these results have for our ability to predict sulphide surface reactivity based on analytical measurements of sulphide trace element tenors.

### **Interrelationships between Bulk Sphalerite Chemistry, Surface Chemistry and Molecular-level Electronic Structure**

Our study indicates that there exist profound and fundamental linkages between the chemical nature of the cation substituent, the bulk structure of the substituted sphalerite, the bonding environment of the associated surface functional groups, and the resultant molecular orbital structure and electronic configuration of the sphalerite surface (Figure 4.4). The ionic size of the cation substituent (measured as a divalent ion in tetrahedral coordination) induces structural distortions in the sphalerite lattice. The cation substituents considered in this study are all larger in ionic size than Zn, and thus all lead to linear increases in the size of the unit cell parameter – in agreement with previous work by Skinner (1961), Harmer *et al.* (2008), and Chen, Chen, and Guo (2010). For example, Cd has the largest difference in size to Zn and results in the largest distortions of the XRD-measured unit cell parameter in Cd-substituted synthetic sphalerites.

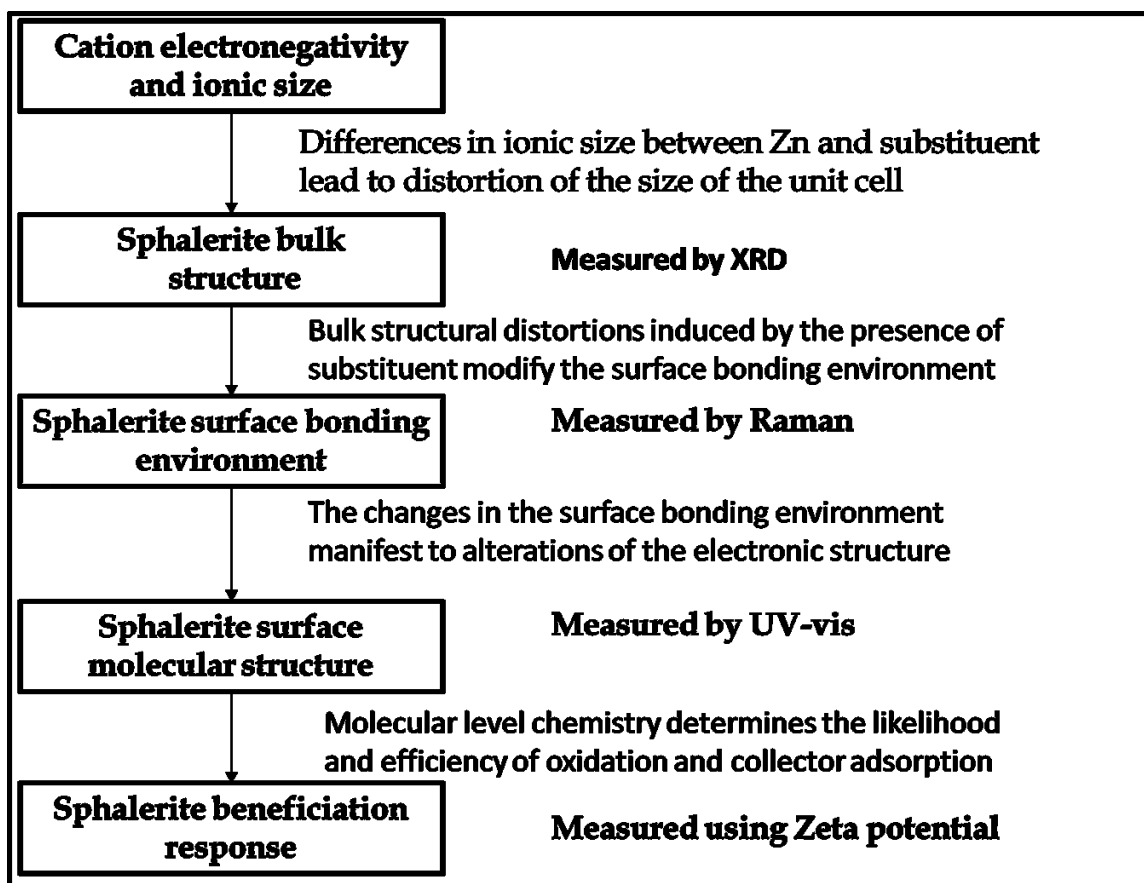


**Figure 4.4.** Diagrammatic overview of how cation substitution in the bulk mineral structure can manifest as modifications to the surface chemistry and thus flotation response of sphalerite. Techniques indicate a simplified work flow towards understanding the important interrelationships (XPS: X-ray photoelectron spectroscopy; XAFS: X-ray absorption fine structure).

These observed structural distortions within the bulk mineral structure translate to differences in the local coordination and bonding environment of the substituted sphalerite mineral surface. The Raman spectroscopy results reported here probe the surface bonding environments of the substituted sphalerites and reveal both the presence of substituent–S bonds at and near the sphalerite surface, and that the nature of the surficial Zn-S bonds changes because of lattice strains induced by the bulk mineral distortions (see next section). For example, the incorporation of Cd (slightly more electronegative, and much larger ionic radius than Zn), results in the presence of Cd-S bonds at the mineral surface, but we also interpret it to result in a stronger average Zn-S bond strength.

The substituent-induced modifications to the sphalerite surface bonding environment will further manifest as differences between the electronic structures of the pure sphalerite and the substituted sphalerites (Figure 4.3b). The resolution of our UV-Vis spectra was sufficient to indicate the variations in the band gap of the substituted sphalerites, and these were found to correlate well ( $r^2 = 0.99$ ) with the measured position of the Raman impurity mode of the corresponding cation substituent (Figure 4.5). Our UV-Vis data, however, could not be used to resolve the influences of the change in the strength of the remaining Zn–S bonds on the average molecular orbital structure (as reflected in the band gap). It is suggested that future work consider the use of X-ray photoelectron spectroscopy (XPS) to better understand the surface bonding environment and its influences on orbital structure.

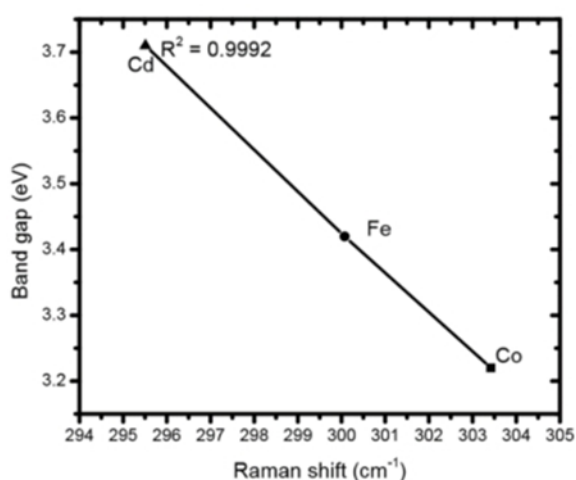


**Figure 4.5.** Relationship between the band gap in substituted sphalerite and the strength of the bond between sulphur and the cation substituent as reflected in the wavenumber position of the impurity mode.

### **Raman Measurements Provide Insights into the Concentration and Chemistry of Trace Metal Substituents in Sphalerite Mineral Structure**

Given the role of surface chemistry in sphalerite flotation (Chandra and Gerson, 2009) it is becoming increasingly important to more fully characterize the sphalerite surfaces in order to design efficient and effective beneficiation circuits and thus responses. Our data reveal that Raman spectroscopy configured to interrogate mineral surfaces is a quick, cheap and useful tool for quantifying the concentrations of trace element substituents within sphalerite. Importantly, our data reveals that the position of the impurity mode can be used to predict the chemical identity of the substituting cation,

with the Raman impurity mode wavenumber position correlating positively with the electronegativity of the substituting divalent atom ( $r^2 = 0.96$ ), and negatively with the atomic radius of the substituting atom ( $r^2 = 0.95$ ). The negative correlation observed with the atomic radius shows that the lattice distortions detected with XRD have no implication for the resultant bond formed. Rather, the chemical nature of the substituting atom is what dictates its interaction with the host molecular cluster. Such variation in the local cluster molecular bonds is visualized in the wavenumber of the impurity modes.

Similarly, by considering the peak intensity ratios between the impurity mode and the transverse optical mode (TO) the Raman spectra can also be used to estimate the relative concentration of the different cation substituents present in sphalerite (Bazuta *et al.*, 2013; Osadchii and Gorbaty, 2010; Figure 4.2b). These estimates can be made using Equations [2], [3], and [4], and similar relationships should be tested for other substituting metal ions. Several studies have illustrated the use of infrared spectroscopy for *in-situ* characterization of the reaction species forming during sphalerite flotation; the use of Raman spectroscopy for *in-situ* analysis can improve flotation efficiency. A quick online Raman analysis will identify the mineral chemistry and thus improve process design/adjustment capabilities.

## **CASE STUDY: SPHALERITE GEOCHEMISTRY AT THE SWARTBERG BASE-METAL SULPHIDE DEPOSIT, NORTHERN CAPE**

The Swartberg ore deposit is one of four Mesoproterozoic stratabound Cu-Pb-Zn-Ag-Ba-Fe-Mn deposits hosted within a medium-to-high grade metamorphosed volcanosedimentary sequence in the Bushmanland Terrane of the Namaqua-Natal Province, South Africa (Rozendaal, Rudnick, and Heyn, 2017). Relative to the other three deposits in the Aggenys-Gamsberg ore district (Broken Hill Deepes, Gamsberg, Big Syncline), the Swartberg deposit is known to contain the highest concentrations of deleterious elements such as Co and Cd. Detailed mineral chemistry analyses have revealed that these elements concentrate within the sphalerite mineral structure (von der Heyden *et al.*, 2017), and that the levels of trace element incorporation vary between orebodies (upper orebody *versus* lower orebody), and within the orebodies

along strike. Figure 6 highlights the spatial trend in the average Cd concentration within individual sphalerite minerals analysed from six sites in the 715 level of the lower orebody. There is an apparent decrease in Cd concentration from NE to SW along strike of this orebody, which is thought to reflect increasing distance away from an interpreted original hydrothermal vent site (Rudnick, 2016).

Our experimental results from the synthetic Cd-substituted sphalerite system suggest that the observed Cd concentration trend in natural sphalerite (Figure 4.6) may manifest as variability in the efficiency of the flotation response. For example, the high-Cd sphalerites (SW extent of the orebody) can be expected to have an onset pH of 8.9 during flotation when activated using  $\text{CuSO}_4$ ; whereas the onset pH is expected to be higher for low-Cd sphalerite found in the NW domain (pH 9.0). This implies that, in order to aid successful interaction with flotation reagents, the operational pH of the flotation circuit must be constantly modified when treating ores with different impurity concentrations. Alternatively, the operational pH can be controlled to selectively beneficiate the low-Cd sphalerite, such that sphalerite with high concentrations of Cd (a deleterious penalty element) will report to the waste stream. It must, however, be stressed that the research is still in its early phase, and future predictive models will necessarily be reliant on a full fundamental understanding of the influences of variable trace metals within the sphalerite mineral structure.

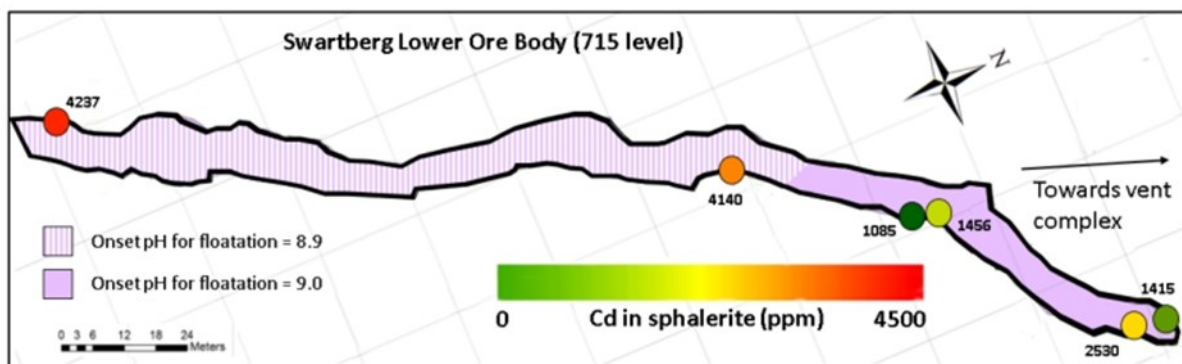


**Figure 4.6.** Distribution of Cd in sphalerite along strike in the lower orebody of the Swartberg deposit. This trace element data can be used to improve efficiencies when beneficiating Swartberg ore by modifying the flotation parameters (e.g. pH) according to the mineral chemistry of the two zones indicated.

## CONCLUSION

Many metallurgical studies have investigated the optimization of flotation behaviour for specific ore mineral assemblages, generally using samples collected from specific orebodies (McClung and Viljoen, 2011; Schouwstra *et al.*, 2010, Cook, Ciobanu, and Williams, 2011). Although such approaches can provide meaningful insights, the transfer of these insights to the optimized beneficiation of other, slightly different ore deposits may be hindered by a lack in fundamental understanding of molecular-level mineral chemistry of the ambient sulphides. To contribute to such a fundamental understanding, we have investigated three binary, substituted sphalerite mineral systems to track the effects of mineral chemistry on the resultant bulk structure, and on the surface chemistry and surface electronic structure of the sphalerites. The last consideration is most important given that the electronic structure and semiconducting properties of the sphalerite surfaces are the ultimate parameters controlling important flotation reactions such as oxidation and collector adsorption (Xu and Schoonen, 2000; Lotter, Bradshaw, and Barnes, 2016). We have linked many of our findings to the basic first-principles chemistry of the cation substituent, and believe that such an approach is crucial towards developing a complete and fundamental understanding of the flotation behaviour of sphalerite. Future work should be devoted towards extending the data-set to other economically important sulphide minerals.

Once these mineral chemistry controls have been more fully constrained, their coupling with existing understanding of mineral liberation and ore mineral associations will greatly advance our capabilities to predict flotation behaviour. This understanding can be used to develop robust and scientifically meritorious geometallurgical models that can be used to optimize base metal sulphide beneficiation design to obtain improved yields during flotation. Furthermore, the insights from first-principles chemistry highlight the tools that may find useful application at mining operations for real-time determination of anticipated mineral behaviour. Here we have demonstrated the potential use of XRD, Raman spectroscopy, and UV-vis (or colour in hand specimen) for predicting flotation response. For hydrothermal ore deposits, it is likely that routine X-ray Fluorescence (XRF) analysis may provide sufficient insight into ambient mineral chemistry (e.g., Cd/Zn ratio (von der Heyden *et al.*, 2017)), however these relationships will need to be tested more rigorously in future research.

## ACKNOWLEDGEMENTS

The authors acknowledge the financial support provided by DST-CIMERA. We are further grateful to Dr Remy Bucker (iThemba Labs) and the staff at the Central Analytical Facility (Stellenbosch University) for their assistance with the XRD and SEM analyses respectively. We thank the reviewers who have substantially aided in strengthening this contribution.

## REFERENCES

Aghazadeh, S., Mousavinezhad, S.K., and Gharabaghi, M., 2015. Chemical and colloidal aspects of collectorless flotation behavior of sulfide and non-sulfide minerals. *Advances in Colloid and Interface Science*, 225, 203-217.

Bradshaw, D. (2014). The role of process mineralogy in improving the process performance of complex sulphide ores. *Proceedings of the XXVII International Mineral Processing Congress*, Santiago, Chile, 20-24 October. Gecamin, Santiago. pp. 1- 23.

Buzatu, A., Buzgar, N., Damian, G., Vasilache, V., and Apopei, A.I. (2013). The determination of the Fe content in natural sphalerites by means of Raman spectroscopy. *Vibrational Spectroscopy*, 68, 220-224.

Chandra, A.P. and Gerson, A.R. (2009). A review of the fundamental studies of the copper activation mechanisms for selective flotation of the sulfide minerals, sphalerite and pyrite, *Advances in Colloid and Interface Science*, 149, 97-110.

Chen, Y., Chen, J., and Guo, J. (2010). A DFT study on the effect of lattice impurities on the electronic structures and floatability of sphalerite. *Minerals Engineering*, 23, 1120-1130.

Cook, N.J., Ciobanu, C.L., and Williams, T. (2011). The mineralogy and mineral chemistry of indium in sulphide deposits and implications for mineral processing. *Hydrometallurgy*, 108 (3-4), 226-228.



Fragomeni, D., Boyd, L.J., Charland, A., Kormos, L.J., Lotter, N.O., and Potts, G. (2005). The use of end-members for grind-recovery modelling, tonnage prediction and flowsheet development at Raglan. *Proceedings of the Canadian Mineral Processors Operators Conference*, Ottawa, January 2005. pp. 75–98.

Gottlieb, P., Wilkie, G., Sutherland, D.N., Ho-Tun, E., Suthers, S., Perera, K., Jenkins, B., Spencer, S., Butcher, A., and Rayner, J. (2000). Using quantitative electron microscopy for process mineralogy applications. *JOM*, 52 (4), 24-25.

Harmer, S.L., Mierczynska-Vasilev, A., Beattie, D.A., and Shapter, J.G. (2008). The effect of bulk iron concentration and heterogeneities on the copper activation of sphalerite. *Minerals Engineering*, 21 (12–14), 1005-1012. doi: 10.1016/j.mineng.2008.02.014

Hope, G.A., Woods, R., and Munce, C.G. (2001). Raman microprobe mineral identification. *Minerals Engineering*, 14 (12), 1565–1577.

Kharbish, S. (2007). A Raman spectroscopic investigation of Fe-rich sphalerite: effect of Fe-substitution. *Physics and Chemistry of Minerals*, 34, 551–558.

Krauzman, M. (1968). Spectre Raman du second ordre de la blende ZnS. *Comptes Rendus Mathematique Academie des Sciences Paris, Series B.*, 1224–1226.

Kullerud, G. (1953). The FeS-ZnS system, a geological thermometer. *Norsk Geologisk Tidsskrift*, 32, 61–147.

Lane, D.J., Cook, N.J., Grano, S.R., and Ehrig, K. (2016). Selective leaching of penalty elements from copper concentrates: A review. *Minerals Engineering*, 98, 110-121.

Li, Y., Lu, A., Wang, C., and Wu, X. (2008). Characterization of natural sphalerite as a novel visible light- driven photocatalyst. *Solar Energy Materials & Solar Cells*, 92, 953-959.

Lotter, N.O., Kowal, D.L., Tuzun, M.A., Whittaker, P.J., and Kormos, L.J. (2003). Sampling and flotation testing of Sudbury Basin drill core for process mineralogy modelling. *Minerals Engineering*, 16, 857-864.

Lotter, N.O., Bradshaw, D.J., and Barnes, A.R. (2016). Classification of the major copper sulphides into semiconductor types, and associated flotation characteristics. *Minerals Engineering*, 96, 177–184. doi: 10.1016/j.mineng.2016.05.016

Lund, C., Lamberg, P., and Lindberg, T. (2013). Practical way to quantify minerals from chemical assays at Malmberget iron ore operations – An important tool for the geometallurgical program. *Mineral Engineering*, 49, 7-16.

McClung, C.R. and Viljoen, F. (2011). A detailed mineralogical assessment of sphalerites from the Gamsberg zinc deposit, South Africa: The manganese conundrum. *Minerals Engineering*, 24 (8), 930-938.

Neuvill, D.R., de Ligny, D., and Henderson, G.S. (2014). Advances in Raman spectroscopy applied to Earth and material sciences. *Spectroscopic Methods in Mineralogy and Materials Sciences*. Henderson, G.S., Neuvill, D.R., and Downs, R.T. (eds). *Reviews in Mineralogy and Geochemistry* 78. Mineralogical Society of America. Chantilly, VA. pp. 509–541.

Osadchii, E.G. and Gorbaty, Y.E. (2010). Raman spectra and unit cell parameters of sphalerite solid solutions ( $\text{Fe}_x\text{Zn}_{1-x}\text{S}$ ). *Geochimica et Cosmochimica Acta*, 74 (2), 568-573.

Pring A., Tarantino S.C., Tenailleau C., Ann, B., Carpenter M.A., Zhang M., Liu Y., and Withers R.I. (2008). The crystal chemistry of Fe-bearing sphalerites: an infrared spectroscopic study. *American Mineralogist*, 93, 591–597.

Rossmann, G.R. (2014). Optical spectroscopy. Spectroscopic methods in mineralogy and materials

sciences. *Reviews in Mineralogy and Geochemistry* 78. Henderson, G.S., Neuvill, D.R., and Downs, R.T. (eds.). Mineralogical Society of America, Chantilly, VA. pp. 371–398.

Rozendaal, A., Rudnick, T.K., and Heyn, R. (2017). Mesoproterozoic base metal sulphide deposits in the Namaqua Sector of the Namaqua-Natal Metamorphic Province, South Africa: a review. *South African Journal of Geology*, 120 (1), 153-186.

Rudnick, T-K. (2016). The genesis of the Swartberg base-metal sulphide deposit, South Africa. MSc thesis, University of Stellenbosch. 207 pp.

Schouwstra, R., de Vaux, D., Hey, P., Malysiak, V., Shackleton, N., and Bramdeo, S. (2010). Understanding Gamsberg – A geometallurgical study of a large stratiform zinc deposit. *Minerals Engineering*, 23 (11-13), 960-967.

Skinner, B.J. (1961). Unit-cell edges of natural and synthetic sphalerites. *American Mineralogist*, 46, 1399–1411.

Von der Heyden, B.P., Rozendaal, A., van Zyl, M.L., and Ukena, C. (2017). Controls on the distribution of the deleterious elements bismuth, cobalt and cadmium in the base metal sulphide deposits of the Mesoproterozoic Aggeneys-Gamsberg Ore District, South Africa. *Proceedings of the 14th Biennial Conference for the Society for Geology Applied to Mineral Deposits*, Quebec, Canada. SGA, Geneva, Switzerland. pp. 693-696.

Xu, Y. and Schoonen, M.A. (2000). The absolute energy positions of conduction and valence bands of selected semiconducting minerals. *American Mineralogist*, 85 (3-4), 543-556.

## Chapter five – Electro-kinetic studies

### Impacts of cation (Co, Cd, Fe) substitution on the geometallurgical response of sphalerite

A presentation of a prepared conference paper

The conference manuscript has been prepared and submitted to the Process Mineralogy 2018 conference which will be hosted by Minerals Engineering International in Cape Town on November 19-21, 2018. I am the lead author of the manuscript, and both Dr. M. Tadie and Dr. B.P. von der Heyden are listed as co-authors.

The manuscript provides key experimental insights into the surface reactivity of synthetic sphalerite under conditions relevant to flotation as a function of the incorporation of three different transition-metal impurities (Cd, Co and Fe). The interpretations presented in the manuscript are based on a thorough evaluation of the electro-kinetic results of sphalerite after the interaction with  $\text{CuSO}_4$  and Sodium Isobutyl xanthate (SIBX). Based on the electro-kinetic measurements presented in the paper. The impacts of three common transition-metal impurities on the flotation response of sphalerite are established. The zeta potential results presented herein were done in triplicates and the presented values are an average from the results. For consideration of the error between the results, error bars on each value is included to illustrate the standard deviation between the three values used.

The acquisition of the data and overall compilation of the manuscript was done by myself as the lead author. Both Dr. M. Tadie and Dr. B.P. von der Heyden contributed on the editing and strengthening of the final draft in their capacity as co-authors. The paper has been peer reviewed at SAIMM 2018 Geometallurgy conference and reviewers made only minor comments. However, the outcome from the peer-review process indicated that the work fell outside of the scope of a Geometallurgy conference and that the paper should instead be submitted to the Process Mineralogy 2018 conference.

# IMPACTS OF CATION (Co, Cd, Fe) SUBSTITUTION ON THE GEOMETALLURGICAL RESPONSE OF SPHALERITE

L. Babedi<sup>1\*</sup>, M. Tadie<sup>2</sup> and B.P. von der Heyden<sup>1</sup>

<sup>1</sup> Department of Earth Sciences, Stellenbosch University, Stellenbosch, South Africa

<sup>2</sup> Department of Process Engineering, Stellenbosch University, Stellenbosch, South Africa

(\*Corresponding author email: [21368546@sun.ac.za](mailto:21368546@sun.ac.za)).

The influence of cation substitution on the flotation response of sphalerite has been widely reported over the past decades with emphasis on the influence of iron but minimal attention on the impacts of other associated impurities. To further expand on this important research concept, sphalerite doped with three common transition-metal (Cd, Co and Fe) impurities was synthesized using a dry experimental method. The influence of each individual cation on the surface charge, Cu-activation and collector adsorption was assessed using electro-kinetic techniques (zeta potential) which provide valuable information on the surface reactivity of impurity bearing sphalerite. The study illustrates different electro kinetic characteristics of sphalerite depending on the nature of the substituting metal resulting in multiple surface products. The study illustrates that maximum recovery of zinc requires a thorough multidisciplinary study and fundamental understanding of the impacts of individual cation substitution on mineral surface reactivity.

## INTRODUCTION

Sphalerite, the main source of zinc metal, commonly occurs in close association with other sulphide minerals (e.g., chalcopyrite, galena) and is found in a variety of base metal sulphide deposits. Sphalerite is known to incorporate varied amounts of transition-metal impurities (e.g. Fe, Mn etc.) through cation substitution reactions (Liu et al., 2014). The beneficiation of sphalerite is typically carried out using flotation technologies (Harmer et al., 2008), which allows the exploitation of previously uneconomical low-grade ores (Bicak and Ekmekci, 2012). The hydrophobic characteristics of sphalerite are induced by reactions involving the attachment of collector molecules such as xanthates moieties. This is particularly successful after sphalerite surface activation caused by the adsorption of Cu ions (Ejtemaei and

Nguyen, 2017, Chandra and Gerson, 2009). The activation process is exceedingly important because the non-activated sphalerite has a wide band gap which results in a low collector adsorption due to the slow electron transfer (Ejtemaei and Nguyen, 2017). In addition, the instability of the zinc-xanthate complexes results in the activation process being a crucial step in sphalerite flotation (Chandra and Gerson, 2009). The actual mechanism and the resultant surface products during copper activation and collector adsorption have been the subject of contrasting results over the years. The interpretation of the contrasting results is largely attributed to the chemistry of sphalerite, with more emphasis attributed to the effects of the contained iron concentration.

Several studies have investigated the impacts of surface oxidation, activator ions, concentration of activators and collector, pH, conditioning time, and iron concentration during copper activation and collector adsorption (Popov and Vucinic, 1990, Harmer et al., 2008, Albrecht et al., 2016). The influence of iron during the flotation of sphalerite has been thoroughly investigated with contrasting findings reported. Makherjee and Sen (1976) report that at pH 3 – 7, an unactivated high iron-bearing sphalerite showed great floatability. Chen et al. (2012) and Boulton et al. (2005) illustrated that the high iron concentration effectively lowered the Cu activation, consequently leading to low flotation recovery. Conversely, Nefedov et al. (1980) reported increased extent of Cu activation with increasing iron concentration. Harmer et al. (2008) suggested that the reported and contrasting findings may largely be attributed to factors associated with conditioning solution, or that may be due to the influence of metal impurities other than Fe.

The selective separation of sphalerite by flotation is based on its hydrophobic characteristics, which can either be natural or induced. Achieving maximum induced hydrophobicity/floatability requires attaching flotation collectors on the surface of the target mineral (Smit and Gnoinski, 2000). Xanthate ions (O-alkyldithiocarbonate, ROCS-2) are frequently used as collectors in sulphide mineral flotation, and thus in sphalerite flotation from different orebodies (Harmer et al., 2008). The semi-conducting properties of sphalerite implies that the reaction responsible for creating a hydrophobic surface is electrochemical (Smit and Gnoinski, 2000). The reaction involves the oxidation of xanthate ions to form a more hydrophobic ions on the mineral surface,

with the oxidation being driven by reduction of oxygen (Smit and Gnoinski, 2000). The general mechanism for Cu activation and the consequent collector adsorption is firstly an ion exchange reaction of Zn with Cu ions to form a Cu-S surface. In the presence of xanthate the Cu surface forms metal xanthates species through surface adsorption or bonding reactions. Finally the surface reduction of oxygen to drive the oxidation of CuROCS-2 to form CuROCS and Dixanthogen (Abrecht et al., 2016, Popov and Vucinic, 1990, Chandra and Gerson, 2009).

The current study forms part of a broader study that seeks to illustrate the use of molecular-level interrogations to better understand and predict the flotation response of sphalerite. This study investigates the impacts of three common transition-metal impurities (Co, Fe, Cd) commonly substituted for Zn in lattice sites of sphalerite. This is achieved by evaluating the influence of those impurities on the surface reactivity of sphalerite as reflected by electro-kinetic studies under flotation related conditions (Cu-activation and collector adsorption). The flotation response as observed in this paper will later be correlated to the molecular-level investigations to better understand improve the understanding of the multiple flotation responses as seen in natural sphalerite containing some of the transition-metal impurities and provide an improved predictability during process design.

## **EXPERIMENTAL**

### **Synthesis of Impurity-doped Sphalerite**

A series of impurity doped sphalerites was synthesised using a dry experimental method for sulphide synthesis (e.g., Kullerud, 1971; Kojima and Sugaki, 1984; Pring et al., 2008). This methodology enables a controlled chemical composition of the final product, through careful and stoichiometric mixing of the constituent elements according to the mineral formula  $MxZ_{1-x}S$  (where M represents the trace metal impurities Co, Fe and Cd). Dopant concentrations ranged between 0 – 4 wt. % for Cd, and between 0 – 1 wt.% for Co (Table 1). All syntheses were conducted at the Experimental Petrology Laboratory at Stellenbosch University, using high purity starting materials procured from Sigma-Aldrich (zinc powder (<150  $\mu$ m, 99.995% trace metal basis), sulphur (trace metal grade >99.99%), cobalt metal powder (<150  $\mu$ m,

>99.99% trace metal basis), cadmium powder (<150  $\mu\text{m}$ , >99.99% trace metal basis), and iron powder (25  $\mu\text{m}$ , > 99.99%).

### **Chemical Characterization**

A set of analytical techniques were used to assess the chemical purity, homogeneity and phase identification of each synthetic sample. The chemical purity and homogeneity was firstly assessed using reflected light microscopy (Nikon Labophot Microscope). Samples were subsequently analysed for elemental distribution using a Zeiss EVO Scanning Electron Microscopy (backscatter and Wavelength Dispersive Spectroscopy (WDS)) operated with an accelerating voltage of 20kV and current of between -19 nA to -21 nA. The elemental mapping confirmed that the reacting phases are distributed evenly without metal zonation, while spot analyses confirmed that no foreign phases were present and showed that the reacting phases retained a sphalerite stoichiometric composition (Table 1). Mineralogical purity was further confirmed using X-ray powder Diffraction (XRD) on a Bruker D8 Powder Diffractometer machine at iThemba Labs, Cape Town, South Africa. Synthetic crystallites were ground to a top size of 50  $\mu\text{m}$  and evaluated for mineral composition and possible spectrum shifts using  $2\theta$  data collection at step size of 0.0340. The XRD data collection was operated at an accelerating voltage of <40 kV and current of 25 mA for Cu K $\alpha$  radiation. The reduction and phase identification was performed using PANalytical X'pert HighScore Plus software.

### **Zeta Potential Measurements**

The zeta potential distribution measurements were collected using a Malvern Zetasizer Nano ZS instrument (University of Cape Town, South Africa). The stock solutions for zeta potential measurements were prepared from analytical grade reagents. Freshly prepared 0.001 M KNO<sub>3</sub> was used as the background electrolyte, with the pH regulated with 0.01 M HCl and 0.01 M NaOH stock solutions. Each sample was ground under acetone using a mortar and pestle to ensure a nominal top-size of <50  $\mu\text{m}$ . After sample drying, a small sub-sample (0.01 g) was transferred into a 15 ml test tube containing 10 ml of 0.001 M KNO<sub>3</sub>. This mixture was shaken vigorously and allowed to condition for 10 min before transferring 2 ml of an aliquot into an electrophoretic cell. For activation and collector adsorption,  $1 \times 10^{-4}$  M of both CuSO<sub>4</sub>



and sodium isobutylxanthate in solution was achieved by adding separately 10  $\mu\text{L}$  of each 0.1 M stock solution ( $\text{CuSO}_4$  and sodium isobutylxanthate) to the 10 ml electrolyte solution with sample and allowed to condition for 10 min. For these experiments, the pH was slightly alkaline ( $\text{pH} \pm 9$ ) and the temperature was controlled at  $25^\circ\text{C}$  for Cu activation and collector adsorption, while unactivated samples were analysed in both acidic and alkaline medium.

## RESULTS AND DISCUSSION

### Chemical Characterization

The doped and pure sphalerite samples synthesized at  $900^\circ\text{C}$  for 7 days showed a homogenous distribution of the various element constituents (Table 1), and their purity was further confirmed by their X-ray diffraction (XRD) patterns. The XRD spectra reflected three prominent diffraction peaks at  $2\theta$  angles of approximately  $28.5^\circ$ ,  $47.5^\circ$ , and  $56.6^\circ$  which are respectively attributed to the 111, 220 and 311 planes of the cubic ZnS mineral structure. The absence of extra peaks indicates that there are no extraneous phases (e.g., wurtzite, zinc oxide) present, and this confirms the mineralogical homogeneity. Relative to pure sphalerite, the impurity doped sphalerites showed minor shifts in the XRD peak positions, indicating small changes to the unit cell parameter resulting from the distortions induced by cation substitution reactions.

**Table 5.1:** Average Scanning Electron Microscopy (SEM) elemental spot analyses for the samples. All values reported in weight percentage and values in parentheses reflect the standard deviation.

Sample	Zn (wt. %)	S (wt. %)	Co (wt. %)	Cd (wt. %)	Fe (wt. %)
ZnS	66.93 ( $\pm 0.42$ )	33.07 ( $\pm 0.42$ )	-	-	-
(Co <sub>0.6</sub> ,Zn <sub>99.4</sub> )S	68.11 ( $\pm 1.70$ )	31.52 ( $\pm 1.68$ )	0.36 ( $\pm 0.05$ )	-	-
(Co <sub>0.9</sub> ,Zn <sub>99.1</sub> )S	66.47 ( $\pm 1.32$ )	32.95 ( $\pm 1.37$ )	0.56 ( $\pm 0.06$ )	-	-
(Co <sub>1.1</sub> ,Zn <sub>98.9</sub> )S	68.08 ( $\pm 1$ )	31.2 ( $\pm 0.98$ )	0.71 ( $\pm 0.05$ )	-	-
(Cd <sub>0.9</sub> ,Zn <sub>99.1</sub> )S	65.66 ( $\pm 1.49$ )	33.2 ( $\pm 1.61$ )	-	1.02 ( $\pm 0.28$ )	-
(Cd <sub>1.8</sub> ,Zn <sub>98.2</sub> )S	65.54 ( $\pm 0.26$ )	32.45 ( $\pm 0.32$ )	-	2.01 ( $\pm 0.08$ )	-
(Cd <sub>3.3</sub> ,Zn <sub>96.7</sub> )S	62.89 ( $\pm 0.32$ )	33.42 ( $\pm 0.56$ )	-	3.68 ( $\pm 0.1$ )	-
(Fe <sub>0.9</sub> ,Zn <sub>99.1</sub> )S	65.93 ( $\pm 1.2$ )	33.29 ( $\pm 0.2$ )	-	-	0.77 ( $\pm 0.35$ )
(Fe <sub>1.8</sub> ,Zn <sub>98.2</sub> )S	64.74 ( $\pm 0.72$ )	33.20 ( $\pm 0.06$ )	-	-	2.07 ( $\pm 0.83$ )
(Fe <sub>3.3</sub> ,Zn <sub>96.7</sub> )S	63.77 ( $\pm 0.49$ )	32.82 ( $\pm 0.1$ )	-	-	3.41 ( $\pm 0.67$ )

## Zeta potential distribution of un-activated impurity bearing sphalerite samples conditioned in both acidic and alkaline media

Zeta potential measurements were conducted to assess the variation in surface charge of sphalerite as a function of the concentration of different substituting impurities (Co, Fe and Cd). The zeta potential distribution results show that based on the chemical nature of the substituting transition-metal impurity, sphalerite exhibits differences in surface charge. In un-activated sphalerite, the magnitude of the negative zeta potential for Cd- and Fe- bearing samples shows similar trends, i.e. increasing from acidic pH to alkaline pH. Conversely, the zeta potential of Co-bearing sphalerite becomes almost neutral, with no change with an increase in impurity concentration and pH.

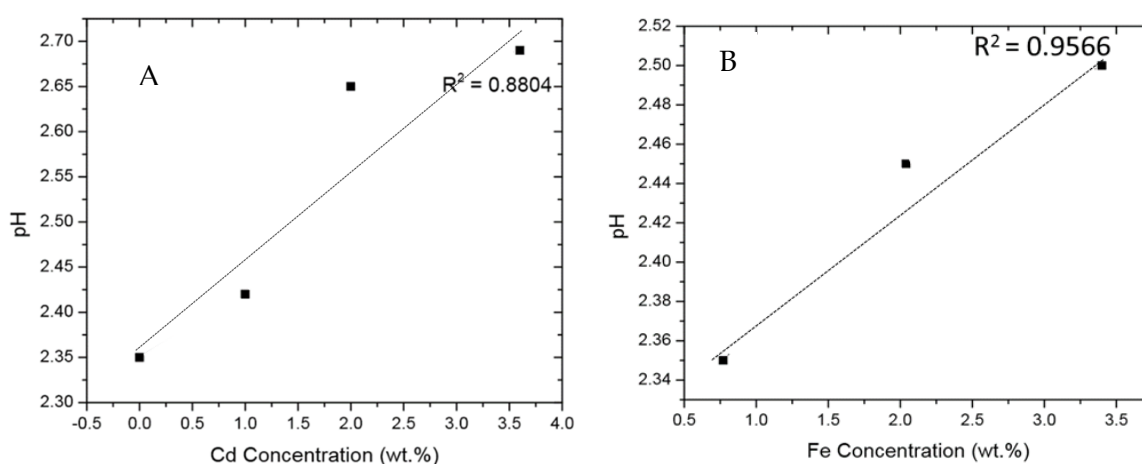


**Figure 5.1a-b:** Correlation between the iso-electric point and the concentration of both iron and cadmium.

The point at which surface charge reversal occurs (the iso-electric point) for an un-activated sphalerite is a well-documented concept with contrasting results reported. Popov and Vucinic, (1990) reported the iso-electric point (iep) for a sphalerite with 13 wt.% Fe at 6.5, Zhang et al., (1992) reported an IEP at 2.5 for sphalerite sample containing 2.8 wt.% Fe, while Albrecht et al., (2016) reported iep less than 4 for a sphalerite containing 0.18 wt.% Fe and variable trace elements. A natural sample with varied amount impurities had an iep at around 3.55, in agreement to the reported iep for natural sphalerite. From figure 1a-b, it is observed that increasing the concentration

of both Fe and Cd results in a shift of the iso-electric point of sphalerite to higher pH. The pure sphalerite exhibits the lowest iep with respect to the impurity bearing sphalerites. For the cobalt bearing samples, an iep was only obtained for the 0.36 wt.% sample at around pH 6. For the samples with > 0.36 wt.% Co, it was not possible to obtain the iep but it is assumed to occur at higher pH compared to the 0.36 wt.%. The correlation between the iso-electric point and impurity concentration is shown in figure 1, a positive correlation ( $r^2=0.96$  for Fe and  $r^2=0.88$  for Cd) between the iso-electric point and impurity (Cd, Fe) concentration is observed. The results presented herein for Cd- and Fe- bearing samples show similar trends as reported by the above mentioned studies on natural sphalerite, i.e. with increasing impurity concentration the iep shift to higher pH.

Popov and Vucinic, (1990) stated that the variation in pH of the iep was largely due to the impurity concentration, solids percentage within a mineral suspension and the duration for conditioning. Based on the different zeta potentials obtained, we also consider the chemical nature of the incorporated impurity to play a pivotal role on the surface characteristics of sphalerite. This is illustrated by the wide differences between zeta potentials of samples with high impurity content (Cd-, Fe-) compared to low Co-bearing samples. The Co-bearing sphalerite exhibited a close to neutral surface charge, with an iep at pH 6 observed only for the sample containing 0.36 wt. % Co. The contrasting behaviour of Co as compared to Cd and Fe illustrate that inclusion of a highly polar atom like Co can not only affect the molecular cluster local structure but also affects the interaction between the parent molecular cluster and incorporated impurity atom. The ability of Co to attract electron density (dipole moment) in the valence orbital affects the distribution of the surface charge of sphalerite thus reflected by the nearly neutral zeta potential.

### **Impacts of impurities on the surface properties of sphalerite in the $\text{CuSO}_4$ activated system**

The effect of impurities on the activation of sphalerite with Cu ions has been a widely researched topic in recent times with several studies reporting contrasting results. Chen et al. (2012) and Boulton et al. (2005) illustrated that the high iron concentration effectively lowered the Cu activation, consequently leading to low flotation recovery.

Conversely, Nefedov et al. (1980) reported a high Cu activation with increasing iron concentration. A large proportion of those studies have focused on the role played by iron content on the Cu activation. The results presented herein assessed the influence of different impurities (Co, Cd and Fe) on the electro kinetic (zeta potential) measurements of a Cu-activated impurity bearing sphalerite in alkaline media. Electro kinetic techniques can be employed to detect surface activation products of sphalerite as illustrated by the different surface charge exhibited by the zeta potential distribution (Laskowski et al., 1997).

The zeta potential values of impurity bearing sphalerite samples activated with  $\text{CuSO}_4$  in an alkaline ( $\text{pH} = 9$ ) solution after conditioning for 10 minutes are shown in figures 2. The results presented in figure 2a-b show that the zeta potential increases with increasing impurity concentration. The increase in the zeta potential for both Cd- and Fe- bearing sphalerite is positively and strongly correlated to increasing impurity concentration, with  $r^2=0.97$  for Cd- and  $r^2=0.99$  for Fe-bearing sphalerite. The Co bearing samples up to 0.56 wt.% shows similar trends to both the Fe and Cd samples, whereas at higher cobalt concentration the zeta potential decreases. The trend in zeta potential across the different sets of samples varied showing the trend  $\text{Fe} > \text{Cd} > \text{Co}$ .

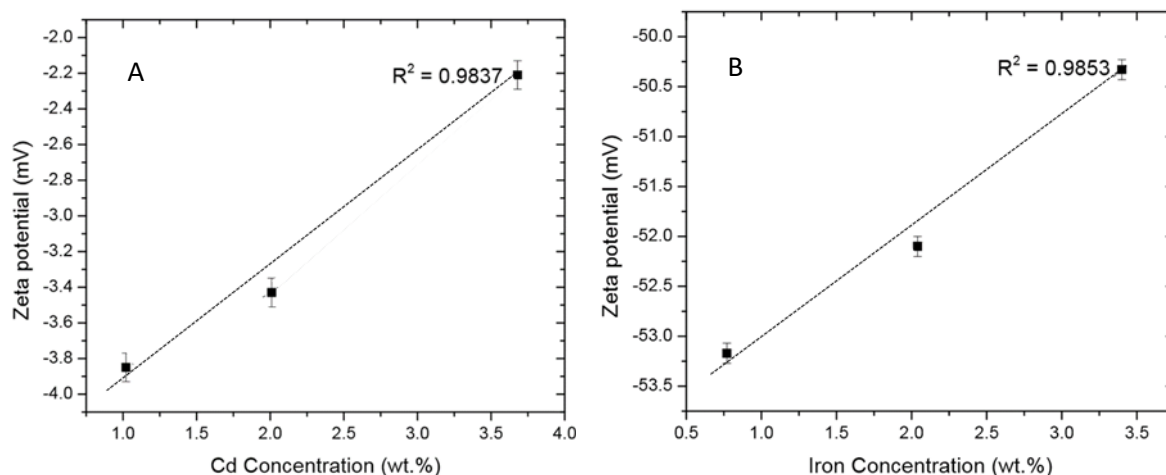


**Figure 5.2a-b:** Zeta potential distribution for Cu-activated impurity bearing sphalerite in alkaline media at pH 9. A represents Cd-sphalerite, while B represents Fe-sphalerite. The magnitude of the negative zeta potential for each sample is different for each set thus not allowing a direct comparison between figure 5.2a and 5.2b.

Several studies have introduced different models to describe the reaction mechanisms occurring during Cu activation. Each of these models highlight the presence of Cu ions at the mineral surface (Gerson et al., 1999, Popov and Vucinic, 1990). The variation of the zeta potential between un-activated and Cu-activated sphalerite is attributed to the product layers on the mineral surface in alkaline media. The change in the zeta potential illustrates the presence of Cu ions on the surface of an impurity-bearing sphalerite (Albrecht et al. 2016). The magnitude of the negative zeta potential for both Fe and Cd activated samples is lower than the negative zeta potential values obtained for un-activated samples. Conversely, the Co samples showed increased negative zeta potential values for the activated samples versus the un-activated Co samples. The negative zeta potential values are lowered with an increase in impurity concentration, indicative of limited available sites for Zn and Cu ion exchange. This can also be attributed to the minimal change on the surface characteristics, thus permitting the electrostatics controlling the Cu ions absorption. Chen et al. (2012) studied the effects of lattice defects due to the incorporation of metal impurities (Fe, Cu and Cd) on sphalerite surface and the consequent copper activation. Their study illustrated that the copper activation of Fe-substituted sphalerite is difficult, since Cu atoms cannot replace the Fe, thereby decreasing the Zn and Cu exchange sites for a Fe-bearing sphalerite. The results presented herein for the un-activated experiments show that the electron withdrawing capabilities of a highly polar element like Co result in the neutralization of the surface charge of sphalerite. The negative zeta potential values exhibited by the Co-bearing sphalerite reflects the presence of the Cu ions on the mineral surface whose magnitude decreases with increased Co concentration.

### **Copper activation-pH of flotation onset**

Hukki et al. (1952) illustrated the zeta potential distribution of sphalerite in both acidic and alkaline media, noting multiple charge reversals with an increase in pH. James and Healy (1972) plotted the zeta potential against pH in the presence of a hydrolysable metal (Cu) ion and obtained three points of charge reversals, naming them Charge Reversals CR1, CR2 and CR3. They interpreted CR1 as the pH (acidic pH) for iep of the mineral, CR2 was the pH (neutral pH) for the electric field induced

surface precipitates, while CR3 is the pH (alkaline pH) associated with the nucleation of the metal hydroxide on the surface. In industrial practice, the flotation of sphalerite is carried in alkaline media in the presence of hydrolysable metal ions (Cu ions) which correspond to CR 3. Thus it is of value to establish the critical onset pH (CR3) for flotation of an activated sphalerite in alkaline media and its relation to impurity concentration. The zeta potential for the different Cu activated impurity-bearing synthetic sphalerite samples was measured between pH 7 and pH 9.4 in order to interrogate the effect of the impurities on the third charge reversal point which is termed the critical onset pH suitable for flotation. The zeta potential for an activated natural sample shows that below pH 5.5, the zeta potential becomes negative indicating the first region of flotation in neutral/acidic media. Above the pH the zeta potential becomes positive until pH 8.57, which is set as the third onset pH of flotation under alkaline media as illustrated by the negative zeta potential attained above 8.57 (Figure 5.3).

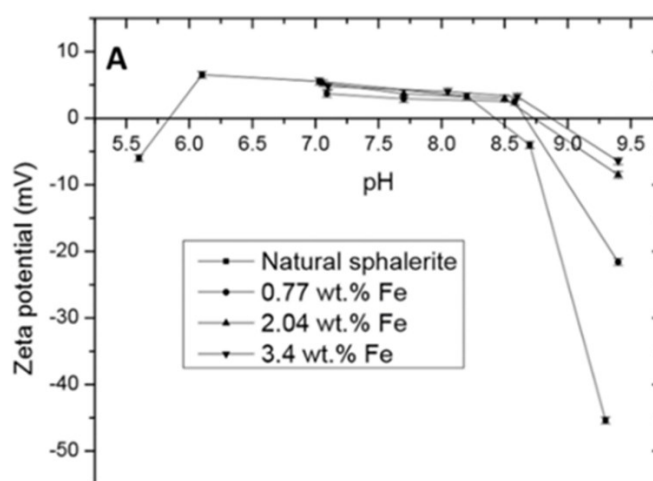


**Figure 5.3:** The variation on the onset pH of flotation with increasing iron concentration within an activated sphalerite conditioned in alkaline media.

Both Fe and Cd-bearing samples results show similar trends i.e. increasing the impurity concentration shifts the critical pH point to higher pH. The dependence of the critical onset pH point of flotation on the impurity concentration is shown in figure 4 by a positive correlation ( $r^2 = 0.99$  for Fe and  $r^2 = 0.75$  for Cd). The Co-bearing samples shows an opposite relation between the critical pH point and impurity concentration as

observed for both Fe- and Cd-bearing samples. Unlike both Fe and Cd, the Co samples (Figure 5.4) have high critical pH points which shift to lower pH with increases in Co concentration. The shift from high pH to low pH of the critical point for flotation of cobalt-bearing samples is correlated ( $r^2=0.91$ ) to increasing Co concentration (Figure 5.4). The values of the  $R^2$  presented herein for the metal impurities illustrate a strong correlation between the impurity concentrations and the onset pH. The linear correlation established (see figure 5.4) for both Cd and Fe confirms that increasing the concentration for both metal impurities increased the onset pH flotation. While a strong negative correlation was established between Co concentration and onset pH, where the Co content lowered the pH.

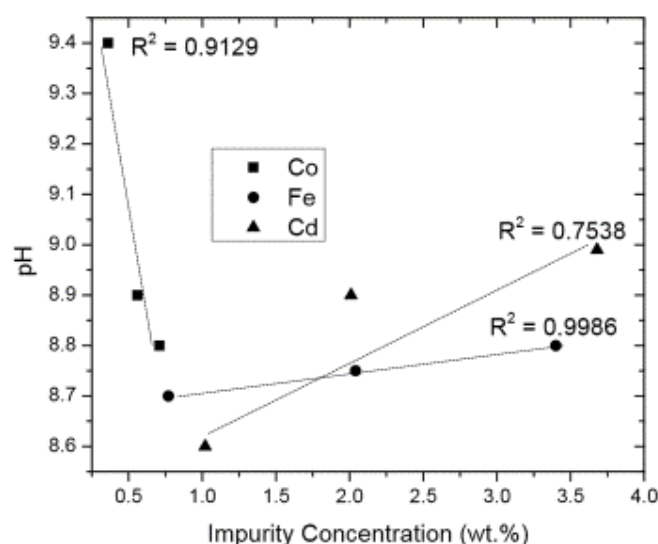


*Figure 5.4: Correlation between the impurity concentration and the change in the critical pH point suitable for flotation in alkaline media.*

### **Influence of transition-metal impurities on collector adsorption**

The influence of impurities during the adsorption of xanthate ( $1 \times 10^{-4}$  M) on the surface of an activated impurity-bearing synthetic sphalerite conditioned in alkaline media (pH 9) is shown in figures 5.5a-b as zeta potential values. The adsorption of xanthate ions ( $EX^-$ ) on the surface of a Cu-activated impurity bearing sphalerite samples showed different behaviour which was dependant on the nature of the substituting metal

impurity for both Co- and Fe-bearing sphalerite, while Cd-bearing sphalerite showed dependence also on impurity concentration. Zeta potential values for both Fe- and Co-bearing samples after conditioning with xanthate remained unchanged across the different impurity concentrations.

Popov and Vucinic, (1990) reported that the adsorption of  $EX^-$  ions on the surface of a Cu-activated sphalerite had no effect on the zeta potential distribution. While the zeta potential distribution for Cd-bearing samples (figure 5.5a) shows a clear correlation ( $r^2=0.99$ ) with the Cd concentration, while both Fe (figure 5b) and Co show no correlation. The different results between the Co-, Fe- with the Cd-bearing sphalerite can be attributed to the influence of the individual impurity on the nucleophilic and electrophilic characteristic of sphalerite (Chen et al., 2010). Based on the Density-Functional Theory results reported by Chen et al. (2010) both Co and Fe will affect the nucleophilic character of sphalerite, while Cd affects the electrophilic character. These will result in a difference in the resultant surface reactions as reflected by the different zeta potential distribution for 3d elements (Co, Fe) and a 4d element (Cd).

The treatment of an activated pure sphalerite with  $EX^-$  resulted in a low negative zeta potential. This can be related to the low flotation recovery achieved by Chen et al. (2012) who explained such behaviour because of the wide band gap exhibited by a pure sphalerite. This results in non-adsorption of oxygen on the mineral surface thus resulting in low rate of xanthate oxidation. Liu et al. (2014) and Popov and Vucinic, (1990) indicated that the interaction between sphalerite, Cu ions and  $EX^-$  in alkaline medium resulted can be expressed in three step reaction mechanisms which include: firstly,  $EX^-$  interaction with Cu ions, followed by the decomposition of Cupric-xanthate to form both Cu- $EX^-$  and dixanthogen occurring at the same time as the reduction of oxygen. Chen et al., 2012 observed both metal xanthate and dixanthogen on the surface of Cd-bearing sphalerite while dixanthogen was absent on Fe-sphalerite surface. The similar trend of both Fe and Co-bearing sphalerite illustrate that both elements induces similar surface species which is associated with the absence of dixanthogen. Conversely, it is assumed that the electrocatalytic capabilities of sphalerite is increased, thus aiding the formation of metal xanthate species and



dixanthogen on Cd-bearing sphalerite surface. The suppressing effect of Cd is noticed with increase in concentration.

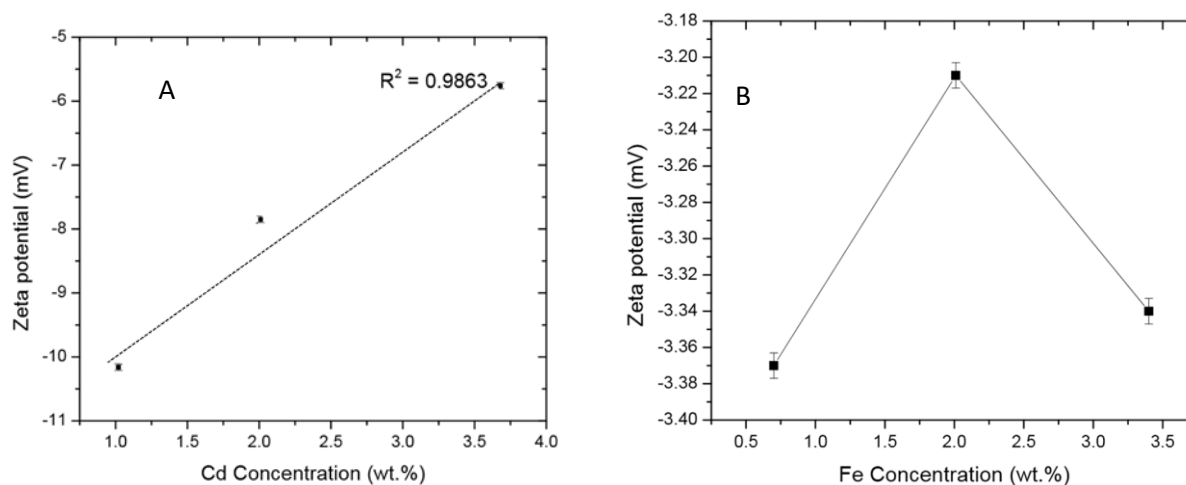


**Figure 5.5:** Zeta potential distribution for different impurity bearing synthetic sphalerite conditioned in an electrolyte solution containing  $1 \times 10^{-4}$  M xanthate and  $1 \times 10^{-4}$  M  $\text{CuSO}_4$  in a 1:1 ratio. Figure 5a-b represents Fe- and Cd-bearing samples respectively.

### Implications to sphalerite flotation and process design

Sphalerite in flotation plants exhibits a low hydrophobic character and thus requires chemical treatment to induce/increase its hydrophobicity (Aghazadeh et al., 2015). This involves the treatment with activator ions (Cu) prior to collector adsorption in an alkaline media, with operations occurring around pH 9. Based on the results presented herein, understanding of the mineral chemistry will permit careful pH adjustment to aid flotation of sphalerite. The different critical onset pH of flotation as a function of the three different impurities implies that operational pH of sphalerite is dependent on the nature of the impurity metals associated with sphalerite. Improving metal recovery from impurity bearing sphalerite requires a high-level understanding of the chemical nature of the substituting metal ions as this also has a bearing on the hydrophobic species on the mineral surface during collector adsorption.

### CONCLUSION

Using an electro-kinetic technique (Zeta potential measurements) the current study has evaluated the influence of cation (Co, Fe and Cd) substitution on the surface reactivity of synthetic sphalerite under flotation related conditions. The results obtained illustrate that the multiple flotation responses of sphalerite as reported in the scientific literature can be attributed to the difference in the transition-metal impurity concentration and their chemical nature. The chemical nature of the substituting metal ion further affects the surface reactivity of sphalerite, and the degree of this influence can be related to the electronegativity of the substituting ion (e.g., Co has a greater influence on sphalerite surface charge than Cd). In alkaline media, the adsorption of Cu ions abstracted from  $\text{Cu}(\text{OH})_{2(\text{aq})}$  (the stable Cu species at pH 9), improves the surface reactivity of sphalerite as illustrated by the negative zeta potential attained by a Cu-activated Co-sphalerite which had a neutral surface charge when un-activated. The onset pH of flotation in an alkaline media showed dependence on the nature of the impurity. The electro-kinetic results revealed different onset pH values for the three-impurity bearing sphalerite sets of samples i.e. Fe and Cd shifts the onset pH to higher values while Co shift the onset point to lower pH. The difference in the chemical nature of the substituting metal also resulted in different surface product during collector adsorption as reflected by the variation in the zeta potential distribution of the three impurity bearing samples. Those variations are attributed to the impacts of the metal impurities on the nucleophilic and electrophilic characteristic of the sphalerite during the collector-mineral interaction. The results presented herein thus illustrate the importance of careful consideration of individual cationic substitution, even at low concentration in complex mineral systems. We maintain that a full and fundamental understanding of the molecular-level dynamics will be crucial towards designing the most efficient beneficiation streams for ores produced from the “Mine of the Future”.

## **ACKNOWLEDGMENTS**

The authors acknowledge the financial support provided by DST-CIMERA and Society of Economic Geology. The authors are further grateful to Dr Remy Bucker (iThemba Labs) and the staff at the Central Analytical Facility (Stellenbosch University) for their assistance with the XRD and SEM analysis respectively.

## **REFERENCE**

Aghazadeh, S., Mousavinezhad, S.K., Gharabaghi, M., 2015. Chemical and colloidal aspects of collectorless flotation behavior of sulfide and non-sulfide minerals. *Advances in Colloid and Interface Science*, Vol. 225, pp 203-217.

Albrecht, T.W.J., Addai-Mensah, J., Fornasiero, D., 2016. Critical copper concentration in sphalerite flotation: Effect of temperature and collector. *International Journal of Mineral Processing*, Vol. 146, pp 15-22.

Bi, C., Pan, L., Xu, M., Yin, J., Guo, Z., Qin, L., Zhu, H., Xiao, Q.J., 2009. Raman spectroscopy of Co-doped wurtzite ZnS nanocrystals. *Chemical Physics Letter*, Vol. 481, pp 220-223.

Boulton, A., Fornasiero, D., Ralston, J., 2005. Effect of iron content in sphalerite on flotation. *Minerals Engineering*, Vol. 18, pp 1120–1122.

Chandra, A.P., Gerson, A.R., 2009. A review of the fundamental studies of the copper activation mechanisms for selective flotation of the sulfide minerals, sphalerite and pyrite, *Advances in Colloid and Interface Science*, Vol.149, pp 97-110.

Chen, Y., Chen, J., Guo, J. 2010. A DFT study on the effect of lattice impurities on the electronic structures and floatability of sphalerite. *Mineral Engineering*, Vol. 23, pp 1120-1130.

Chen, Y., Chen, J., Lan, L., Yang, M., 2012. The influence of impurities on the flotation behaviours of synthetic ZnS. *Mineral Engineering*, Vol. 27-28, pp 65-71.

Ejtemaei, M., Nguyen, V.A., 2017. A comparative study of the attachment of air bubbles onto sphalerite and pyrite surfaces activated by copper sulphate. *Mineral Engineering*, Vol. 109, pp 14-20.

Harmer, S.L., Mierczynska-Vasilev, A., Beattie, D.A., Shapter, J.G., 2008. The effect of bulk iron concentration and heterogeneities on the copper activation of sphalerite. *Minerals Engineering*, Vol. 21, pp 1005-1012.

Laskowski, J.S., Liu, Q., Zhan, Y., 1997. Sphalerite activation: flotation and electrokinetic studies. *Mineral Engineering*, Vol. 10, pp 787-802.

Liu, J., Wen, S., Deng, J., Chen, X., Feng, Q. 2014. DFT study of ethyl xanthate interaction with sphalerite (110) surface in the absence and presence of copper. *Applied Surface Science*, Vol. 311, pp 258-263.

Mukherjee, A.D. and Sen, P.K., 1976. Flotability of sphalerite in relation to its iron content. *J. Mines, Metals, Fuels*, Oktober: 327.

Nefedov, V.I., Salyn, Ya.V., Solozhenkin, P.M., Pulatov, G.Yu., 1980. X-ray photoelectron study of surface compounds formed during flotation of minerals. *Surface and Interface Analysis*, Vol 2, pp 170–172.

Popov, S.R., Vucinic, D.R., 1991. The ethylxanthate adsorption on copper –activated sphalerite under flotation-related conditions in alkaline media. *International Journal of Mineral Processing*, Vol. 30, PP 229-244.

Smit, J.T., Gnoinski, J., 2000. *Electrochemistry: Contaminant Ions and Sulphide Mineral Interactions*. Unplished.

Zhang, Q., Rao, S.R., Finch, J.A. 1992. Flotation of sphalerite in the presence of iron ions. *Colloids and Surfaces*, Vol. 66, pp 81-89.

## Chapter Six – Discussion

The chapter expands on the prior understanding presented in both chapter 4 and chapter 5 by tying the two chapters into a comprehensive knowledge of the influence of metal impurities on sphalerite. This section presents a detailed discussion of the influence of three metal impurities on the bulk structure, surface characteristics, and electronic structure and how such variations influence the flotation response of sphalerite. Table 6.1 summarises the key observations from both chapter 4 and 5 and relates these to the physico-chemical characteristics of the substituting transition metal impurity. The chapter also illustrates how the nature of the surface bonding environment impacts the electronic structure of the sphalerite surface which in turn controls the interaction of sphalerite with flotation reagents (i.e., Cu-activators and collectors). The systematic evaluation presented herein illustrates how molecular-level investigations can be related to flotation response, and the findings have strong implications for enabling predictive capabilities during process design. The chapter begins by evaluating the impacts of a 4d metal (Cd) and compare such influence on the pure sphalerite, this is because both Zn and Cd have similar electronic structure and any changes induced by Cd would easily be noticed and explained. Based on the differences between a 4d and 3d metal impurities, the chapter proceed to discussing the major differences of the impacts of a 4d (Cd) metal impurity and 3d (Co and Fe) metal impurities. The penultimate section herein is the overall inter-relation of the bulk structure, surface bonding and electronic structure, and how they can relate to the flotation response of sphalerite. The last point covered is an illustration of the implication of cation substitution to sphalerite flotation and process design.

**Table 6.1:** Summary of the influence of metal impurities on the structure, surface bonding, electronic structure and flotation response of sphalerite.

Metal impurity	Ionic radius (pm)	Electro negativity	Electronic structure	Unit cell parameter	Bond length	Bond strength	Vibrational Energies	Band gap	Un-activated	Cu-activated	Cu-activation+ xanthate
Zn	88.0	1.65	[Ar] 4d <sup>10</sup> 5s <sup>2</sup>	lowest	longest	weakest	smallest	Wide	No influence	No influence	Weak interaction
Cd	109.0	1.69	[Kr] 4d <sup>10</sup> 5s <sup>2</sup>	Highest	long	weak	small	wide	Minimal influence	Minimal influence	Low influence
Co	88.5	1.88	[Ar] 3d <sup>7</sup> 4s <sup>2</sup>	lowest	shortest	strongest	highest	narrowest	High influence	Minimal influence	Highest influence
Fe	92.0	1.83	[Ar] 3d <sup>6</sup> 4s <sup>2</sup>	low	short	strong	High	narrow	Minimal influence	Minimal influence	High influence

## **The impacts of the Cd on the structure, surface bonding, electronic structure and flotation response of sphalerite.**

### **Influence of Cd on the bulk structure and surface bonding of sphalerite**

The isoelectric substitution of different transition-metal impurities is known to impact the bulk structure of sphalerite (Skinner, 1961, Barton and Toulmin, 1966, Lepetit et al., 2003, Harmer et al., 2008, Chen et al., 2010, Osadchii and Gorbaty, 2010, Buzatu et al., 2013, Chareev et al., 2017). The results presented in Chapter 4 and Appendix III illustrate that an increased Cd concentration induces X-ray diffraction line broadening, which results in changes to the unit cell parameter. The incorporation of Cd resulted in a linear increase of the unit cell parameter of sphalerite. The relationship between sphalerite chemical composition (i.e. Cd concentration) and the crystal distortions are reflected by the linear relationship ( $r^2= 0.9857$ ) between the unit cell parameter and Cd concentration. This agrees with several reported evaluations of unit cell parameters, which showed a consensus that increasing metal impurity concentration resulted in a linear increase of the unit cell parameters (Skinner, 1961, Osadchii and Gorbaty, 2010, Chareev et al., 2017). Despite the clear correlation between the unit cell parameter and Cd concentration, such trends are only observed for sphalerite with lower concentrations (<26 mol.%) of impurity (Osadchii and Gorbaty, 2010). The magnitude of the unit cell parameters reflects the impact of the presence of a metal impurity (i.e. Cd) whose ionic size is larger to that of Zn, hence the consequent structural dilatations at different Cd concentrations. The current dataset of Cd-bearing sphalerite was compared with the dataset previously presented by Skinner (1961). Both datasets evaluated Cd-bearing sphalerite that had been synthesised at 900°C, and the concentration range of this sphalerite was slightly lower than that of Skinner (1961). The unit cell parameters for Cd-sphalerite samples presented herein were comparable to the results of Skinner, (1961), however the current data-set had slightly higher unit cell parameters. Such differences can be attributed to possible experimental discrepancies such as morphology of the final product (i.e. crystallite size), furnace calibration, and stress and strain.

Both XRD and Raman spectroscopy are composition sensitive techniques, as such it is possible to quantitatively correlate both the bulk structure and surface bonding features as induced by the incorporation of Cd. This is possible because the distortions

caused by impurities to the bulk structure, will also reflect as changes/distortions to the bonding environment in the tetrahedral coordination sited at the surface of sphalerite. Raman is highly sensitive to any compositional variation within a mineral, thus making it an ideal technique for measuring any changes brought about by the presence of impurities.

The ability of sphalerite to incorporate different transition-metal impurities in lattice sites means that a composition sensitive technique such as Raman can illustrate the impacts of metal impurities on the surface bonding characteristics of a sphalerite molecular cluster. Hope et al. (2001) and Mernagh and Trudy, (1997) reported that the nature of a pure sphalerite structure should be reflected by a single first order band that is both Infrared and Raman active. Because pure sphalerite does not have a center of inversion, however, the first order mode is split into a Transverse optical mode (TO) where the atomic vibrations are perpendicular to the incident light and a Longitudinal optical mode (LO) where the atomic vibrations are parallel (Hope et al., 2001). The characteristic difference between the pure sphalerite spectrum and the Cd-bearing sphalerite spectra is the introduction of a new mode at frequency higher than TO and lower than LO modes (figure 5.3).

The main surface feature that reflects the influence of Cd on the local bonding environment in the molecular cluster is the absolute wave number position of the Cd induced impurity mode. The Cd-S induced mode occurs around  $295\text{ cm}^{-1}$ , this thus reflects the weaker nature of the Cd-S bond within a sphalerite molecular cluster. Several studies, noticeably Zigone et al., (1982), Sandoval et al., (2003), Osadchii and Gorbaty, (2010) and Buzatu et al., (2013) have illustrated the varied mode positions for different transition-metal impurities incorporated within lattice sites of sphalerite. Buzatu et al., (2013) attributed the variation in the mode position Fe-S and Zn-S to the strength of the bond i.e. the vibrational energy difference required to vibrate each bond. According to Buzatu et al., (2013) such energy differences can be attributed to the differences in the ionic size between  $\text{Zn}^{2+}$  and the substituting metal impurity. Based on the Raman measurements of different substituted sphalerites, my study agree with Bazatu and coworkers (2013) that the impurity mode reflects the vibrations arising from new impurity-sulphur bonds in the local coordination environment. This is because the intensity ratios (Impurity mode/TO) of the Raman peak correlates linearly with the concentration of the substituting metal impurity (figure 4.2, chapter 4).



The strength of the resultant Cd-S bond, because of its low chemical polarity will be weaker compared to both Fe-S and Co-S bonds, thus requiring less energy to vibrate as illustrated by the lower Raman mode position of the Cd-S bond (Buzatu et al., 2013). The minimal influence of Cd on the surface bonding environment is shown on the Raman spectrum of a high Cd-bearing sphalerite, whereby the prominent first order Zn-S mode (LO) remained independent of the Cd concentration (Karbish, 2007). Karbish, (2007) observed a single Cd induced mode at lower frequencies for Cd-rich (7 wt.%) natural sphalerite. Such Cd behaviour is however different with sphalerite samples containing high content of polar atoms such as Fe, which induces an inflection point indicating a phase transition because of the change in the physico-chemical properties of sphalerite (Barton and Toulmin, 1966, Buzatu et al., 2013). The introduction of Cd in lattice sites will result in a greater lattice distortion due to ionic size, however because of chemical identity (i.e. electronegativity) it induces minimal alterations to the surface bonding.

It is broadly illustrated that variation in the unit cell parameters is attributed to the lattice induced distortions, which depend on the concentration and ionic size of the substituting metal impurity. Raman data illustrates the involvement of the metal impurities on the bonding environment of sphalerite molecular cluster. Both sets of analytical instruments present information that can be interlinked, this is because of the dependence of the lattice distortions on the bonding nature within a molecular cluster. The relation between the structural distortions and the surface features at different Cd concentration is presented in figure 6.1, where the XRD lattice parameter is correlated to the ratio of the impurity mode to the transverse optical mode. The positive correlation ( $r^2 = 0.8967$ ) observed in figure 6.1 suggests a strong relation between the magnitude of bulk structural distortions and the impurity mode/TO ratio reflecting the concentration of the impurity incorporated. This then implies that based on the relative intensities observed on Cd-bearing Raman spectra, it is possible to assume quantitatively the magnitude of the lattice distortions incurred to the mineral by the presence of the impurities. Although peak position of the impurity induced mode is dependent on the chemical properties of the substituting metal, however the intensity of the Cd mode is independent of its chemical identity (i.e. electronegativity) but rather depends on the Cd concentration.

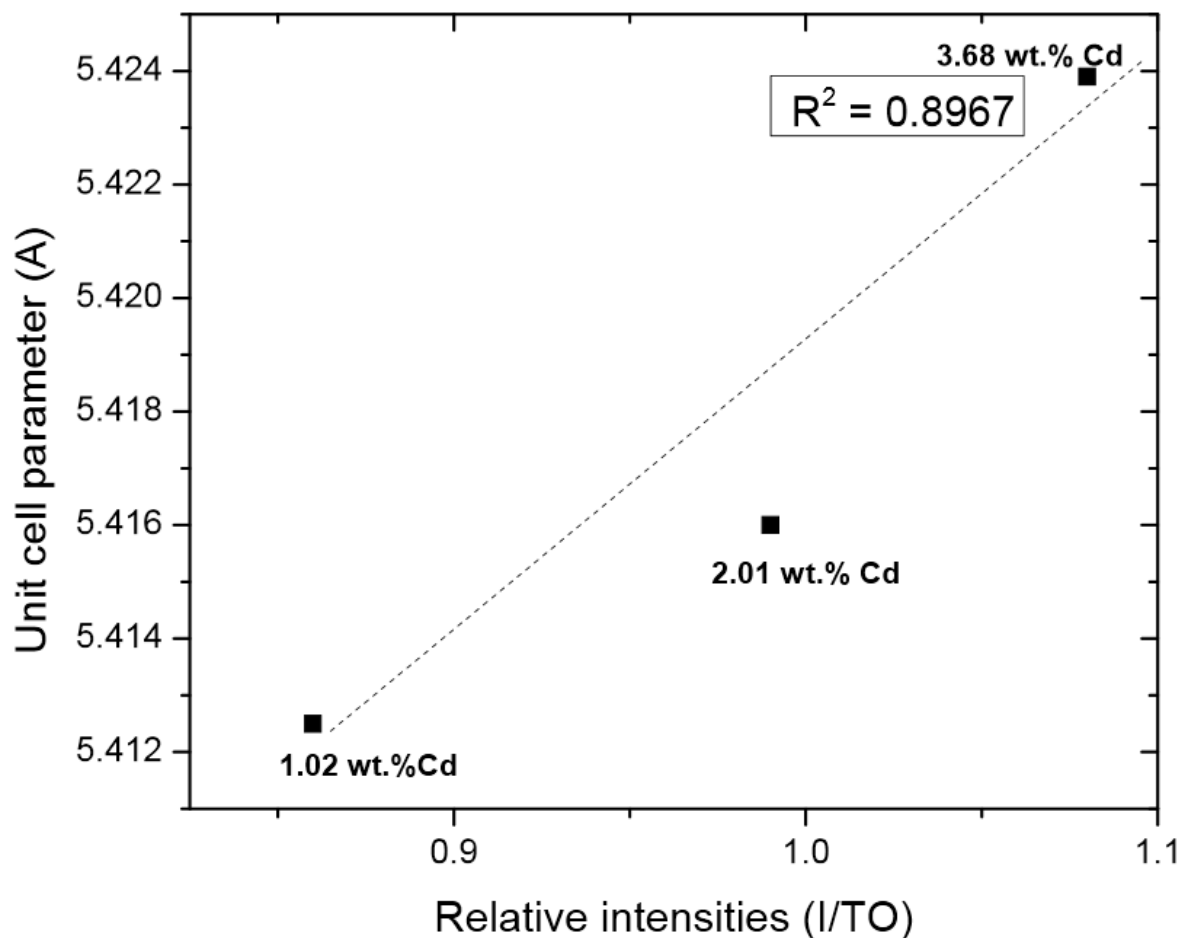


**Figure 6.7:** Evolution of the relative intensities (I/TO) of three sets of impurity bearing sphalerite samples as a function of the unit cell constant variations.

The correlation between the Cd induced lattice distortions and the surface features provides an understanding on how the nature of the new Cd-S bond influences the host ZnS molecular cluster. Cd has the largest ionic radius of the elements studied and is least polar, thus its substitution for Zn will result in the formation of a longer bond with minimal alterations to the molecular polarity of the Zn-S cluster. Due to the longer Cd-S bonds within sphalerite, the magnitude of lattice strain induced is increased. As shown in Appendix III, the lattice parameter of Cd-bearing sphalerite increases with increasing Cd concentration, but the extent of lattice strain is higher than for both Co and Fe. This means that the magnitude of the lattice constant although not diagnostic can be used as a reflection of the nature of the metal impurity incorporated and can be corroborated by the position of the metal impurity induced mode position on a Raman spectrum.

## **The relation of Cd induced surface bonding, electronic structure characteristics and the flotation (i.e. Cu-activation and collector adsorption) response of Cd-bearing sphalerite**

The critical step during the sphalerite flotation is the ability to render the mineral surface hydrophobic. This is typically achieved through the attachments of organic surfactants such as xanthate ions after activation using Cu ions (Chandra and Gerson, 2009). The processes controlling the chemical interactions between the mineral surface and collector are crucial to flotation and thus to the overall beneficiation response of sphalerite. A consensus amongst several reported studies (Lascelles et al., 2001, Chandra and Gerson, 2009, Nedjar and Barkat, 2013) that the sphalerite surface can be rendered hydrophobic during flotation by two reaction mechanisms. The first the formation of a chemical bond between the metal sulphide and the adsorbed xanthate molecule. The second mechanism involves the formation of oxidation products on the mineral surface because of the electrochemical oxidation of adsorbed xanthate. Such interactions are highly dependent on the structure, chemistry and electronic properties of the sphalerite surface which acts as a catalyst for the necessary reactions. The Raman spectroscopy and UV-vis diffuse reflectance interrogations presented herein illustrate that the incorporation of the metal impurities induces different bonding features which can be corroborated by the variation of the band gap measured for sphalerite surfaces.

The UV-vis data (Appendix III) indicate that the incorporation of Cd at different concentration results in a narrowing of the band gap of sphalerite. This reflects changes to key electronic properties of the sphalerite surface such as the position of the conduction and valence band energies and the fermi-level. The pure sphalerite used in this study was found to have a wide band gap of (3.76 eV), while Li et al. (2008) and Xia et al. (2018) band gap of 3.4 eV and 3.7 eV respectively for pure sphalerite. It was also proposed that the band structure of a pure sphalerite comprises valence band which is made up of S 3p and Zn 3 d electronic character; and the conduction band made up of Zn 4s Zn 4p and some S 3p character (figure 6.2) (Li et al., 2008).

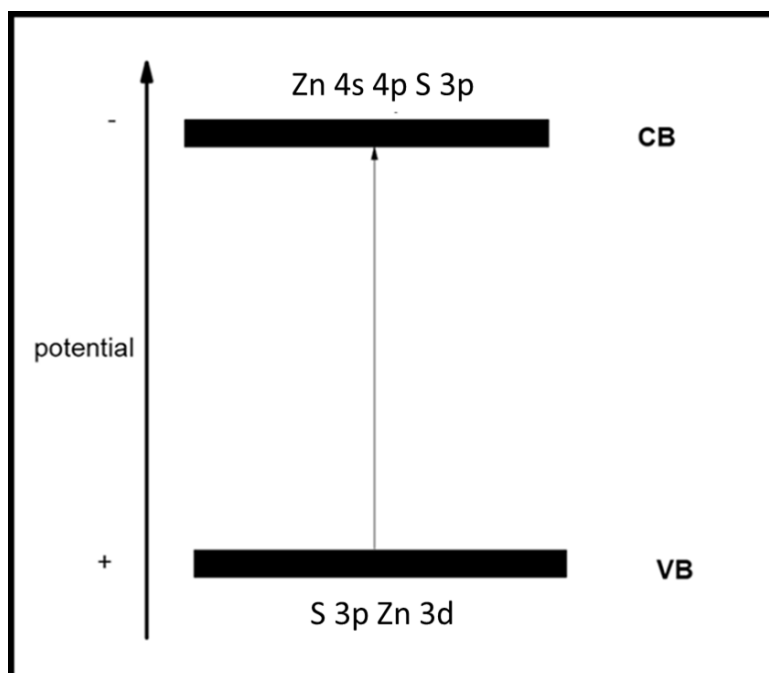


**Figure 6.8:** Proposed band structure of pure sphalerite.

The influence of metal impurities on the electronic properties of sphalerite is dependent on the concentration and the chemical nature (i.e. electronegativity) of the metal incorporated in lattice site. The reduction of the band gap is dependent on the nature of the impurity incorporated as shown by the different UV-vis absorption edges exhibited by sphalerite after the addition of the three different transition-metal (Co, Fe and Cd) impurities. Several studies have illustrated proposed band structures for different impurity bearing sphalerites (Lawniczak-Jablonska et al., 1999, Li et al., 2008), and both studies proposed that the band gap was narrowed by the valence band moving towards a more negative potential.

According to Chen et al. (2010), Cd does not affect the electronic properties of sphalerite significantly, this is because both Zn and Cd exhibit similar electronic configurations. From the UV-vis results presented herein, it was shown that at 1.02 wt.% Cd, the band gap shifted slightly (3.71 eV) as compared to the pure sphalerite (3.76 eV), but only shifted to 3.68 eV at higher Cd concentration (2.01 and 3.68 wt.%). Based on that observation, it is postulated that although the main control for the variation in electronic properties is constrained in the chemical nature of the substituting metal impurity, the concentration of the impurity also plays a role. Lawniczak-Jablonska et al., (1999) showed that in a mixed crystal system ( $\text{Zn}_{1-x}\text{Fe}_x\text{S}$ ), the formation of the valence band includes electrons from the Fe 3d orbital hybridized

with S 3p orbital. Based on such observation, the Cd 4d electrons will also participate in the formation of the valence band of a  $Zn_{1-x}Cd_xS$ . In this mixed system, the conduction band will comprise both Zn 4s and 4p character and Cd 5s and 5p character. Due to the higher Cd concentration, the valence band of sphalerite moves towards the conduction band, thereby decreasing the band gap as illustrated in figure 6.2.

The electronic structure distortions are a manifestation of the changes to the surface bonding interactions (i.e., as investigated using Raman spectroscopy). From previous sections it was established that Raman spectra provide valuable information on the nature of the new metal-sulphur bonds based on the position and relative intensity of the impurity mode. Figure 6.3 illustrates the relationship between the UV-Vis measured band gap of different impurity-doped sphalerite surfaces and the Raman shift of each impurity mode. It is shown that Cd incorporation into the sphalerite structure has minimal effect on the band gap of sphalerite, because Zn and Cd atoms exhibit similar valence electron configurations (Chen et al., 2010). The similarity between the atoms is reflected by the wide band gap exhibited by the Cd-sphalerite samples, which is complemented by the low vibrational energy required for Cd-S bonds. Buzatu et al. (2013) established the dependence of vibrational energies on bond strength, stating a decrease in vibrational energy with decreasing bond strength; hence, Cd-S due to its weak bond strength required a low energy of vibration. Balabin and Sack. (2000), Hope et al. (2001), Osadchii and Gorbaty. (2010) showed that the incorporation of polar atom like Fe would result in an increase of the free energy thus altering the surfacing bonding characteristics of sphalerite. In contrast to Fe, as shown in the current study and Karbish et al. (2007) the incorporation of Cd at high concentration has minimal influence on the surface bonding features of Zn-S molecular cluster. The electronic configuration similarities between Cd and Zn means that during the Cd-substitution in sphalerite there is a minimal gain in free energy of the system relative to substitution of Zn with a high polar atom. Critical to the behaviour of the Raman character and band gap of the gain energy with the incorporation of different transition metal.

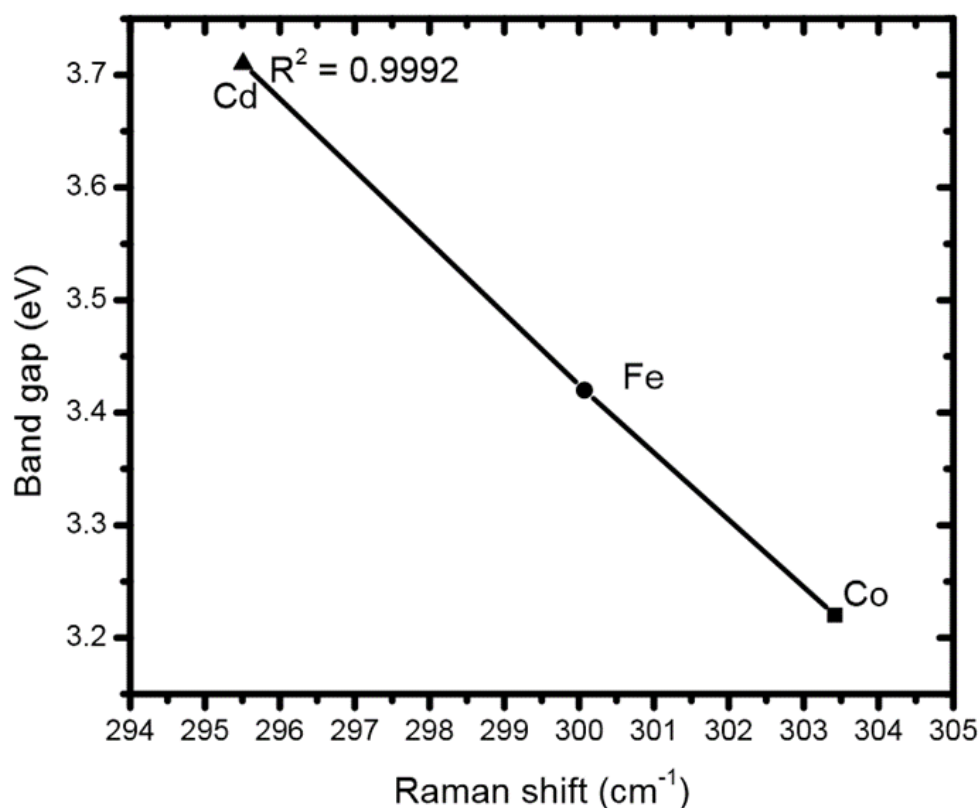


**Figure 6.9:** Correlation between the strength of the bond as reflected by the impurity mode position with the variation of the individual band gap.

Cation substituent induced alterations to the electronic properties of the sphalerite surface greatly affects the way in which sphalerite interacts with flotation reagents (i.e. activators and collectors) to become hydrophobic and float during beneficiation (Harmer et al., 2008, Chen et al., 2010). This is because the fundamental control of the sphalerite-collector interaction lies in the energy difference between the mineral surface and the organic surfactant (Xu and Schoonen, 2000). The electron transfer can only occur between the mineral surface and the collector when the difference in their respective molecular orbital energies are comparable. The redox potential of the collector must be slightly higher than the conduction band energy of sphalerite (Xu and Schoonen, 2000). Another contributor to the mineral surface-collector interaction is the type of semi-conductor (n-type or p-type). Chen et al. (2010) suggested that the oxidation of xanthate to dixanthogen is fundamentally controlled by the electrostatic attractions between the mineral surface and the collector and that these are highly favoured for p-type compared to n-type semiconductor mineral surfaces. The variation of the Co-, Fe- and Cd-bearing sphalerite during activation and collector interactions as reflected by the zeta potential distribution presented in chapter 5 is explained based

on surface charge difference, the frontier molecular orbital theory, variation of the conduction band energies and the fermi level shifts.

### **The influence of Cd on Cu activation and the flotability of sphalerite**

Prior to collector adsorption, it is widely understood that Cu-activation of sphalerite is critical to aid maximum recovery of zinc metal, however such activation mechanism is strongly controlled by the electrostatic energy of the host Zn-S cluster. Both Raman and UV-vis data showed that the chemical characteristics of Zn and Cd are not significantly different and thus Cd-substitution has limited impact on the geometrical configuration of the local cluster of the Zn-S molecule, thus resulting in the sphalerite surface retaining its negative surface charge. The influence of Cd on the surface reactivity of sphalerite is minimal at low Cd concentration as corroborated by the minimal change of the band gap as compared to pure sphalerite. Several authors have indicated that the isoelectric point (IEP) of sphalerite is dependent on the impurity concentration, hence different IEP values have been reported (Popov and Vucinic, 1990, Zhang et al., 1992, Albrecht et al., 2016). Several reported (Popov and Vucinic, 1990, Chandra and Gerson, 2009, Albrecht et al., 2016) interpretations on changes of IEP of sphalerite has been attributed to variation in Fe concentration with minimal literature on the impacts of other associated metal impurities such as Cd. In the same manner to Fe behaviour in natural sphalerite, it is shown in this study that increasing Cd concentration shifts the IEP to higher pH values. The type of information presented on the Raman and UV-vis can be used as a predictive tool to infer surface charge properties of sphalerite because the surface charge of mineral is dependent of the influence of the metal impurity on both surface bonding and the electronic characteristics.

The impacts of Cd on the surface reactivity of sphalerite dictated the response during Cu-activation. It is strongly illustrated herein that Cd-S bonds formed within sphalerite cluster are weaker, and thus easily broken. It is with this interpretation that just like Zn, Cd would easily exchange with Cu ions during activation of a Cd-bearing sphalerite. The nature of the Cd bond as illustrated by Raman data thus controls the ability of the metal impurity to be replaced in lattice sites with Cu ions. The Cu ion coverage of the sphalerite surface during activation is reflected by the increased negative zeta potential (see chapter 5) of sphalerite (Popov and Vucinic, 1990, Albrecht et al., 2016).

The wide band gap and absence of surface bonding alterations as shown by Raman and UV-vis data suggests that a pure sphalerite favours Cu-activation because it can be interpreted that there exists an increased availability of sites for Cu/Zn exchange. The increased Cu ion coverage for pure sphalerite is reflected by the high magnitude (-17.533 mV) of the negative zeta potential as compared to the Cd-bearing sphalerite samples. According to Gerson et al. (1999) successful absorption of Cu ions into pure sphalerite lattice site is controlled by the breakage of the Zn-S bond, which is relatively weak as compared to the metal impurity-S bonds. Taking into consideration such interpretation, the current study suggests that the ease at which the Cd-S bond is broken will also control the extent of Cu-activation process of sphalerite with Cd in lattice. Based on the prior interpretations of the Raman data it is now known that the weaker Cd-S would easily be broken, with Cd removed in lattice site for Cu, thus explaining the high negative zeta potential for sphalerite with low Cd concentration. The minimal influence of Cd at low concentration is also reflected by small change (see chapter 5) on the onset pH of flotation (around pH 8.5), thus at low Cd content sphalerite retains its flotation characteristics. However, increasing Cd content to 3.68 wt.% induced changes in the surface bonding feature (i.e. the Cd-S induced mode dominated the Zn-S induced TO mode) thus illustrating stoichiometric deviation and change in the energetic states of Cd-sphalerite due to high Cd content (Write and Gale, 2010). This implies that the influence of Cd would thus only be experienced at elevated concentration, as more Cd-S bonds start to dominate the Zn-S molecular cluster in a dipole-dipole interaction as reflected by the disappearance of TO mode at high Cd content. The change in the surface bonding characteristics at high Cd concentration means that the electrostatic behaviour of sphalerite with Cu ions is compromised and gives rise to poor absorption of Cu ions. This is shown by the decreasing magnitude of the negative zeta potential and the shift in the onset pH to higher values at high Cd concentration. It is thus imperative to have a broad understanding of the surface bonding features and electronic structure respectively as this can enhance the predictive knowledge on the way impurities influence Cu-activation and consequently the flotation response. This can be interpreted as the presence of more Cd ions within lattice sites of sphalerite, thus the minimal difference between Cd and Zn can only be experienced at higher concentration hence Cu-activation is impacted at elevated Cd concentrations.



## **The influence of Cd on the electron transfer between collector and sphalerite surface**

The incorporation of metal impurities (Cd, Fe and Co) in lattice structure of sphalerite induces different donor and acceptor levels within the band structure which are responsible for the variation in the conduction band and valence band energies (Morrison, 1990). The direct electron transfer between sphalerite and xanthate is permitted by the energy difference of sphalerite conduction band orbitals (i.e. HOMO and LUMO) and xanthate in an aqueous medium (Xu and Schoonen, 2000). Increasing the concentration of the metal impurities can be interpreted as a continued alteration of the conduction band energies due to the contribution of the metal impurities. The Raman study presented herein illustrated new vibrational features that represent a formation of new metal impurity (Cd-S) bonds within the molecular cluster of sphalerite and due to their bond strength, they are correlated to the band gap sphalerite. Considering the gain in energy of sphalerite as a function of metal impurity clusters (Osadchii and Gorbaty, 2010), it is assumed that such gained energy is attributed to the contribution of the metal impurity on the energy levels of the conduction band molecular orbitals (i.e. LUMO and HOMO). A fundamental illustration of the process governing the collector-mineral surface oxidation is presented in figure 6.4. The overall mineral-collector interaction and consequent oxidation of xanthate is dictated by the ability of electron transfer between the three components (figure 6.4). Such interactions are best described by the energy difference in the conduction band orbitals using the frontier orbital model, while the consequent oxidation of xanthate can be explained by electrochemical potential (fermi level) model (Saur and Sustmann, 1980, Xu and Schoonen, 2000, Yu and Zhu, 2000, Chen et al., 2010, Chen et al., 2012).

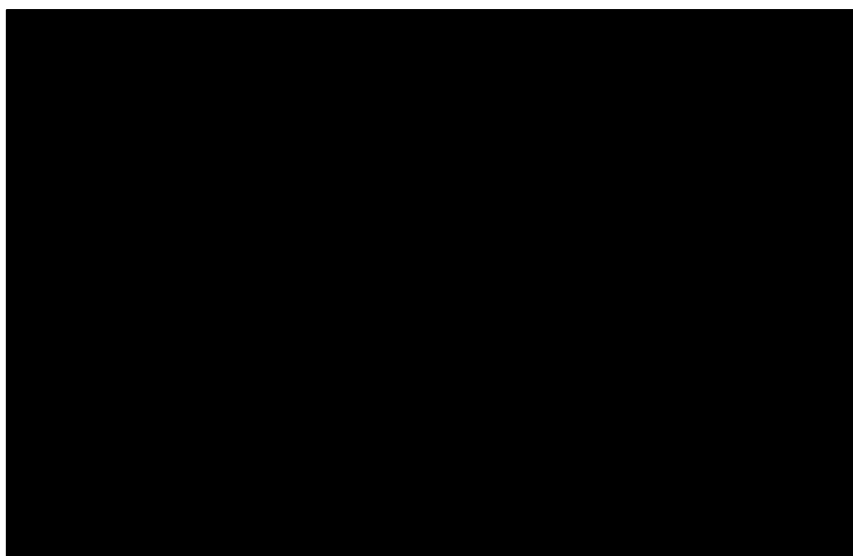


**Figure 6.4:** *Electron transfer process that occurs during the mineral surface interaction with collector and consequent oxidation (modified from Xu and Schoonen, 2000).*

Figure 6.4 shows a fundamental process that occurs between the mineral surface and collector and the consequent oxidation. In this case, xanthate orbital (HOMO) is the electron donor to the conduction band orbital (LUMO) on the mineral surface (i.e. sphalerite), while oxygen orbital (LUMO) acts as an electron acceptor of the donated electrons from the HOMO orbital of sphalerite to complete the overall oxidation process. The impacts of Cd on the LUMO orbital of sphalerite is relatively minimal as compared to the other 3 d metal impurities, this is because Cd has similar 4d outer-shell configuration with Zn thus will not alter the electronic structure significantly (Chen et al., 2010). The implication of the incorporation of the Cd in lattice sites of sphalerite is that; Cd-bearing sphalerite (like pure sphalerite) exhibit a high conduction band energy and wide band gap because of the nucleophilic character of Cd. The treatment of both Cd-bearing and pure sphalerite would thus require an aqueous donor with a higher energy than the high conduction band energy exhibited by both minerals to ensure that electron transfer is energetically viable (i.e. moves from high state to lower state).

In accordance to the frontier molecular theory which explains the energy difference between the two frontier orbitals (HOMO and LUMO), the reaction between xanthate and sphalerite during the flotation process utilizes the HOMO orbital of xanthate (donor) and the LUMO orbital of sphalerite (acceptor), (Xu and Schoonen, 2000, Chen et al.,

2010). Chen et al., (2010) used a density functional theory (DFT) to calculate different energy states of both the HOMO of xanthate and the LUMO of different impurity bearing sphalerite. Using the frontier molecular theories, the interactions of the HOMO and LUMO orbitals involved in the reaction can be represented by:

$$\Delta E = E^{\text{ZnS}}_{\text{LUMO}} - E^{\text{X}}_{\text{HOMO}} \quad [2]$$

where  $E^{\text{ZnS}}_{\text{LUMO}}$  represent the energy of the LUMO of sphalerite upon the addition of metal impurity and  $E^{\text{X}}_{\text{HOMO}}$  represents the energy of the HOMO orbitals of xanthate (Chen et al., 2010). The frontier energy of the HOMO of xanthate is -5.40 eV, while the LUMO energies of both pure and Cd-bearing sphalerites are -2.7 eV and -3.43 eV respectively (Chen et al., 2010). The value of the  $\Delta E$  is used to predict if the presence of the metal impurities would favour the electron transfer or not, Chen et al., (2010) suggested that the higher the value of  $\Delta E$  indicative of a weaker interaction with Xanthate. The wide band gap of both pure and Cd-sphalerite shown herein thus reflect minimal energy change of the LUMO energies as function of Cd incorporation at different concentrations. The  $\Delta E$  for both pure sphalerite and Cd-bearing sphalerite is higher reflecting a weak interaction with xanthate, thus explaining the low flotation recoveries associated with a pure sphalerite. Similarly, equation 2 can be used to explain the interaction of the mineral surface (donor) with oxygen (acceptor). The interaction between mineral surface orbitals and oxygen is then represented by:

$$\Delta E = E^{\text{ZnS}}_{\text{HOMO}} - E^{\text{O}_2}_{\text{LUMO}} \quad [3]$$

For such interactions, the HOMO orbitals (-5.60 eV for pure sphalerite, -5.49 eV for Cd-bearing sphalerite) are responsible for the donation of electrons to the LUMO of oxygen (-4.74 eV) (Chen et al., 2010). Applying equation 3 then the resultant  $\Delta E$  for the pure and Cd-bearing sphalerite are highest thus suggesting that the incorporation of Cd would not favour the interaction with oxygen.

### **Impacts of Cd on the oxidation of xanthate to dixanthaogen**

Several studies have shown that the sphalerite-xanthate interaction characterized by oxidation of xanthate ions to form a more hydrophobic dixanthogen ion on the mineral surface (Smit and Gnoinski, 2000, Lascelles et al., 2001, Chandra and Gerson, 2009). However, different studies have shown the absence of dixanthogen, while other have illustrated the presence of dixanthogen after the electrochemical reaction with

sphalerite (Popov and Vucinic, 1990, Vucinic et al., 2006, Chen et al., 2012). The difference in the electrochemical potential of both xanthate and sphalerite dictates the formation of dixanthogen. Several authors have illustrated that the oxidation of xanthate to dixanthogen enhances the mineral surface hydrophobic character and occurs at the same time as the oxygen reduction (Richardson and O'Dell, 1985, Smit and Gnoinski, 2000, Chen et al., 2012). Depending on the mineral chemistry of sphalerite two possible products form i.e. metal xanthate and dixanthogen (Vucinic et al., 2006, Chen et al., 2012).

The oxidation of xanthate to dixanthogen is electrochemical in nature thus will be controlled by the chemical potential (i.e. Fermi level energies) (Chen et al., 2012). The principle of chemical potential states that electrons will only move from higher potential to lower potential (Chen et al., 2000). It is thus imperative to establish the fermi level energies of the different impurity bearing sphalerite and relate them to the chemical potential to discern whether the reaction is energetically favourable for oxidation or not. Chen et al., (2012) used Dmol3 software to calculate the fermi level energies of common impurity bearing sphalerite samples and butyl xanthate. Both pure and Cd-sphalerite exhibit wide band and lower fermi level values which favours the electron transfer from xanthate to the mineral surface (Harmer et al., 2008, Chen et al., 2010, Chen et al., 2012). This results in the oxidation of xanthate to dixanthogen, however, Abramov and Avdohin, (1977) stated that because of a wide band, pure sphalerite does not allow the adsorption of oxygen thus resulting in poor xanthate oxidation. Despite the wide band gap of Cd-sphalerite, the presence of Cd in lattice is then used as a reaction site for oxygen hence the formation of dixanthogen is permitted unlike with pure sphalerite where oxygen reduction is impossible due to the absence of the reaction side (Chen et al., 2012).

### **Major difference between the impacts of 3d (Fe and Co) and 4d (Cd) atoms on the bulk structure, surface bonding, electronic structure and flotation response.**

The impacts of Fe on the structure, surface characteristics, electronic structure and consequently the flotation response of sphalerite are widely documented (Skinner, 1961, Boulton et al., 2005, Karbish et al., 2007, Harmer et al., 2008, Chen et al., 2010,

Osadchii and Gorbaty, 2010, Chen et al., 2012, Chareev et al., 2017). Most interpretations of cationic substitution associated with sphalerite has been illustrated with Fe substitution, thus its influence is comprehensively understood. Similarly, like any other transition-metal both Fe and Co can easily be incorporated into the tetrahedral coordination of sphalerite through the simple 1:1 ratio substitution with Zn (Harmer et al., 2008). Amongst the three metals used, Fe is widely evaluated because it's the only metal impurity that is found in almost all-natural sphalerite (Harmer et al., 2008, Cook et al., 2009, McClung and Viljeon, 2011). However, due to the different chemical nature between both 3d (Co and Fe) and 4d (Cd), the overall interrelation between the 3d metals induced structural and chemical alterations and the flotation response varies to that of a 4d metal (Cd).

As stated in chapter 4 the magnitude of the impurity induced lattice distortions is dependent on the impurity concentration and the ionic size of metal impurity incorporated. Despite the slight differences in the  $\text{Co}^{2+}$  and  $\text{Fe}^{2+}$  impurity concentrations relative to  $\text{Cd}^{2+}$ , the magnitude of their induced lattice distortions as reflected by the unit cell parameters are less than the distortions caused by Cd incorporation. The results show that increasing the Fe and Co concentration showed similar linear correlations when plotted against unit cell parameter ( $r^2 = 0.979$  for Fe and  $r^2 = 0.99$  for Co). The relationship between Fe concentration and unit cell parameter presented herein agrees to the reported relationships established in literature at different concentrations (Lepetit et al., 2003, Osadchii and Gorbaty, 2010, Chareev et al., 2017). In table 1 it is shown that both Co and Fe are highly electronegative and have smaller ionic size as compared to Cd, thus the nature of the Co/Fe-S bond will be shorter and stronger than the Cd-S (Gibbs et al., 1998). Based on the nature of the Co/Fe-S bonds, it postulated that the short bonds formed would not incur a greater lattice distortion as compared to the longer bonds of Cd-S, hence the unit cell parameters of Fe and Co are smaller than that of Cd. This is because highly polar atoms like Co can draw electron density towards themselves thus shortening the length of the bond, thus causing minimal distortions to the host bulk structure. The linear relation between the Fe concentration and unit cell parameter was maintained in a similar manner as with Cd samples due to the low Fe concentration used.

The ability of a polar atom (e.g. Co) to draw electron density closer as compared to Cd during coordination with S gives rise to the shorter and stronger bonds thus requiring different vibrational energies than weaker bonds formed by Cd. The Raman results showed that the vibrational mode for Co-S and Fe-S occurs at higher wavenumbers as compared to the Cd-S vibrations. This illustrates that stronger bonds require high vibrational energies compared to weaker bonds (Buzatu et al., 2013). Osadchii and Gorbaty, (2010) stated that the presence of polar atoms such as Fe results in a gain in free energy, while Hope et al., (2001) stated the incorporation of a strongly polarizing Fe atom in a sphalerite lattice site results in the alteration of the vibrational properties. Although the concentrations of both polar atoms used in this study were relatively low, it was illustrated that Co induces a new vibrational mode at higher wavenumbers on the vibrational properties at higher concentration will show comparable trends to those reported for Fe (Hope et al., 2001). Such impacts are shown by the diversion of the linear relationship between the unit cell parameter and Fe concentration, and by the disappearance of the prominent Zn-S mode (LO) at elevated Fe content (Hope et al., 2001, Osadchii and Gorbaty, 2010).

The incorporation of 3d transition metal impurities with different outer shell electrons to Zn significantly affects both the surface bonding interaction and the band gap as compared to the results obtained for a 4d transition metal impurity (Cd). Figure 6.3 illustrates that the stronger and more polar Co-S or Fe-S bonds within sphalerite molecular cluster result in a narrowing of the band gap. The positive correlation between bond strength and band gap of impurity bearing sphalerite reflects the polarizing ability of a highly polar Fe-S bond on the less-polar Zn-S cluster. The consequent interaction changes the overall dipole moment of the host molecular cluster. The presence of either Co-S or Fe-S within Zn-S cluster creates dipole-dipole interactions, which are dominated by the metal impurity bonds. The dominance of the metal impurity bonds over the host cluster is reflected by the narrowed band gap at elevated Co and Fe concentrations because of the increased cluster free energy (Osadchii and Gorbaty, 2010). Such variation indicates that a polar atom will result in far greater influence on the sphalerite flotation response because of the greater changes to key electronic properties at the sphalerite surface (e.g., the conduction band energies and the fermi level).

## **The influence of both Co and Fe on Cu-activation and electron transfer between collector and sphalerite surface**

The ability of Cu ions to easily remove both Zn and Cd in lattice sites is the main driver for both pure and Cd-bearing sphalerite having a better activation product as compared to both Co and Fe-bearing sphalerite. This is because both metals form weaker bonds, which can be easily broken to allow the replacement of Zn and Cd by Cu ions. However, the incorporation of highly polar atoms like Co and Fe form stronger bonds as illustrated by the Raman that are not easily broken during activation. This means that instead of having Cu ions incorporated in mineral lattice sites, they remain in solution due to the limited availability of sites resulting in poor Cu-ion coverage on the surface of sphalerite. The minimal Cu ions coverage on the mineral surface is illustrated by the reduced negative zeta potential acquired by the Co-bearing sphalerite (see chapter 5), but the value decreases at elevated Co concentration. The major difference between the influence of Co and Fe is illustrated by the variation on the onset pH (pH 9 conducive for flotation) of flotation of sphalerite. Osadchii and Gorbaty, (2010) have suggested that Fe induces energy changes of sphalerite implying therefore that Co is a far greater polar atom than Fe and will alter the sphalerite surface energy greatly thus affecting the electrostatics governing Cu-activation. This is reflected by different onset pH (see chapter 5) for Co and Fe-bearing samples.

The increased concentration of the two metal impurities induces greater changes to the energy levels of the conduction band orbitals responsible for the interaction with xanthate and oxygen as shown in figure 6.4. Both metal impurities are highly electrophilic thus instead of donating electrons into the conduction band of sphalerite, they withdraw thus altering the energy levels of sphalerite's conduction band orbitals. The lowered conduction band energy of both Co- and Fe- bearing sphalerite makes the two metal impurities favourable for the reaction with xanthate as illustrated by figure 6.4. Based on equation 2 it is found that the  $\Delta E$  of both Fe- and Co- bearing sphalerite indicate that the incorporation of such metal impurities will be beneficial for the interaction with xanthate (Chen et al., 2010). Both Co and Fe-bearing samples have lower  $\Delta E$  which indicate that electrons can be transferred between the HOMO orbital (-5.40 eV) of xanthate to the most reactive orbital (LUMO (-3.59 eV Fe, -3.5 eV

Co)) of sphalerite's conduction band. While equation 3 illustrated that the energy difference  $\Delta E$  between the HOMO (-4.33 eV Fe, -5.31 eV Co) orbital of sphalerite and the LUMO orbital of oxygen (-4.74 eV) are smaller thus both metal impurities would favour reaction with oxygen. However, the oxidation of xanthate to dioxanthogen is controlled by the fermi level energies.

The ability of Cu ions to easily remove both Zn and Cd in lattice sites is the main driver why both pure and Cd-bearing sphalerite have a better activation product as compared to both Co and Fe-bearing sphalerite. This is because both metals form weaker bonds, which can easily be broken to allow the replacement of Zn and Cd by Cu ions. However, the incorporation of highly polar atoms like Co and Fe form stronger bonds as illustrated by the Raman that are not easily broken during activation. This means that instead of having Cu ions incorporated in mineral lattice sites, they remain in solution due to the limited available sites resulting to poor Cu-ions coverage on the surface of sphalerite. The minimal Cu ions coverage on the mineral surface is illustrated by the minimal negative zeta potential acquired by the Co-bearing sphalerite (see chapter 5), but the value decreases at elevated Co concentration. The major difference between the influence of Co and Fe is illustrated by the variation on the onset pH of flotation of sphalerite. Osadchii and Gorbaty, (2010) have suggested that Fe induces energy changes of sphalerite implying therefore that Co is a far greater polar atom than Fe and will alter the sphalerite surface energy greatly thus affecting the electrostatics governing Cu-activation. This is reflected by different onset pH (see chapter 5) for Co and Fe-bearing samples.

The increased concentration of the two metal impurities induces greater changes to the energy levels of the conduction band orbitals responsible for the interaction with xanthate and oxygen as shown in figure 6.4. Both metal impurities are highly electrophilic thus instead of donating electrons into the conduction band of sphalerite, they withdraw thus altering the energy levels of sphalerite's conduction band orbitals. The lowered conduction band energy of both Co- and Fe- bearing sphalerite makes the two metal impurities favourable for the reaction with xanthate as illustrated by figure 6.4. Based on equation 2 it is found that the  $\Delta E$  of both Fe- and Co- bearing sphalerite indicate that the incorporation of such metal impurities will be beneficial for the interaction with xanthate (Chen et al., 2010). Both Co and Fe- bearing samples



have lower  $\Delta E$  which indicate that electrons can be transferred between the HOMO orbital (-5.40 eV) of xanthate to the most reactive orbital (LUMO (-3.59 eV Fe, -3.5 eV Co)) of sphalerite's conduction band. While equation 3 illustrated that the energy difference  $\Delta E$  between the HOMO (-4.33 eV Fe, -5.31 eV Co) orbital of sphalerite and the LUMO orbital of oxygen (-4.74 eV) are smaller thus both metal impurities would favour reaction with oxygen. However, the oxidation of xanthate to dixanthogen is controlled by the fermi level energies.

### **The influence of metal impurities on the electrochemical oxidation of xanthate to dixanthogen**

The behaviour of both Co- and Fe-bearing sphalerite samples during the interaction with collector (see chapter 5) significantly varies to both the pure and Cd-bearing sphalerite thus indicating different surface products. Popov and Vucinic, (1990) and Chen et al. (2012) illustrated that some sphalerite samples had dixanthogen while it was absent on other samples. The interpretation of the difference in the zeta potential distribution of Co- and Fe-sphalerite and pure/Cd-sphalerite is based on the ability to oxidize xanthate to dixanthogen. This is controlled by the impacts of both Co and Fe on the fermi level energies of sphalerite (Chen et al., 2012) due to the electrochemical nature of the oxidation reaction of xanthate to dixanthogen.

The fermi level values of Co- and Fe-sphalerite are higher than xanthate, thus electrons cannot flow from xanthate to mineral surface, hence the absence of dixanthogen (Chen et al., 2000). The presence of metal impurity as possible reaction site for oxygen cannot be translated to the formation of a hydrophobic dixanthogen if the fermi level of the mineral is higher than the fermi level of xanthate. Such behaviour can also be corroborated by the neutral surface charge exhibited by unactivated Co-sphalerite as compared to Fe-sphalerite. The extreme influence of Co on the chemical makeup of sphalerite makes it the most detrimental impurity compared to Fe, even when incorporated at low concentration.

### **Overall inter-relation of the bulk structure, surface chemistry and electronic structure to the flotation response of sphalerite**

The current study uses a set of analytical techniques to establish correlations between the bulk structure, surface characteristics, electronic structure and the surface

reactivity under flotation related conditions as a function of three common metal impurities. The study illustrates a profound and fundamental correlation between the chemical nature of the cation substituent, the bulk structure of the substituted sphalerite, the bonding environment of the associated surface functional groups, and the resultant molecular orbital structure and electronic configuration of the sphalerite surface. A key to the all-round linkage is the characteristics of the subsequent metal impurity-Sulphur cluster, forming within the molecular cluster of sphalerite with increased concentration of the metal impurities. The structural distortions of sphalerite are reflected by the variation of the lattice constant whose magnitude shows dependence on the ionic size of the incorporated transition-metal impurity. The ionic size and polarity of the metal impurity dictates the bond strength and the consequent interaction with Zn-S. For example, Cd has the largest difference in size to Zn and results in the largest distortions of the XRD-measured unit cell parameter in Cd-substituted synthetic sphalerites. This is incurred by the formation of Cd-S which has the longest bond length amongst the three impurities.

These observed structural distortions within the bulk mineral structure translate to differences in the local coordination and bonding environment of the substituted sphalerite mineral surface. Based on the Raman spectroscopy results presented herein it was possible to probe the bonding characteristics of sphalerite as a function of cation substitution and relate such surface bonding features to the bulk structural distortions as shown by the lattice constants. The lattice distortions are related to the bonding features based on the nature of the subsequent metal impurity bonds within sphalerite, which are dependent on the ionic size and electronegativity of the metal impurity. For example, the new longer Cd-S bond is relatively weak, and mildly polar compared to the other metal impurities thus will require lower energy of vibration, which is illustrated by the occurrence of Cd-S induced mode at lower Raman shift ( $295\text{ cm}^{-1}$ ). It is thus possible to correlate the lattice constant to the type of bond (size and strength) and the energy required for vibration.

The impurity-induced distortions to the sphalerite surface bonding environment will further manifest as differences between the electronic structures of the pure sphalerite and the impurity-bearing sphalerites. The UV-Vis data was enough to indicate the variations in the band gap of sphalerites as a function of cation substitution, and these were found to correlate well ( $r^2 = 0.99$ ) with the measured position of the Raman

impurity mode of the corresponding metal impurity. The introduction of new metal bonding within the sphalerite affects the host molecular cluster and such effects are illustrated by the variation in the band gap. Sphalerite exhibits a wide band gap (3.76 eV), the substitution of Zn with a metal impurity such as Cd, which has similar properties (i.e.  $Nd^{10}$  configuration) results in minimal changes in the electronic properties. This implies that greater change in the bonding environment manifests due to alterations of the electronic properties (i.e. band gap, fermi level, valence and conduction band energies). The substitution of a highly polar atom such as Co creates new short, strong bonds within the molecular cluster, thus resulting in a dipole-dipole interaction with the host Zn-S. Such interactions illustrate the variation of the electronic properties.

The variation in the band gap indicate changes to key electronic properties of sphalerite such as the conduction band and valence band energies, and fermi levels. Harmer et al. (2008) and Chen et al. (2010) stated that key to the fundamental understanding of the flotation behaviour lies with the electronic properties of sphalerite. The UV-vis data shown in chapter 4 reflects an inference of the variation in both the conduction band energies and the fermi level energies of sphalerite as function of cation substitution. The alteration of the electronic structure influences the way sphalerite will interact with flotation reagents, thus the greater the alterations to the electronic structure may results to poor flotation response. Figure 5 shows the overall inter-relation between the bulk structure, surface characteristics, electronic structure and flotation. The flow sheet indicates the ability to inter-relate the flotation response to key changes in the electronic structure, and how the variation in the electronic structure can be related to both surface bonding and the bulk structural distortions. The inter-relation established herein is critical to the modification of process parameters during the beneficiation of sphalerite and improves the predictive capabilities during process design.

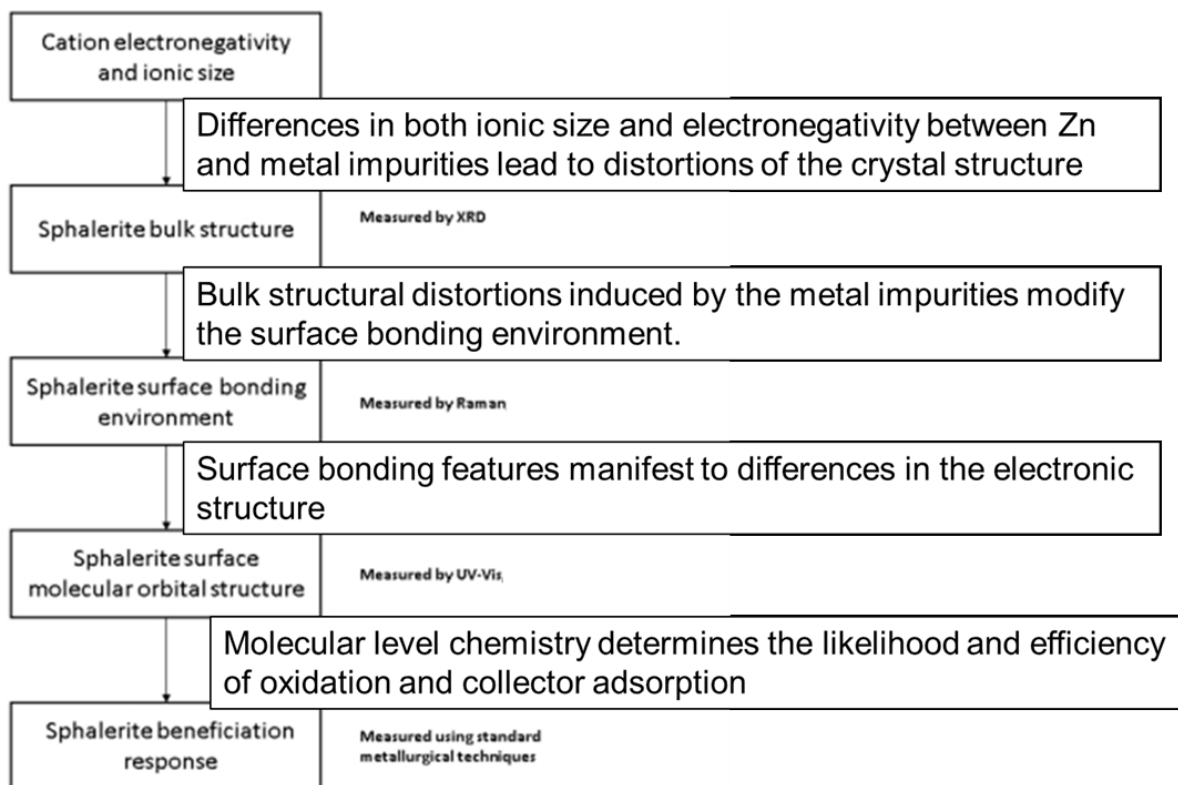


**Figure 6.5:** Diagrammatic overview of how cation substitution in the bulk mineral structure can manifest as modifications to the surface chemistry and thus flotation response of sphalerite.

## Implications for sphalerite flotation and predictive capabilities during process design

The optimization of flotation recoveries and improved predictive capabilities during process design of sphalerite involves a broader knowledge on variety data-sets, which include a substantive molecular-level mineral chemistry. The role of molecular-level mineral chemistry on the flotation response of sphalerite has not fully been resolved in numerous literatures. It is thus important to complement the empirical geometallurgical studies (McClung and Viljoen, (2011), Schouwstra et al., 2010, Cook et al., 2011) with a substantive experimental data-set addressing the knowledge gap (i.e. lack of molecular-level insights) presented in such studies. The empirical approaches provide meaningful insights, however the shortcoming associated with such approaches is a lack in fundamental understanding of molecular-level mineral chemistry and its impact on the consequent flotation response. This has resulted in several contrasting metallurgical (i.e. Cu-activation and collector adsorption)

interpretations on the optimisation of flotation behaviour of sphalerite in natural systems. The current study illustrated the importance of building up a thorough molecular-level understanding of the influence of individual cation substitution on the bulk structure, surface bonding environment and electronic structure of sphalerite. This provided insights on the influence of individual metal impurity on the Cu-activation and collector interactions. The study indicates that the incorporation of Fe, Co and Cd induces different geometallurgical responses of sphalerite, thus illustrating the importance of critical molecular -level interrogations.

The evaluation of the impacts of each metal impurity reflected that an understanding of the response of sphalerite behaviour to both Cu-activation and collector adsorption is controlled by the chemical nature (i.e. Electronegativity) of the cation. The current study evaluated three common metal impurities with varying chemical polarity (chemical polarity trend:  $\text{Co} > \text{Fe} > \text{Cd}$ ) and was shown that they induce different impacts. The role of Co, Fe and Cd substitutions within sphalerite mineral structure, and inferred their effects on flotation by carefully evaluating their zeta potential response under alkaline conditions has been interrogated. Cobalt significantly modifies the surface charge of sphalerite, resulting in a close to neutral charge in both alkaline and acidic media for an unactivated sphalerite without collector. The slight change in the zeta potential after the addition of Cu ions in Co-sphalerite samples illustrates minimal adsorption of Cu ions thus reflecting that sphalerite can never self-activate due to the presence of Co ions. This implies that a processing stream with Co bearing mineral will require a significant addition of both Cu ions and collectors to aid maximum recovery. While the incorporation of both Fe and Cd show minimal alterations on the surface charge of sphalerite thus resulting in better chances of self-activation and the eventual Cu-activation.

Several studies have illustrated that the flotation of sphalerite is aided by successful Cu-activation prior to collector adsorption (Lascelles et al., 2000, Harmer et al., 2008 Chandra and Gerson, 2009, Albrecht et al., 2016). This involves the treatment with activator ions (Cu) prior to collector adsorption in an alkaline media (to suppress pyrite), with operations occurring around pH 9. The incorporation of the metal impurities at different concentration in lattice sites means that the number of available sites for Cu ions adsorption is reduced. This would result in lower Cu ions coverage on the mineral surface which will translate into poor flotation recoveries as illustrated by the decrease

in the magnitude of the negative zeta potential (see chapter 5) of the activated samples. In addition, the metal impurities influence the pH at which sphalerite flotation will start occurring in alkaline media, thus a well-established molecular-level mineral chemistry gives insights on the pH adjustment of the flotation circuits. The different critical onset pH of flotation as a function of the three different impurities implies that operational pH of sphalerite is dependent on the nature and concentration of the impurity metals associated with sphalerite. Improving metal recovery from impurity bearing sphalerite requires a high-level understanding of the chemical nature of the substituting metal ions as this also has a bearing on the hydrophobic species on the mineral surface during collector adsorption.

The last consideration is most important given that the electronic structure of the sphalerite surfaces is the ultimate parameter controlling important floatation reactions such as oxidation and collector adsorption (Xu and Schoonen, 2000; Lotter et al., 2016). The broad understanding of the mineral chemistry of sphalerite provides critical information about the mineral-collector interaction and the possible formation of the more hydrophobic dixanthogen. The alterations to key electronic properties such as fermi levels and mineral's conduction band orbitals energies as a function of metal impurities becomes detrimental to the floatability of sphalerite. It is key to understand the electronic properties of sphalerite due to its chemistry and be able to associate that with energy levels of the collector in use. Such an approach will enhance our understanding of why some sphalerite surfaces react well to other collectors, while others do not. This will be critical to improving capabilities to predict flotation response of sphalerite and thus optimise beneficiation design. The predictability of flotation response of sphalerite depends on an in situ mineral surface characterization to establish the impacts of the different metal impurities on the overall molecular cluster. The application of Raman spectroscopy in processing plants would provide useful insights on the influence of difference metal impurities on the surface characteristics of sphalerite and infer such influence on the adjustment of key flotation parameters such pH and type of collector.

## **Chapter Seven – Conclusions and Recommendations**

Using a suite of analytical techniques (XRD, Raman spectroscopy, UV-vis diffuse reflectance and Zeta Potential measurements), the influence of cation (Cd, Co, Fe) substitution on the structural, surface and electronic characteristics of synthetic sphalerite and illustrated their effects on the minerals' ultimate surface reactivity has been evaluated. To achieve this, three sets of impurity (Cd, Co, Fe) bearing sphalerite were synthesised using a dry experimental method for 7 days at 900°C. The application of a molecular-level knowledge of the impacts of cation substitution on sphalerite chemistry and the consequent surface reactivity has evoked the following conclusions, which are derived in relation to the key questions presented in chapter one:

**Key question 1:** *What are the common bulk structural distortions and surface characteristics associated with individual cationic substitution of Zn in lattice sites of sphalerite?*

The impacts of cation substitution on the crystal structure of sphalerite were studied using X-ray diffraction analysis, while Raman spectroscopy was used to interrogate the variation in the surface-bonding environment of sphalerite as a function of the incorporation of the three trace impurities.. Based on the XRD structural evaluations, it is concluded that:

- The incorporation of the three-common transition metals induces line broadening of the diffraction patterns thus moving the Bragg's peaks to higher position. This is interpreted as lattice strains reflected by the distribution of the variable unit cell parameters.
- The extent of lattice distortions is related to the impurity concentration and the ionic size of the substituent metal. This is shown by the linear increase of the lattice constant with increasing concentration. The magnitude of the lattice constant is dependent on the ionic size of the metal impurity. For example, Cd has the largest ionic size amongst the metal impurities tested and reflected the largest lattice distortions (as measured using the lattice constants). However, the use of XRD as a diagnostic tool to reveal the identity of the incorporated metal impurity is thus limited and will require additional use of other analytical instruments such as scanning electron microscope (SEM).

Based on the surface bonding evaluations, it is concluded that:



- The incorporation of metal-impurities in lattice sites of sphalerite induced a new Raman mode, the position of which is dependent on the chemical identity of the impurity.
- The introduction of metal impurity does not affect the position of the prominent first order Raman modes (LO and TO) of sphalerite, however it shows a correlation with the ratio of the impurity mode to the TO mode. It is also shown on the Raman results that it is not possible to illustrate the effect of lattice induced distortions on the Zn-S bonds as reflected by the lack of correlation to both Zn-S modes (TO and LO) with increased impurity concentration.
- The ratio (I/TO) between the impurity mode and the transverse optical mode (TO) the Raman spectra can also be used to estimate the relative concentration of the different cation substituents present in sphalerite.
- The position of impurity mode is related to strengths of the bonding interaction with Co>Fe>Cd. This is illustrated by the occurrence of the Co-induced mode at higher wavenumbers ( $303\text{ cm}^{-1}$ ) compared to the Cd and Fe-induced modes at lower wavenumbers ( $295\text{ cm}^{-1}$  and  $300\text{ cm}^{-1}$  respectively).

**Key question 2:** *Can we relate such bulk structural distortions to the surface bonding characteristics of a Zn-S molecular cluster?*

- The position of the new mode can be used to predict the lattice distortions, this is because based on the Raman modes reflects the type of bond and its vibrational energy, thus a low vibrational energy can be correlated to large lattice distortion as is the case with Cd.

**Key question 3:** *What are the influences of the metal impurities on the electronic structure of sphalerite?*

Sphalerite is a semi-conductor and exhibits a wide band gap, but the addition of metal impurities shifts the onset of the absorption edges to higher wavelengths. The shift in the absorption edge is interpreted as narrowing of the band gap caused by cation substitution. The extent of the band gap variation is related to the chemical nature of the metal impurity and vibrational energies (e.g. The weaker metal impurity bond (i.e. Cd-S) requires low vibrational energies thus resulting in minimal changes in the band gap of sphalerite, while stronger impurity bonds result in greater narrowing of the band



gap). The substitution of Zn with a metal impurity that has similar outer-shell configuration leads to minimal change to the band, while the substitution of Zn with a highly polar 3d metal such as Co greatly narrows the band gap.

**Key question 4:** *How does the influence of cation substitution on the surface bonding environment be related to the changes to the electronic structure of sphalerite?*

The variation in the bonding environment as reflected by the Raman spectroscopy manifests as changes to the electronic properties of synthetic sphalerite (as shown by UV-vis data presented herein). The variation in the band gap energies is attributed to the influence of the new metal-S bond on the host molecular cluster. The presence of a high polar bond such as Co-S within the sphalerite cluster creates a dipole-dipole interaction within the molecular cluster thus narrowing the band gap, while a weakly bond such as Cd-S causes minimal effect on the electronic structure as reflected by the small shift in the band gap energies.

**Key question 5:** *Do the different metal impurities give sphalerite different flotation response?*

Using electro-kinetic techniques (Zeta potential measurements), the current study has interrogated the impacts of cation (Co, Fe and Cd) substitution on the surface reactivity of synthetic sphalerite under flotation related conditions. The following key conclusions are made:

- The multiple flotation responses of sphalerite (as reported in the published literature) can be attributed to the concentration and nature of transition-metal impurities present in the sphalerite structure. The nature of the substituting metal ion further affects the surface reactivity of sphalerite.
- In alkaline media, the adsorption of Cu ions abstracted from  $\text{Cu}(\text{OH})_{2(\text{aq})}$  (the stable Cu species at pH 9) improved the surface reactivity of sphalerite. This was illustrated by the negative zeta potential attained by a Cu-activated Co-sphalerite which had a neutral surface charge when unactivated.
- However, the variation in the chemistry of sphalerite affects the onset pH of flotation in an alkaline media, which showed dependence on the nature of the impurity i.e. with increasing impurity concentration the onset pH shifted to different values depending on the metal impurity incorporated.

- Based on the nature of the substituting metal, different reaction products are observed during collector adsorption. This is illustrated by the different zeta potential distributions of Cd-bearing sphalerite and Co-bearing, which is interpreted as the presence of dixanthogen on the surface of Cd-bearing sphalerite and absent on both Fe- and Co-sphalerite surfaces. Those variations are attributed to the impacts of the metal impurities on the nucleophilic and electrophilic characteristics of sphalerite, which then affects how the mineral surface interact with collector.

**Key question 6:** *Can these molecular-level insights (1-4) positively impact predictive capabilities during the design of sphalerite beneficiation circuits?*

The results presented herein thus illustrate the importance of careful consideration of individual cation substitution reactions which can have strong impacts on sphalerite behaviour at even at low concentration in complex mineral systems. Based on the results presented herein it is maintained that a broader understanding of sphalerite flotation response is constrained to detail molecular-level investigations in addition, it is also believed that a full and fundamental understanding of the molecular-level dynamics will be crucial towards designing the most efficient beneficiation streams for ores produced from the “Mine of the Future”.

### **Recommendations:**

Critical to the fundamental understanding of the flotation response of sphalerite is a substantive molecular -level interrogation prior to detailed process design. Our study has illustrated systematic correlation of the structure, surface chemistry, electronic structure and their relation to flotation. It was illustrated that the key to the formation of hydrophobic species on the mineral surface was dictated by the difference in the electrochemical potential between both xanthate and sphalerite. Given this new understanding, the following recommendations arise:

1. The expansion of the current dataset to other trace metals (e.g., Mn, Bi etc.), and other mineral systems (e.g., chalcopyrite galena etc). The goal is to establish a substantive geometallurgical framework with a better understanding on the theoretical prediction of flotation response for any ore deposit based on molecular-level mineral chemistry fundamental considerations.

2. The development Raman techniques for in-line evaluation of complex sphalerite ores so that processing can be modified in real time. The spectral resolution of the Raman would need to be high enough to resolve all substituents present in the sphalerite structure.

3. It is also recommended that going forward with the improved knowledge of the electronic structure of impurity bearing sphalerite should be used as a catalyst to probe the possibility of synthesising xanthate species whose electronic structure can allow the transfer of electrons to a substituted sphalerite. This concept is very broad but if it is thoroughly expanded can be the key to finally being able to generate hydrophobic species (i.e. dixanthogen) on all substituted sphalerite, thus exploiting low grade ores previously deemed uneconomical.

## References

- Abramov, A.A., Avdohin, V.M., 1977. Oxidation of Sulfide Minerals in Beneficiations Processes. Gordon and Breach Science Publishers, Amsterdam.
- Aghazadeh, S., Mousavinezhad, S.K., Gharabaghi, M., 2015. Chemical and colloidal aspects of collectorless flotation behavior of sulfide and non-sulfide minerals. *Advances in Colloid and Interface Science*, Vol. 225, pp. 203-217.
- Albrecht, T.W.J., Addai-Mensah, J., Fornasiero, D., 2016. Critical copper concentration in sphalerite flotation: Effect of temperature and collector. *International Journal of Mineral Processing*, Vol. 146, pp 15-22.
- Balabin A. I. and Sack R. O. (2000) Thermodynamics of (Zn, Fe)S sphalerite. A CVM approach with large basis clusters. *Mineral Magazine*, Vol. 64, pp. 923–943.
- Barton, P. B. Jr., Toulmin P. III. 1966. Phase relations involving sphalerite in the Fe-Zn-S system. *Economic Geology*, Vol. 61, pp. 815-849.
- Bi, C., Pan, L., Xu, M., Yin, J., Guo, Z., Qin, L., Zhu, H., Xiao, Q.J., 2009. Raman spectroscopy of Co-doped wurtzite ZnS nanocrystals. *Chemical Physics Letter*, Vol. 481, pp 220-223.
- Boulton, A., Fornasiero, D., Ralston, J., 2005. Effect of iron content in sphalerite on flotation. *Minerals Engineering* 18, 1120–1122.

Chandra, A.P., Gerson, A.R., 2009. A review of the fundamental studies of the copper activation mechanisms for selective flotation of the sulfide minerals, sphalerite and pyrite, *Advances in Colloid and Interface Science*, Vol.149, pp 97-110.

Chareev, D.A., Osadchii, V.O., Shiryayev, A.A., Nekrasov, A.N., Koshelev, A.V., Osadchii, E.G. 2017. Single-crystal Fe-bearing sphalerite: synthesis, lattice parameter, thermal expansion coefficient and microhardness. *Physical Chemistry Minerals*, Vol. 44, pp 287-296.

Chen, Y., Chen, J., Guo, J. 2010. A DFT study on the effect of lattice impurities on the electronic structures and floatability of sphalerite. *Mineral Engineering*, Vol. 23, pp 1120-1130.

Chen, Y., Chen, J., Lan, L., Yang, M., 2012. The influence of impurities on the flotation behaviours of synthetic ZnS. *Mineral Engineering*, Vol. 27-28, pp 65-71.

Chen, J.H., Feng, Q.M., Lu, Y.P. 2000. Energy band model of electrochemical flotation and its application (II) – energy band model of xanthate interacting with sulphide minerals. *The Chinese Journal of Nonferrous Metals*, Vol. 10, pp. 426–429.

Cook, N.J., Ciobanu, C.L., Pring, A., Skinner, W., Shimizu, M., Danyushevsky, L., Saini-Eidukat, B., Melcher, F. 2009. Trace and minor elements in sphalerite: A LA-ICPMS study. *Geochimica et Cosmochimica Acta*, Vol. 73, pp. 4761-4791.

Cook, N.J., Ciobanu, C.L., and Williams, T. 2011. The mineralogy and mineral chemistry of indium in sulphide deposits and implications for mineral processing. *Hydrometallurgy*, Vol. 108 (3-4), pp. 226-228.

Ejtemaei, M., Nguyen, V.A., 2017. A comparative study of the attachment of air bubbles onto sphalerite and pyrite surfaces activated by copper sulphate. *Mineral Engineering*, Vol. 109, pp14-20.

Harmer, S.L., Mierczynska-Vasilev, A., Beattie, D.A., Shapter, J.G., 2008. The effect of bulk iron concentration and heterogeneities on the copper activation of sphalerite. *Minerals Engineering*, Vol. 21, pp 1005-1012.

Hope, G.A., Woods, R., and Munce, C.G. 2001. Raman microprobe mineral identification. *Minerals Engineering*, Vol. 14 (12), pp 1565–1577.

Kharbish, S. 2007. A Raman spectroscopic investigation of Fe-rich sphalerite: effect of Fe-substitution. *Physics and Chemistry of Minerals*, Vol. 34, pp 551–558.

Lawniczak-Jablonska, K., Kachniarz, J., Spolnik, Z.M. 1999. X-ray emission valence band spectra from  $Zn_{1-x}Fe_xS$  excited by electrons. *Journal of Alloys and Compounds*, Vol. 286, pp 71-75.

Laskowski, J.S., Liu, Q., Zhan, Y., 1997. Sphalerite activation: flotation and electrokinetic studies. *Mineral Engineering*, Vol. 10, pp 787-802.

Lepetit P., Bente K., Doering T. and Luckhaus S. (2003) Crystal chemistry of Fe-containing sphalerites. *Physical Chemistry Minerals*. Vol. 30, pp 185–191.

Li, Y., Lu, A., Wang, C., and Wu, X. 2008. Characterization of natural sphalerite as a novel visible light- driven photocatalyst. *Solar Energy Materials & Solar Cells*, Vol. 92, pp 953-959.

Lotter, N.O., Kowal, D.L., Tuzun, M.A., Whittaker, P.J., and Kormos, L.J. 2003. Sampling and flotation testing of Sudbury Basin drill core for process mineralogy modelling. *Minerals Engineering*, Vol. 16, pp 857-864.

McClung, C.R. and Viljoen, F., 2011. A detailed mineralogical assessment of sphalerites from the Gamsberg zinc deposit, South Africa: The manganese conundrum. *Minerals Engineering*, Vol.24, pp 930-938.

Mernagh, T.P., Trudu, A.G. 1993. A laser Raman microprobe study of some geologically important sulphide minerals. *Chemical Geology*, Vol. 103, pp 113-127.

Mukherjee, A.D. and Sen, P.K., 1976. Flotability of sphalerite in relation to its iron content. *J. Mines, Metals, Fuels*, Oktober: 327.

Nedjar, Z., Barkat, D. 2013. Electrochemistry of copper activation of sphalerite and potassium isobutyl xanthate (KIBX) synthesized collectors adsorption. *Iranian Journal of Chemical Engineering*, Vol. 10, pp 4.

Nefedov, V.I., Salyn, Ya.V., Solozhenkin, P.M., Pulatov, G.Yu., 1980. X-ray photoelectron study of surface compounds formed during flotation of minerals. *Surface and Interface Analysis*, Vol 2, pp 170–172.

- Popov, S.R., Vucinic, D.R., 1991. The ethylxanthate adsorption on copper –activated sphalerite under flotation-related conditions in alkaline media. *International Journal of Mineral Processing*, Vol. 30, pp 229-244.
- Richardson, P.E., O'Dell, C.S. 1985. Semiconducting characteristics of galena electrodes relationship to mineral flotation. *Journal of the Electrochemical Society*, Vol. 132, pp 1350–1356.
- Sauer, J., Sustmann, R., 1980. Mechanistic aspects of diels–alder reactions: a critical survey. *Angewandte Chemie International Edition in English*, Vol. 19 (10), pp 779–807.
- Sandoval, S.J., Rivera, S.A. L. 2003. Influence of reduced mass differences on the Raman spectra of a ternary mixed compound:  $Zn(1-x)Fe(x)S$  and  $Zn(1-x)Mn(x)S$ . *Physical Review*, Vol. 68, 054303.
- Schouwstra, R.P., de Vaux, D., Hey, P., Bramedeo, S. 2010. Understanding Gamsberg – A geometallurgical study of a large stratiform zinc deposit. *Mineral Engineering*, Vol. 23, pp 960-967.
- Skinner, B.J. (1961). Unit-cell edges of natural and synthetic sphalerites. *American Mineralogist*, Vol. 46, pp 1399–1411.
- Smit, J.T., Gnoinski, J., 2000. *Electrochemistry: Contaminant Ions and Sulphide Mineral Interactions*. Unpublished.
- Vucinic, D.R., Lazic, P.M., Rosic, A.A. 2006. Ethyl xanthate adsorption and adsorption kinetics on lead-modified galena and sphalerite under flotation conditions. *Colloids and Surfaces*, Vol. 279, pp 96-104.
- Wright, K., Gale, J.D. 2010. A first principles study of the distribution of iron in sphalerite. *Geochimica et Cosmochimica Acta*, Vol. 74, pp 10-16.
- Xia, C., Winckelmans, N., Prins, P.T., Bals, S., Gerritsen, H.C., Donega, C.D. 2018. Near-Infrared-Emitting  $CuInS_2/ZnS$  Dot-in-Rod Colloidal Heteronanorods by Seeded Growth. *Journal of the American Chemical Society*, Vol. 140, pp 5755-5763.
- Xu, Y. and Schoonen, M.A. (2000). The absolute energy positions of conduction and valence bands of selected semiconducting minerals. *American Mineralogist*, Vol. 85 (3-4), pp 543-556.

Yu, Q.S., Zhu, L.G. 2000. The Introduction of Molecular Design. Higher Education Press, Beijing.

Zhang, Q., Rao, S.R., Finch, J.A. 1992. Flotation of sphalerite in the presence of iron ions. *Colloids and Surfaces*, Vol. 66, pp 81-89.

Zigone, M., Vandevyver, M., Talwar, D.N., 1981. Raman scattering and local force variations due to transition-element impurities in zinc sulphide crystals: Effect of pressure application. *Phys Rev B*24:5763–5778.

## APPENDIX I

### IMPACT OF CATION SUBSTITUTION (Cd, Co) ON THE GEOMETALLURGICAL RESPONSE OF SPHALERITE.

**L. Babedi<sup>a\*</sup>, M. Tadie<sup>b</sup>, P. Neethling, and B.P. von der Heyden<sup>a</sup>**

*<sup>a\*</sup> Department of Earth Sciences, Stellenbosch University, South Africa,  
21368546@sun.ac.za*

*<sup>b</sup> Department of Process Engineering, Stellenbosch University, South Africa*

#### **Abstract**

The effects of trace element substitutions in sphalerite mineral structure on optimised floatation response have not been fully constrained or fully understood. To further this important field of study, this contribution focusses specifically on mineral and surface chemistry, and electro-chemistry of Cd- and Co- substituted synthetic sphalerites using Raman spectroscopy and Zeta potential experimentation. Raman spectroscopy illustrates that the presence of these impurities results in the introduction of a new mode, the relative intensity of which can be correlated (Cd  $r^2=0.95$  and Co  $r^2= 0.99$ ) to the dopant concentration. Comparison to X-ray Diffraction results measuring the unit cell parameter further shows that this relative intensity (Cd  $r^2=0.81$  and Co  $r^2= 0.99$ ) may provide insights into the degree of lattice strain within the mineral structure. The zeta potential distribution of an un-activated Cd-sphalerite show no detrimental effect as function of Cd content. Although the iso-electric point shifted from 2.45 at 1 wt.% Cd to 2.69 at 3.68 wt.% Cd, the zeta potential remained negative at alkaline media. Conversely, cobalt at low concentration of 0.36 wt.% had a detrimental effect on the surface charge, resulting to a close to neutral zeta potential at different pH. The adsorption of Cu ions on the surface of Co-bearing sphalerite conditioned in an alkaline media slightly increases the zeta potential of Co-sphalerite. While the Cd-bearing sphalerite decrease in negative zeta potential at >1 wt.% Cd indicating a complete exchange between Cu and Zn. The results presented herein illustrate that, based on the chemical nature of the substituting metal; sphalerite will exhibit multiple response to flotation reagents. Maximum recovery of zinc can thus only be achieved through multidisciplinary study and fundamental understanding of the effects of cation



substitution on mineral structure and surface chemistry, the latter necessarily affecting the floatation response.

**Key words: sphalerite, Surface chemistry, electro-chemistry, zeta potential, iso-electric point, floatation.****Introduction**

Zinc is an important metal used primarily in the alloying industry, particularly in the manufacture of brass. Although it can be won from non-sulphidic ores, its primary ore mineral sphalerite (ZnS) which is mined, commonly in association with zinc and copper minerals, from a variety of base metal deposit types. The beneficiation of these complex ores relies heavily in the use of floatation technologies (e.g., Aghazadeh et al., 2015) which, when optimised, enable exploitation of even low-grade ores that would otherwise be uneconomical (Bicak and Ekmekci, 2012). Because of its large band gap, sphalerite is a semi-conducting mineral that requires activation using copper sulphate or copper nitrate to improve the efficiency of collector adsorption reactions (Ejtemaei and Nguyen, 2017, Chandra and Gerson, 2009).

Despite the volumes of early work devoted to understanding the mechanisms of Cu activation and collector adsorption at sphalerite mineral surfaces, the impacts of cation substitution reactions on sphalerite response to beneficiation has still not been fully resolved at the fundamental or molecular level. Harmer and co-workers (2008) have investigated the changes that these cation substitution reactions cause to sphalerite mineral structure, whereas Chen et al. (2012) related the incorporation of selected trace metal impurities (Cu, Fe and Cd) in sphalerite mineral structure to the mineral's floatation response. The latter authors invoked that changes in the sphalerite crystal structure resulted in changes to the associated electronic properties of the mineral surface e.g., band gap, fermi level, and ratio of charge carrier concentration (Chen et al., 2012). Here we build on the existing body of work by specifically focusses on the effects that Cd and Co substitution reactions have on the surface structure and surface reactivity of synthetic sphalerite using a combination of Raman spectroscopy and Zeta potential experimentation. Our results are interpreted as to further understand the fundamental molecular-level controls on sphalerite response to floatation, as crucial step towards an ultimate design of optimised beneficiation circuits based on careful analysis and understanding of mineral chemistry.

## Methods

### Synthesis of Impurity-doped Sphalerite

A series of impurity doped sphalerites was synthesised using the dry experimental method for sulphide synthesis (e.g., Kullerud, 1971; Kojima and Sugaki, 1984; Pring et al., 2008). This methodology enables a controlled chemical composition of the final product, through careful and stoichiometric mixing of the constituent elements according to the mineral formula  $M_xZ_{1-x}S$  (where M represent the trace metal impurities (Co and Cd). Dopant concentrations ranged between 0 – 4 wt. % for Cd, and between 0 – 1 wt. % for Co (Table 1). All syntheses were conducted at the Experimental Petrology Laboratory at Stellenbosch University, using high purity starting materials procured from Sigma-Aldrich (zinc powder (<150  $\mu\text{m}$ , 99.995% trace metal basis), sulphur (trace metal grade >99.99%), cobalt metal powder (<150  $\mu\text{m}$ , >99.99% trace metal basis), and cadmium powder (<150  $\mu\text{m}$ , >99.99% trace metal basis)).

For each synthesis, the relevant mass of each starting material was ground in an agate mortar using an acetone medium to prevent undesired oxygen from interacting with the chemical system. The finely ground homogenous mixture was transferred into a 12 mm diameter Pyrex tube which was subsequently evacuated under low vacuum conditions and then flushed with argon gas to remove excess oxygen, and finally sealed. The sealed tubes were heated in a muffle furnace at 400°C for two days and at 900°C for one day to allow complete reaction of the phases to produce crystalline sphalerite. To fully ensure chemical homogeneity and a complete reaction, the initial crystallites were removed from their tubes, reground under acetone, and reacted for a further one day at 400°C and finally for four days at 900°C. A total of seven samples were produced following this experimental protocol (Table 1), and, for comparative purposes, a further natural sphalerite (iron poor) sample was selected from the Stellenbosch University Department of Earth Sciences' ore mineral library.

**Table 3:** Average Scanning Electron Microscopy (SEM) elemental spot analyses for the samples. All values reported in weight percentage and values in parentheses reflect the standard deviation.

Sample	Zn (wt. %)	S (wt. %)	Co (wt. %)	Cd (wt. %)
ZnS	66.93 ( $\pm 0.42$ )	33.07 ( $\pm 0.42$ )	-	-

(Co <sub>0.6</sub> ,Zn <sub>99.4</sub> )S	68.11 (±1.70)	31.52 (±1.68)	0.36 (±0.05)	-
(Co <sub>0.9</sub> ,Zn <sub>99.1</sub> )S	66.47 (±1.32)	32.95 (±1.37)	0.56 (±0.06)	-
(Co <sub>1.1</sub> ,Zn <sub>98.9</sub> )S	68.08 (±1)	31.2 (±0.98)	0.71 (±0.05)	-
(Cd <sub>0.9</sub> ,Zn <sub>99.1</sub> )S	65.66 (±1.49)	33.2 (±1.61)	-	1.02 (±0.28)
(Cd <sub>1.8</sub> ,Zn <sub>98.2</sub> )S	65.54 (±0.26)	32.45 (±0.32)	-	2.01 (±0.08)
(Cd <sub>3.3</sub> ,Zn <sub>96.7</sub> )S	62.89 (±0.32)	33.42 (±0.56)	-	3.68 (±0.1)

## Chemical and Structural Characterizations

A range of analytical techniques was applied to firstly ensure the chemical and mineralogical homogeneity within each synthetic sample, and secondly to derive molecular-level insights into the structural changes that result when trace metal dopants are incorporated into the sphalerite crystal structure. Initial sample interrogation was performed using reflected light microscopy (Nikon Labophot Microscope), and this was subsequently supported by detailed chemical mapping using a Zeiss EVO Scanning Electron Microscope (SEM) at the Central Analytical Facility at Stellenbosch University (figure 1). The SEM data was collected both in back-scatter mode and by using the Wavelength Dispersive Spectroscopy (WDS) sensor, and operating conditions were set at an accelerating voltage of 20kV and a current of between -19 nA to -21 nA.

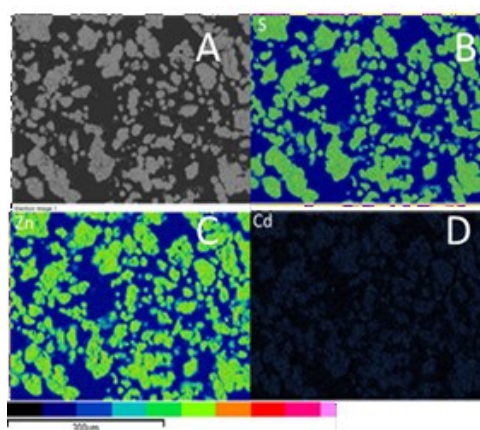


**Figure 1a:** Back-scatter image of Cd 1.02 wt. % Cd-substituted sphalerite. **1b-d:** Elemental maps showing homogenous distribution of elemental constituents within the sphalerite crystallites with an average crystallite size of 18 nm.

Mineralogical purity was further confirmed using X-ray powder Diffraction (XRD) on a Bruker D8 Powder Diffractometer machine at iThemba Labs, Cape Town, South Africa. Synthetic crystallites were ground to a top size of 50  $\mu\text{m}$  and evaluated for mineral composition and possible spectrum shifts using  $2\theta$  data collection at step size of 0.0340. The XRD data collection was operated at an accelerating voltage of <40 kV and current of 25mA for  $\text{CuK}\alpha$  radiation. The reduction and phase identification was performed using PANalytical X'pert HighScore Plus software.

The Raman spectra were collected at room temperature at the department of Physics (Stellenbosch University) using a MicroHR Horiba Jobin Yvon Raman spectrometer equipped with two-dimensional Synapse ICCD detector. An Nd:YAG ion laser emitting at 532 nm was used for the excitation of Raman spectra, and spectra were collected over the region 200 – 400  $\text{cm}^{-1}$  using a exposure time of 1s. Collected spectra were processed using PeakFit v 4.12, SYSTAT softwares, where they were truncated and corrected for background signal drift using a Gaussian fit.

### **Zeta Potential Measurements**

The zeta potential distribution measurements were collected using a Malvern Zetasizer Nano ZS instrument (University of Cape Town, South Africa). The stock solutions for zeta potential measurements were prepared from analytical grade reagents. Freshly prepared 0.001 M  $\text{KNO}_3$  was used as the background electrolyte, with the pH regulated with 0.01 M HCl and 0.01 M NaOH stock solutions. Each sample was ground under acetone using a mortar and pestle to ensure a nominal top-size of <50  $\mu\text{m}$ . After sample drying, a small sub-sample (0.01 g) was transferred into a 15 ml test tube containing 10 ml of 0.001 M  $\text{KNO}_3$ . This mixture was shaken vigorously and allowed to condition for 10 min before transferring 2 ml of an aliquot into an electrophoretic cell. For Cu activation experiments, 10  $\mu\text{L}$  of  $1 \times 10^{-4}$  M  $\text{CuSO}_4$  added to the electrolyte prior to analysis. For these experiments, the pH was slightly alkaline ( $\text{pH} \pm 9$ ) and the temperature was controlled at 25°C.

### **Results and Discussion**

## Chemical and Structural Characterization

The doped- and pure- sphalerite samples synthesized at 900°C for 7 days showed a homogenous distribution of the various element constituents (Fig. 1, Table 1), and their purity was further confirmed by their X-ray diffraction (XRD) patterns. The XRD spectra reflected three prominent diffraction peaks at  $2\theta$  angles of approximately 28.5°, 47.5°, and 56.6° which are respectively attributed to the 111, 220 and 311 planes of the cubic ZnS mineral structure. The absence of extra peaks indicates that there are no extraneous phases (e.g., wurtzite, zinc oxide) present, and this confirms the mineralogical homogeneity indicated by the complementary SEM results (Fig. 1). Relative to pure sphalerite, the impurity doped sphalerites showed minor shifts in the XRD peak positions, indicating small changes to the unit cell parameter resulting from the distortions induced by cation substitution reactions. The structural changes induced by the incorporation of impurity metals into the sphalerite structure were further probed by Raman spectroscopy.

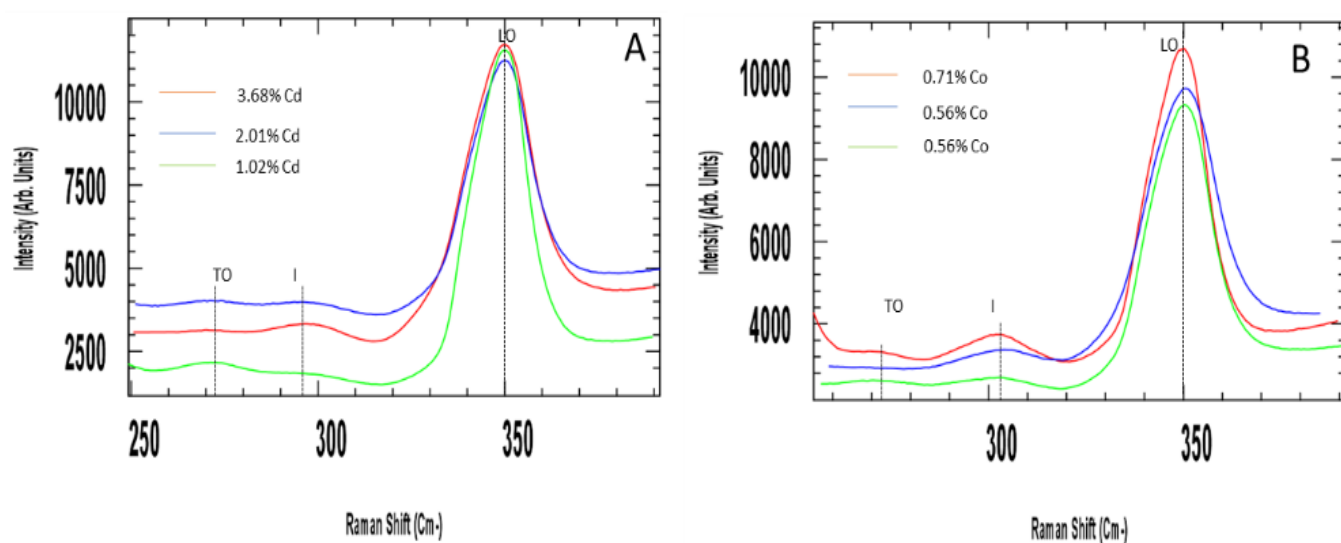


*Figure 10 - Raman spectra of a pure synthetic sphalerite sample with mode assignment adopted from Hope et al., 2000 with the truncated spectra of both Co and Cd bearing sphalerite samples illustrating the development of a new mode with increasing impurity concentration.*

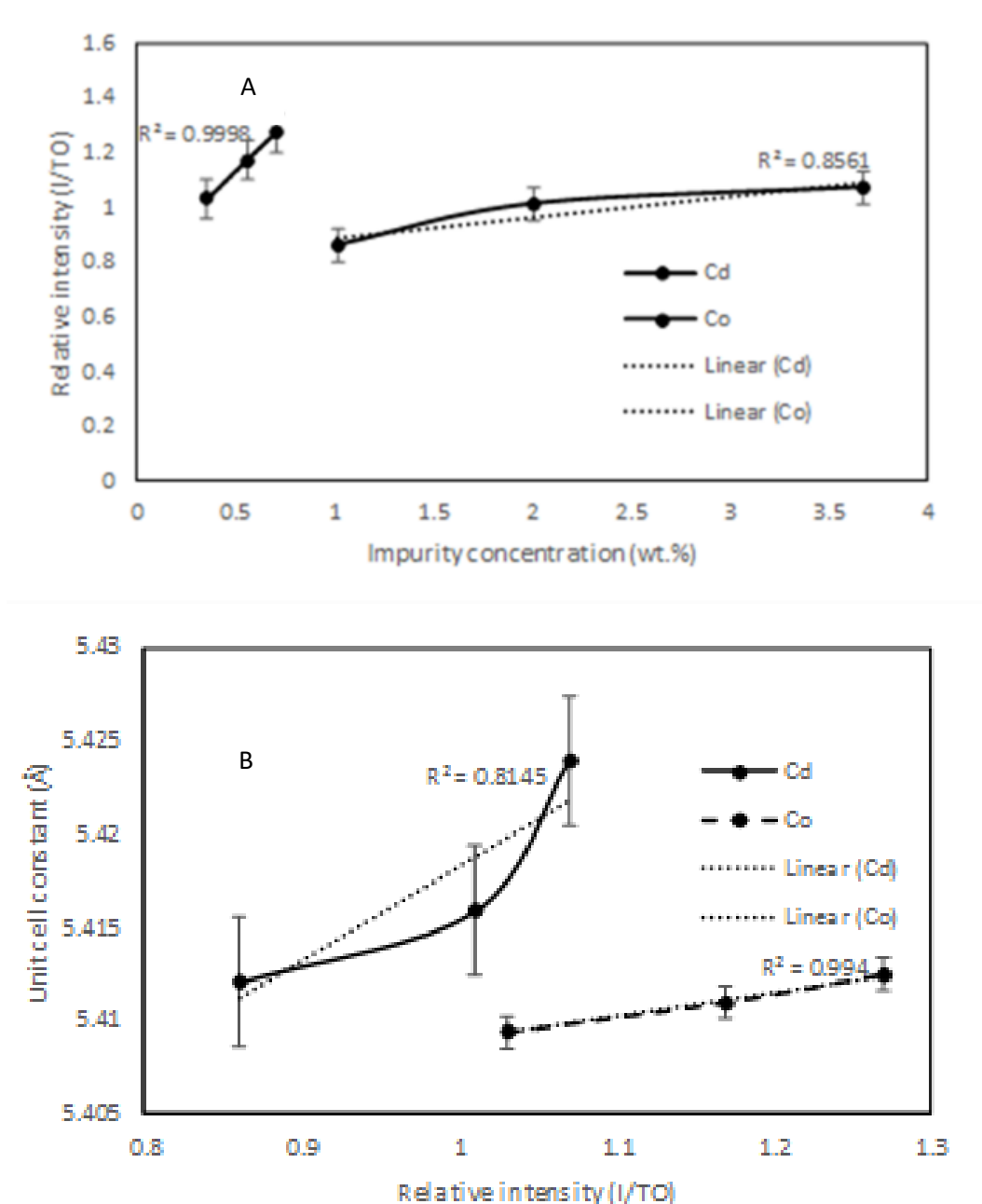


Figure 3a-b: The dependence of relative intensities (I/TO) on impurity concentration (3a), while 3b illustrate the correlation between the unit cell constant and the relative intensities of the impurity-induced mode and TO mode (I/TO).

The relative intensity of the impurity mode (I) relative to the primary transverse optic mode (TO) illustrates the dependence of the mode intensity on the impurity concentration Cd ( $r^2 = 0.85$  and Co ( $r^2 = 0.99$ ) respectively (Fig. 3a), indicating that Raman spectroscopy may be used to predict trace metal concentrations in sphalerite structure. The I/TO ratio further shows a positive relationship ( $r^2 = 0.81 - 0.99$ ; Fig. 3b) with shifts in the unit cell parameter (measured using XRD), reflecting the fact that the

trace element substituents modify both the bulk lattice structure of the sphalerite, and accordingly, its surface structure (as reflected in the surface-sensitive Raman spectra). Our data also show that the positions of the LO and TO shift as a function of impurity concentration (e.g., LO at  $350.32\text{ cm}^{-1}$  for the 0.36 wt% Co but shifts to  $350.57\text{ cm}^{-1}$  at 0.56 wt.% Cd), which agrees well with previous work by Nien and Chen (2006) and further confirms the interplay between dopant concentration, lattice structure and surface bonding (and thus reactivity).

### Dopant Effects on the Reactivity of Un-activated Sphalerite

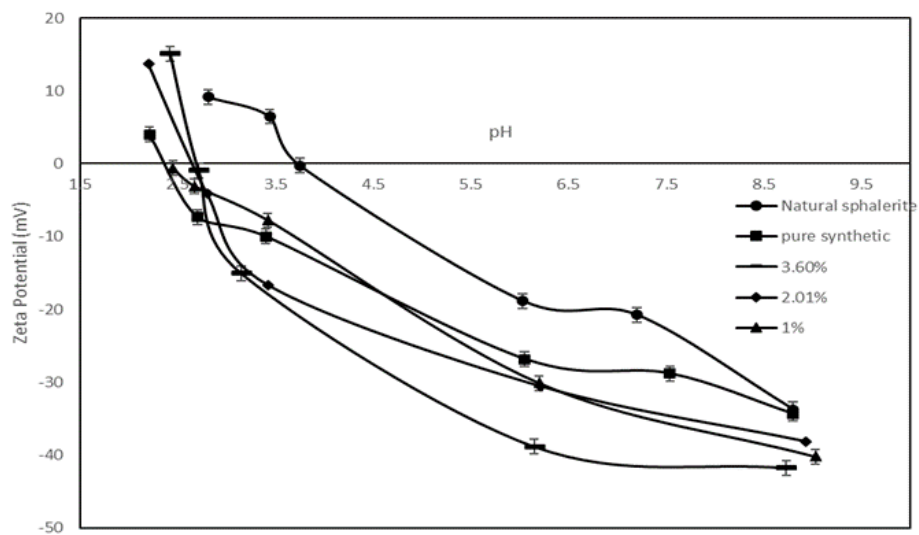
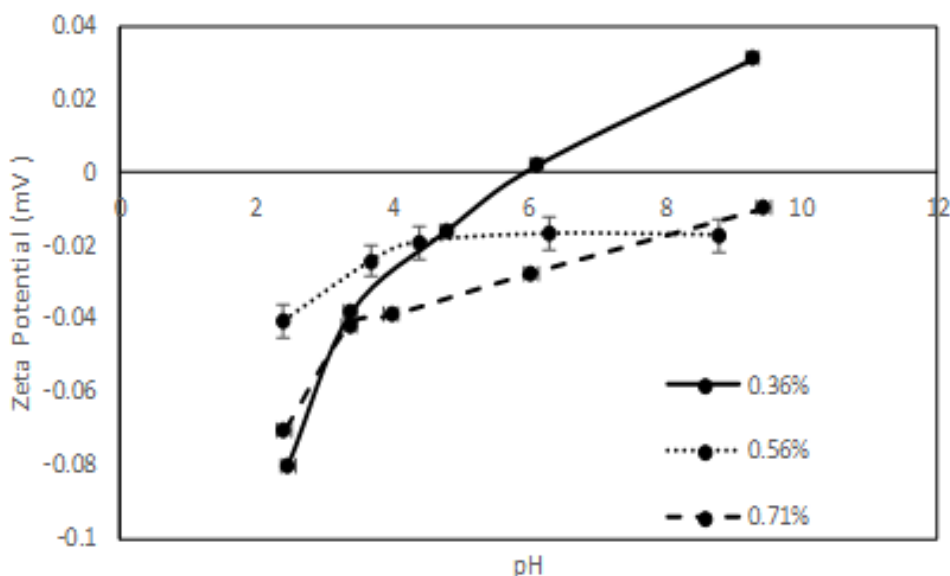


Figure 4 - Plots of unactivated cadmium bearing sphalerite and a single natural sphalerite samples (0.01g) as function of pH in  $1 \times 10^{-4}\text{ M KNO}_3$  (10 ml) as a background electrolyte.



*Figure 5 - Plots of unactivated cobalt bearing sphalerite and a single natural sphalerite samples (0.01g) as function of pH in  $1 \times 10^{-4}$  M KNO<sub>3</sub> (10 ml) as a background electrolyte.*

Zeta potential measurements were performed to assess the surface reactivity of sphalerite with varied cation substitution. Figures 4 and 5 show the zeta potential distribution of unactivated impurity-bearing sphalerite samples conditioned in an alkaline media (pH 9). The results highlight the variable zeta potential response as a function of the geochemical nature of the substituting impurity. Relative to pure sphalerite, the zeta potential for Cd-doped sphalerite becomes more negative, although this phenomenon does not appear to follow a discernible trend with increasing concentration of substituent. The magnitude of the zeta potential is lowered by the incorporation of cobalt (Fig. 5), until the potential is almost neutral.

Several studies have illustrated that sphalerite with varying impurity content exhibit different iso-electric points (iep). Popov and Vucinic (1990) found the iso-electric point at pH 6.5 for a sphalerite sample with 13 wt. % Fe. Our data indicate a strong correlation between the iso-electric point and the concentration of Cd substituting into the sphalerite structure (Fig. 6). The iep for the sample containing 0.36% of Co was found to occur at pH 6, and we unfortunately unable to collect data for the other Co-doped sphalerites in both alkaline and acidic media, indicating that Co shift the iep to



a higher pH. Popov and Vucinic (1990) reported that iep of sphalerite was dependent on factors such as impurity content, solid percent in solution, the time of conditioning and the measuring technique. In addition to the above-mentioned factors, this study suggest that the nature of the impurity plays a significant role on the variation of the iep.

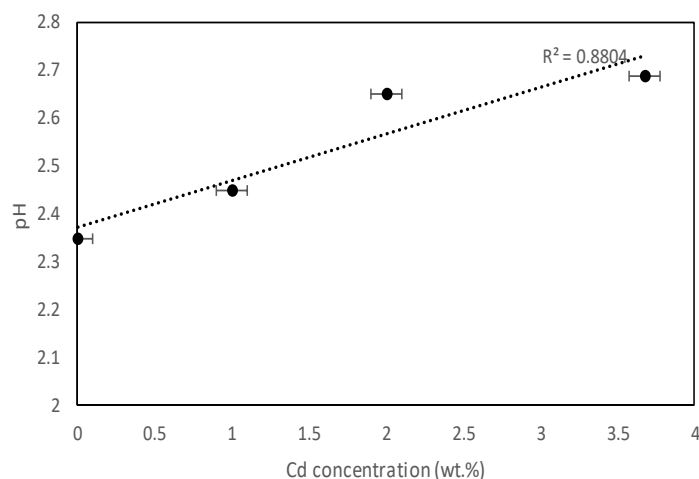


Figure 6 - Variation of the iso-electric point as a function of cadmium concentration.

It was illustrated with Raman spectroscopy that both Cd and Co induce new vibrational features due to their contrasting mass difference and chemical polarity. In agreement with Karbish et al. (2007), sphalerite retains its vibrational characteristics even at high cadmium contents. This shows that the chemical characteristics of Zn and Cd are not significantly different and thus Cd-substitution has limited impact on the geometrical configuration of the local cluster of the Zn-S molecule, thus resulting in the sphalerite surface retaining its negative surface charge. Conversely, the incorporation of a more highly polar atom like Co or Fe will result in a different distribution of the valence electron density of the molecule. The associated dipole moment causes variations in the internal packing structure of the parent molecule, thus changing the preferred local electrostatic energy of the Zn-S cluster. The occurrence of the cobalt-induced modes at higher wavenumbers compared to the Cd induced modes would thus be attributed to the variation in the electrostatic energies of both molecules. The resulting effect on surface properties, as illustrated with the Zeta potential distribution of Co bearing sphalerite (Fig. 5), is neutralisation of the surface charge caused by the electron withdrawing effects of even low concentrations of Co.

## Dopant Effects on Electro-kinetics Properties of Sphalerite in the $\text{CuSO}_4$ Activated System

The effect of impurities on the activation of sphalerite with Cu ions has been a widely researched topic in recent times with several studies reporting contrasting results. A large proportion of those studies have focused their attention on the role played by iron content on the Cu activation. Here we investigate the zeta potential distribution of Co- and Cd-bearing sphalerite samples activated with  $\text{CuSO}_4$  in an alkaline solution for 5 minutes (Fig. 7). The current study measures the electro-kinetic properties of sphalerite activation in an alkaline media, since Cu activation of sphalerite in typical processing circuits is usually performed at high alkaline pH to suppress pyrite and recover sphalerite (e.g., Albrecht et al., 2016).

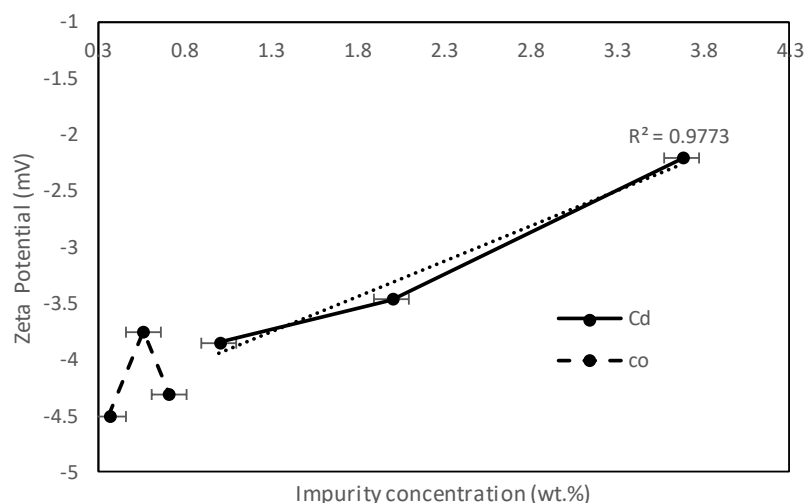


Figure 7 - Comparison of the zeta potential distribution of a Cu-activated pure and cd-bearing sphalerite.

The zeta potential distribution for an activated sphalerite is sensitive to the Cd concentration, with increasing Cd concentration resulting in a lowering of the zeta potential (Fig.7). This decrease in the negative Zeta potential is associated with adsorption of copper hydroxide species on the sphalerite after all the zinc atoms have been substituted with copper ions (Fornaserio and Ralston, 2006). Chen et al. (2012) also illustrated that Cd bearing sphalerites are easily activated with Cu as results of

the minimal changes on electronic structure of sphalerite due to the incorporation of Cd. A Cd-sphalerite retains its surface characteristic thus permits the electrostatics involved during the Cu ions absorption. Conversely, the activation of Co-bearing sphalerite with Cu ions results in a more negative zeta potential indicating that Cu adsorption occurs at the mineral surface. The change in the zeta potential distribution is attributed to the variation in the surface charge, which is dependent on the surface electronic state of impurity-bearing sphalerite. Due to the differences in the geochemical properties of the substituting metal, the surface charge of sphalerite displays variable zeta potential behaviour between the Co- and Cd- substituted sphalerites in alkaline media. Albrecht et al. (2016) stated that the electrostatic interaction between the negatively charged sphalerite surface and the positively charged copper ions ( $\text{Cu}(\text{OH})^+$ ) is responsible for the adsorption of copper. The results from the un-activated experiments show that cobalt is a highly polarizing atom, and thus it will draw the bonding electrons towards itself thus neutralizing the negative surface of sphalerite. Chen et al., (2012) studied the effects of lattice defects due to the incorporation of metal impurities (Fe, Cu and Cd) on sphalerite surface and the consequent copper activation. Their study illustrated that the copper activation of Fe-substituted sphalerite is difficult, since Cu atoms cannot replace the Fe, thereby decreasing the Zn and Cu exchange sites for a Fe-bearing sphalerite. Similarly, the low negative zeta potential acquired for a Co-bearing sphalerite illustrate that limited amount Cu ions that get adsorbed on mineral surface due to limited substitutional site. Conversely, Cd low cadmium content has less effect on the Cu adsorption because the Cu ions can replace the Cd ions that occupy the zinc site, thus increase the floatability of a Cd-bearing sphalerite.

### **Implications to Sphalerite Flotation and Predictive Capabilities During Process Design**

Previous studies have shown that the presence of trace element impurities within sphalerite structure has a negative effect on the floatation recovery of zinc metal (Harmer et al., 2008). Our study indicates that although the incorporation of the Co and Cd induces lattice strains in the sphalerite structure, the magnitude of the lattice distortions does not actually correlate to the geometallurgical response of an impurity bearing mineral. Rather, the chemical properties (e.g., electronegativity) of the substituting metal can be expected to play a more significant role in modifying

floatation response. Chen et al. (2012) have shown a low floatation recovery for Fe-bearing sphalerite in comparison to Cu and Cd bearing sphalerite. We have interrogated the role of Co and Cd substitutions within sphalerite mineral structure and inferred their effects on floatation by carefully evaluating their zeta potential response under alkaline conditions. Cobalt significantly modifies the surface charge of sphalerite, resulting to a close to neutral charge in both alkaline and acidic media for an unactivated sphalerite without collector. The slight change in the zeta potential after the addition of both Cu ions signals that Co-sphalerite can never self-activate due to the presence of Co ions, thus a processing stream with Co bearing will require a significant addition of both Cu ions and collectors to aid maximum recovery. Based on the zeta potential distribution of an un-activated Cd-sphalerite, it is visible that the incorporation of Cd at low concentration <1 wt.% has no detrimental effect on the floatation of sphalerite. A low Cd-bearing sphalerite will have a self-activating capability compared to a Co-sphalerite. When present at high concentration, Cd will start to suppress the floatation behaviour of sphalerite, thus based on a thorough mineralogical and chemical characterization; the predictive capabilities during process design can be enhanced.

## **Conclusion**

Using a suite of analytical techniques (XRD, Raman spectroscopy and Zeta Potential measurements), we have interrogated the influence of cation (Cd, Co) substitution on the structural characteristics and geometallurgical response of synthetic sphalerite. The substituting ions induce measurable distortion to the sphalerite structure, which consequently alters both the vibrational properties and surface structure of the mineral. The extent of the distortions are highly dependent on the concentration and nature of the substituting metal impurity, as reflected by both XRD and Raman spectroscopy. The nature of the substituting metal ion further affects the surface reactivity of sphalerite, and the degree of this influence can be related to the electronegativity of the substitution ion (e.g., Co has a greater influence on sphalerite surface charge than Cd). Zeta potential measurements indicate that surface reactivity of sphalerite is highly dependent on the nature and concentration of the substituting metal. This is reflected by the varied electro kinetic response of Cd- and Co- sphalerite samples. Co draws valence electrons density towards itself thus neutralizing the surface charge of

sphalerite, while Cd a less polar atom thus not cause a significant change to the surface charge at low concentration but its suppressing effect is noticed at higher concentration. Our results thus highlight the importance of considering molecular level interactions in complex mineral systems. We maintain that a full and fundamental understanding of the molecular-level dynamics will be crucial towards designing the most efficient beneficiation streams for ores produced from the “Mine of the Future”.

## **Acknowledgments**

The authors acknowledge the financial support provided by DST-CIMERA. The authors are further grateful to Dr Remy Bucker (iThemba Labs) and the staff at the Central Analytical Facility (Stellenbosch University) for their assistance with the XRD and SEM analysis respectively.

## **References**

- Albrecht, T.W.J., Addai-Mensah, J., Fornasiero, D., 2016. Critical copper concentration in sphalerite flotation: Effect of temperature and collector. *International Journal of Mineral Processing*, Vol. 146, pp 15-22.
- Bi, C., Pan, L., Xu, M., Yin, J., Guo, Z., Qin, L., Zhu, H., Xiao, Q.J., 2009. Raman spectroscopy of Co-doped wurtzite ZnS nanocrystals. *Chemical Physics Letter*, Vol. 481, pp 220-223.
- Chandra, A.P., Gerson, A.R., 2009. A review of the fundamental studies of the copper activation mechanisms for selective flotation of the sulfide minerals, sphalerite and pyrite, *Advances in Colloid and Interface Science*, Vol.149, pp 97-110.
- Chen, Y., Chen, J., Guo, J. 2010. A DFT study on the effect of lattice impurities on the electronic structures and floatability of sphalerite. *Mineral Engineering*, Vol. 23, pp 1120-1130.
- Chen, Y., Chen, J., Lan, L., Yang, M., 2012. The influence of impurities on the flotation behaviours of synthetic ZnS. *Mineral Engineering*, Vol. 27-28, pp 65-71.

- Ejtemaei, M., Nguyen, V.A., 2017. A comparative study of the attachment of air bubbles onto sphalerite and pyrite surfaces activated by copper sulphate. *Mineral Engineering*, Vol. 109, pp14-20.
- Harmer, S.L., Mierczynska-Vasilev, A., Beattie, D.A., Shapter, J.G. The effect of bulk iron concentration and heterogeneities on the copper activation of sphalerite
- Hope, G.A., Woods, R., Munce, C., 2001. Raman microprobe mineral identification. Eleventh Annual V. M. Goldschmidt Conference, Hots Springs.
- Kharbish S., 2007. A Raman spectroscopic investigation of Fe-rich sphalerite: effect of Fe-substitution. *Physical Chemistry Minerals*, Vol. 34, pp 551–558.
- Kullerud, G. 1971. Experimental Techniques in Dry Sulfide Research. In , Ulmer, G. C., Ed., *Research Techniques for High Pressure and High Temperature*. Springer-Verlag, pp. 288 – 315.
- McClung, C.R. and Viljoen, F., 2011. A detailed mineralogical assessment of sphalerites from the Gamsberg zinc deposit, South Africa: The manganese conundrum. *Minerals Engineering*, 24(8), 930-938.
- Osadchii, E.G., Gorbaty, Y.E. 2010. Raman spectra and unit cell parameters of sphalerite solid solutions ( $\text{Fe}_x\text{Zn}_{1-x}\text{S}$ ). *Geochimica et Cosmochimica Acta*, Vol. 74, pp 568-573.
- Popov, S.R., Vucinic, D.R., 1991. The ethylxanthate adsorption on copper –activated sphalerite under flotation-related conditions in alkaline media. *International Journal of Mineral Processing*, Vol. 30, PP 229-244.
- Prestidge, C.A., Skinner, W.M., Ralston, J., Smart, R. St C., 1996. Copper (II) activation and cyanide deactivation of Zn sulfide under mildly alkaline conditions, *Applied Surface Science*, Vol.108, pp 333-344.
- Ralston, J and Healy, T W, 1980. Activation of zinc sulphide with  $\text{Cu}^{2+}$ ,  $\text{Cd}^{2+}$  and  $\text{Pb}^{2+}$ , *International Journal of Mineral Processing*, 7(175-201):203-217.
- Sandoval, S.J., Rivera, A.L., Irwin, J.C., 2003. Influence of reduced mass differences on the Raman spectra of ternary mixed compounds:  $\text{Zn}_{1-x}\text{Fe}_x\text{S}$  and  $\text{Zn}_{1-x}\text{Mn}_x\text{S}$ . *Phys Rev B*68:3031–3039.
- Skinner, B.J., 1961 Unit-cell edges of natural and synthetic sphalerites. *American Mineralogist*, Vol 46, 1399–1411.

Yung-Tang Nien, Y.T., Chen, I.G., 2006. Raman scattering and electroluminescence of ZnS:Cu,Cl phosphor powder. *Applied Physics Letters*, Vol. 89, 261906.

Zigone, M., Vandevyver, M., Talwar, D.N., 1981. Raman scattering and local force variations due to transition-element impurities in zinc sulphide crystals: Effect of pressure application. *Phys Rev B*24:5763–5778.

## APPENDIX II

author	elements wt.%										
	Fe	Mn	Cd	Co	Zn (major)	Cu	Ga	Ag	Ge	In	Pb
McClung and Viljoen, (2011)	25	14	0.16	0.64	-	-	-	-	-	-	-
Pring et al., 2008	12.8	0.3	0.3	-	53.6	-	-	-	-	-	-
Zhang et al., 1992	2.8	-	-	-	63.8	0.1	-	-	-	-	0.38
Boulton et al., 2005	0.3	-	-	-	66.7	0.06	-	-	-	-	0.07
Boulton et al., 2005	12.5	-	-	-	53.2	0.47	-	-	-	-	0.24
Harmer et al., 2008	0.02	-	0.11	-	-	-	-	-	-	-	-
Harmer et al., 2008	0.19	-	0.58	-	-	0.03	-	-	-	-	-
Harmer et al., 2008	8.14	1.31	0.22	-	-	-	-	-	-	-	-
Harmer et al., 2008	14.79	0.36	0.62	-	-	-	-	-	-	-	-
Tong et al., 2007	20.05	-	-	-	45.12	-	-	-	-	-	-
Mirmezami et al., 2003	0.3	-	-	-	65	0.1	-	-	-	-	-
Mirmezami et al., 2003	17.5	-	-	-	40	0.4	-	-	-	-	0.04
Mirmezami et al., 2003	13.2	-	-	-	48	0.1	-	-	-	-	0.2
Mirmezami et al., 2003	8.2	-	-	-	51	1.3	-	-	-	-	0.1
Gerson et al., 1999	0.49	-	-	-	66.9	0.06	-	-	-	-	0.04
Gigowski et al., 1991	0.25	0.0012	0.09	-	66	0.0067	0.08	0.0001	0.0026	0.0001	0.08
Gigowski et al., 1991	3.05	0.012	0.38	-	62.51	0.044	0.002	0.0006	0.0066	0.0005	0.17
Gigowski et al., 1991	1.2	0.0092	0.11	-	60.9	0.018	0.0046	0.0035	0.0008	0.0002	0.08
Gigowski et al., 1991	12	0.33	0.2	-	53.4	0.02	0.0003	0.0003	0.0005	0.0038	0.0003
Gigowski et al., 1991	0.38	0.0016	0.29	-	66	0.01	0.0002	0.0001	0.0026	0.0001	0.0001
Gigowski et al., 1991	0.35	0.001	0.41	-	66.31	0.046	0.009	0.0005	0.021	0.0001	0.065
De Gyves, 1998	4.08	0.0032	0.3724	0.0196	59.4	0.1633	0.0112	0.0392	0.0072	0.0064	-
De Gyves, 1998	2.86	0.0117	0.2273	0.0216	60.94	0.0416	0.0033	0.0017	0.0031	0.0024	-
De Gyves, 1998	1.92	0.0044	0.0735	0.0361	63.16	0.0561	0.0013	0.0027	0.0054	0.0005	-
De Gyves, 1998	3.76	0.0073	0.13	0.0446	58.63	0.4487	0.0046	0.0029	0.0019	0.0091	-
George et al., 2016	8.8	0.2392	0.1045	0.0076	-	0.0584	0.0002	-	-	0.0004	-
George et al., 2016	0.1525	0.0358	0.1634	0.0285	-	0.0616	0.0001	0.0002	-	0.00078	-
George et al., 2016	9	1.66	0.0884	0.0128	-	0.0071	0.00026	0.0001	-	0.000069	-
Frenzel et al., 2016	0.44	0.0018	0.36	0.0006	-	0.035	0.0042	0.0012	0.0063	0.0002	-
Frenzel et al., 2016	3	0.059	0.24	0.0002	-	0.031	0.0011	0.0016	0.00036	0.001	-
Frenzel et al., 2016	3.7	0.073	0.21	0.001	-	0.0001	0.0019	0.0013	0.00022	0.0022	-



## APPENDIX III

This appendix presents the sets of results that are not shown on the entire thesis but have been not shown in both chapters 4-6.

### Impurity induced surface characteristics of sphalerite

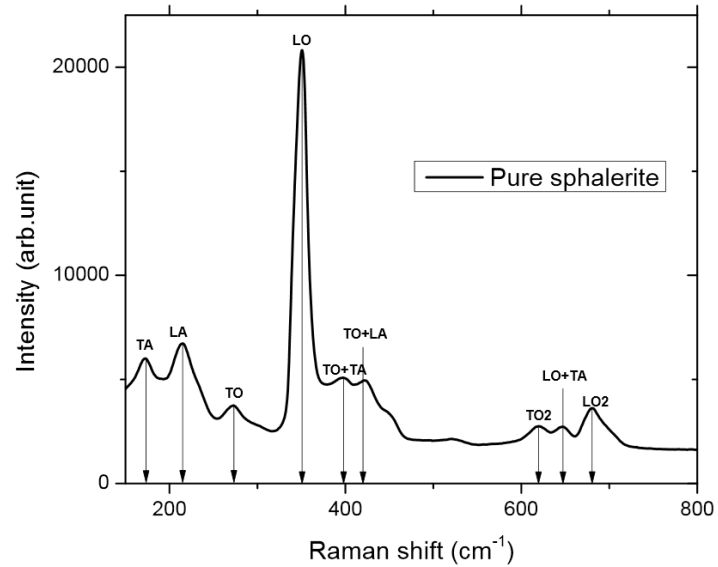


**Figure 11:** Raman spectrum of a pure sphalerite sample with mode assignment adopted from Hope et al., 2001.

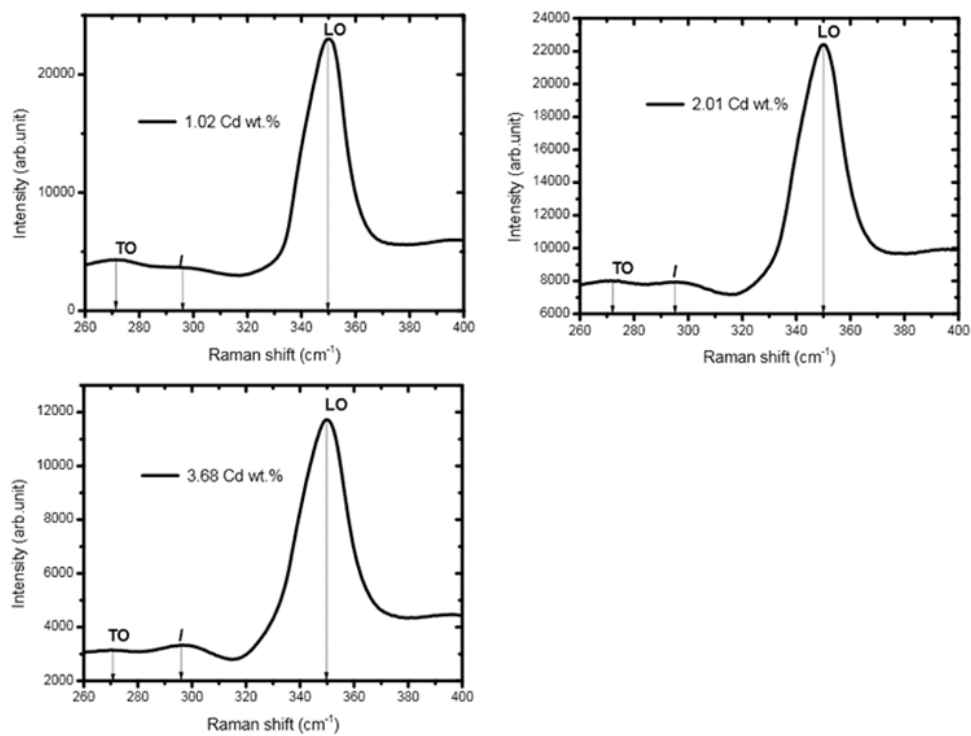


**Figure 12:** Evolution of the impurity induced Raman mode with increasing cadmium concentration within sphalerite lattice site. The impurity mode is denoted as I, appearing approximately around 295 cm<sup>-1</sup>.

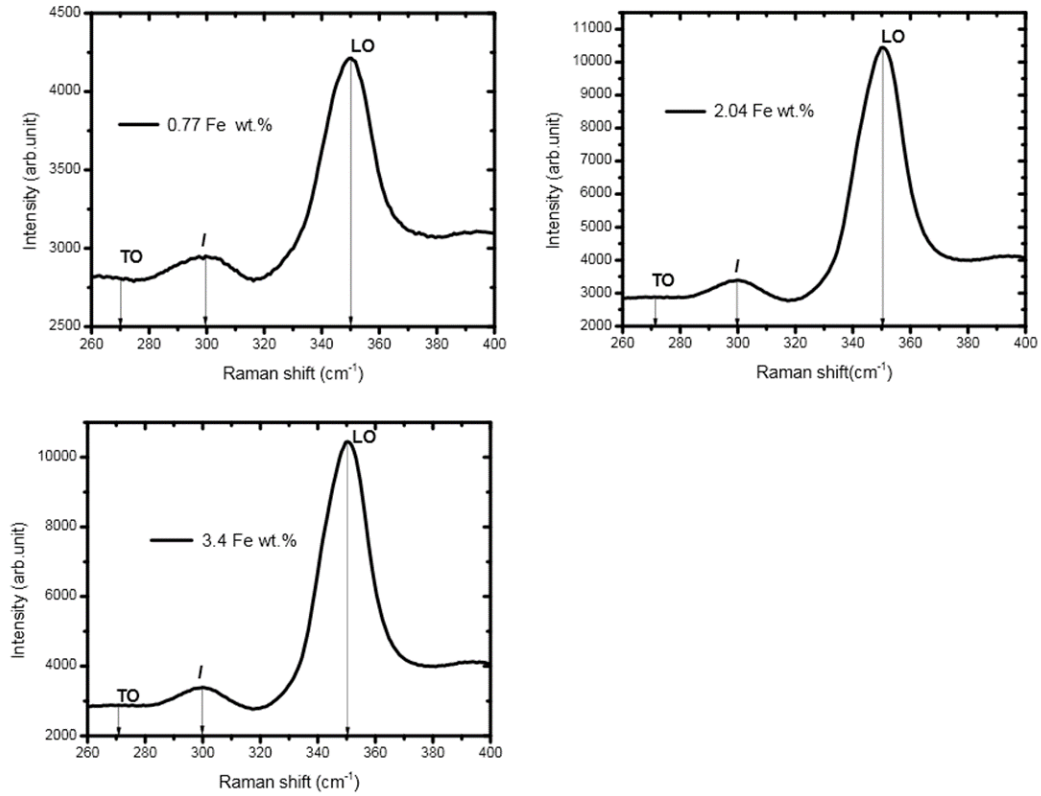


**Figure 13:** Evolution of the impurity induced Raman mode with increasing iron concentration within sphalerite lattice site. The impurity mode is denoted as I, appearing approximately around 300 cm<sup>-1</sup>.

### Influence of impurities on the band structure of sphalerite

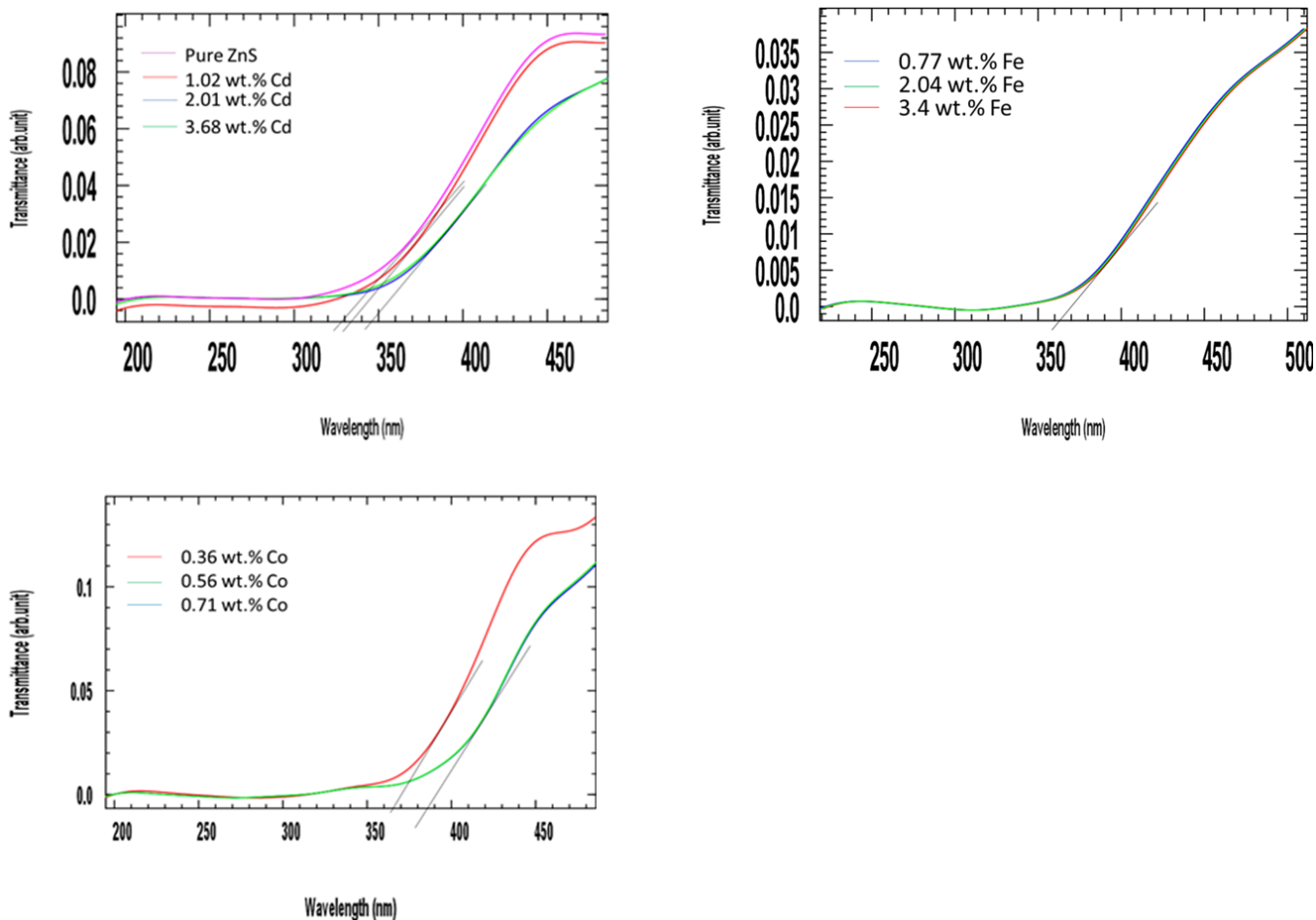


**Figure 14:** UV-vis diffuse reflectance spectra of pure sphalerite and impurity (Fe, Cd and Co) bearing sphalerite.

**Influence of impurities on sphalerite flotation response as reflected by electro-kinetic measurements**

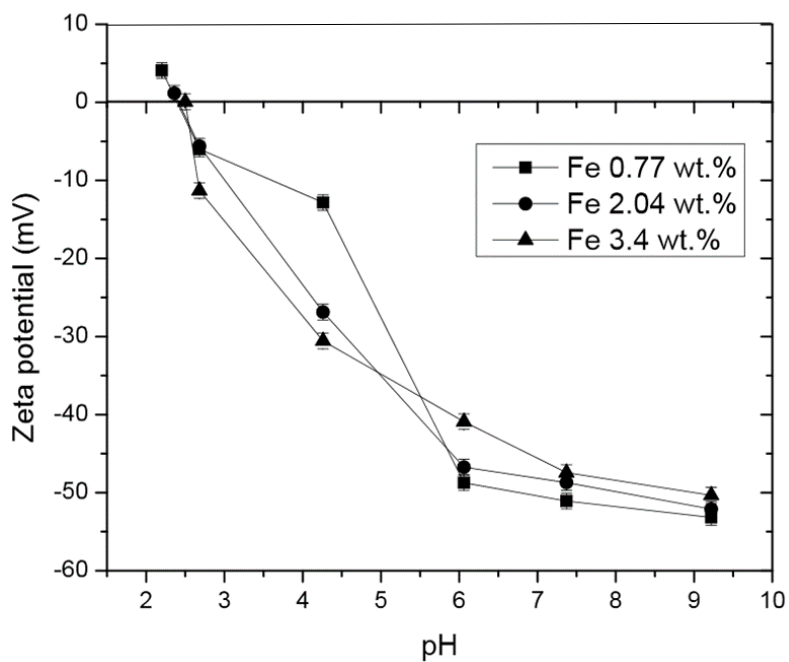


**Figure 15:** Zeta potential distribution of unactivated Fe-bearing sphalerite conditioned for 5 min in both acidic and alkaline electrolyte solution.

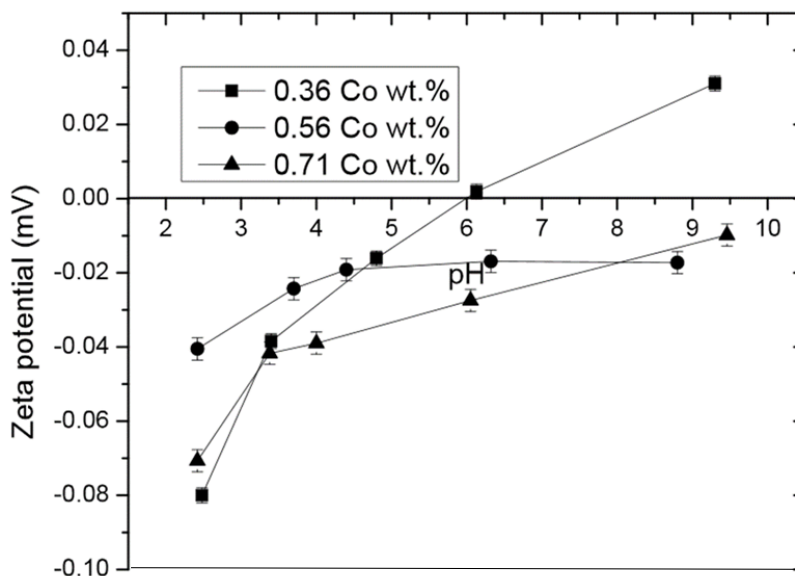


**Figure 16:** Zeta potential distribution of a Co-bearing sphalerite conditioned in an acidic and alkaline electrolyte solution for 5min.

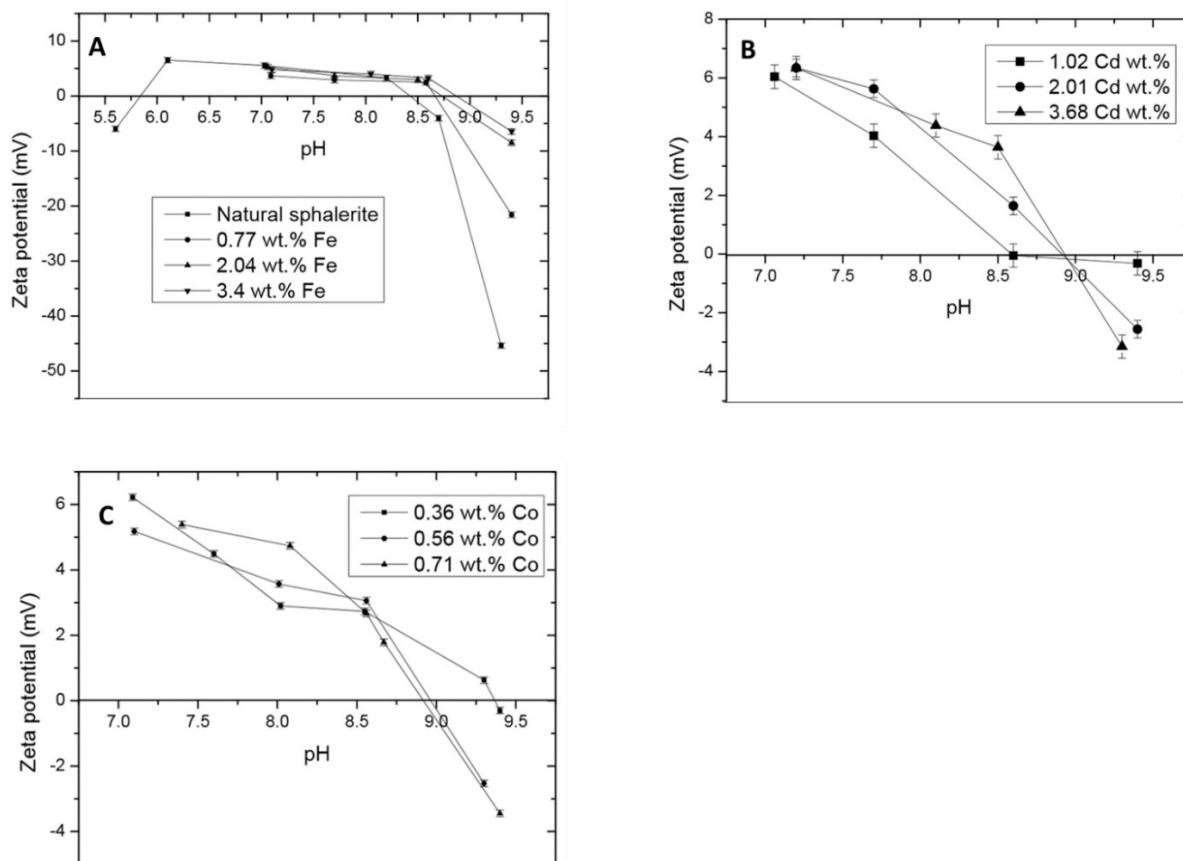


**Figure 17:** Zeta potential distribution for Cu-activated impurity bearing synthetic sphalerite samples at different pH points.

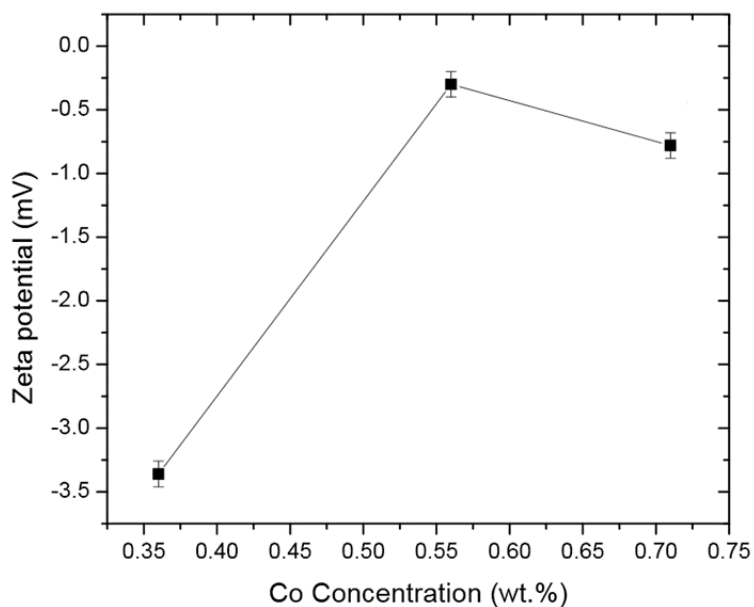


**Figure 18:** Zeta potential distribution for different Co-bearing synthetic sphalerite conditioned in an electrolyte solution containing  $1 \times 10^{-4} \text{ M CuSO}_4$ .

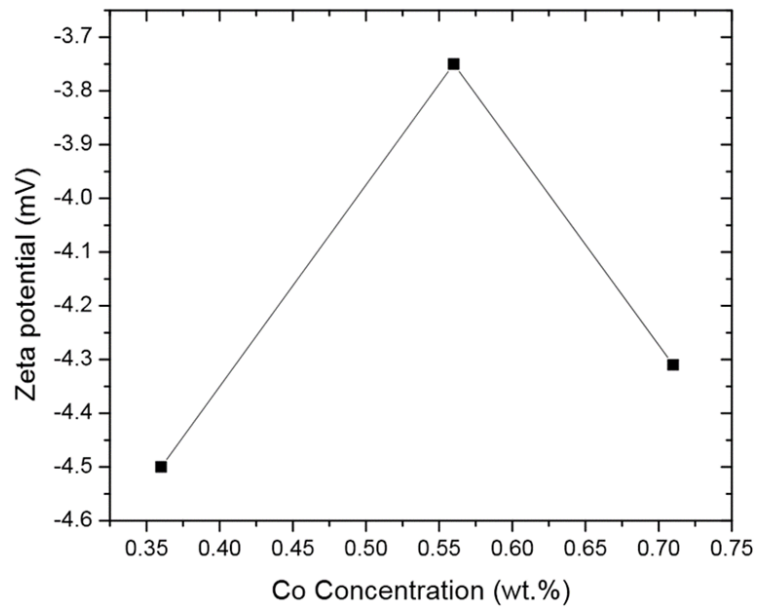


**Figure 19:** Zeta potential distribution for different impurity bearing synthetic sphalerite conditioned in an electrolyte solution containing  $1 \times 10^{-4}$  M xanthate and  $1 \times 10^{-4}$  M  $\text{CuSO}_4$  in a 1:1 ratio.